Ricardo Arbach Fernandes de Oliveira

On the drag coefficient in particle agglomerates: a CFD approach to propose a new drag correlation

São Carlos

2023

Ricardo Arbach Fernandes de Oliveira

Estudo do coeficiente de arraste em aglomerados de partículas: uma nova correlação de coeficiente de arraste utilizando CFD

São Carlos

2023

Ricardo Arbach Fernandes de Oliveira

On the drag coefficient in particle agglomerates: a CFD approach to propose a new drag correlation

Doctoral Thesis presented to the Graduate Program in Chemical Engineering of the Federal University of São Carlos as a partial requirement to obtain the degree of Doctor in Chemical Engineering.

Federal University of São Carlos

Graduate Program in Chemical Engineering

Advisor: Prof. Dr. Gabriela Cantarelli Lopes

São Carlos

2023

UNIVERSIDADE FEDERAL DE SÃO CARLOS

Centro de Ciências Exatas e de Tecnologia
Programa de Pós-Graduação em Engenharia Química

Folha de Aprovação

Defesa de Tese de Doutorado do candidato Ricardo Arbach Fernandes de Oliveira, realizada em 31/07/2023.

Comissão Julgadora:

Profa. Dra. Gabriela Cantarelli Lopes (UFSCar)

Prof. Dr. Gabriel Henrique Justi (UNIPAMPA)

Profa. Dra. Liliana de Luca Xavier Augusto (UTFPR)

Prof. Dr. Antonio Jose Gonçalves da Cruz (UFSCar)

Prof. Dr. Thiago Faggion de Pádua (UFSCar)

O Relatório de Defesa assinado pelos membros da Comissão Julgadora encontra-se arquivado junto ao Programa de Pós-Graduação em Engenharia Química.

Acknowledgements

I would like to express my gratitude, first and foremost, to my parents, Luis and Roseli, who have always supported and encouraged me throughout these years of post-graduate studies. As an essential part of this work, they have always been there to assist me, providing both moral support during moments when I doubted my ability to complete the work and technical support when I faced challenges with the fundamentals of mathematics and, during periods of financial difficulties, as my *mécènes*. Every achievement throughout these years has their special and direct involvement.

To my advisor, Professor Gabriela Cantarelli Lopes, I am grateful not only for her technical expertise, raising intriguing questions about the work during hours of meetings that led to reflections and helped in developing a solid piece of research, but also for her enthusiastic, patient, and captivating way of working, which has always served as motivation for my dedication throughout my master's and doctoral studies.

I extend my appreciation to the technical staff of the didactic laboratory, Gabriel and Tiago, who have always been very approachable, helpful, and patient in explaining the functioning of the equipment.

To my laboratory friends, Ayuba, João, Karla, and Victor, whose friendships and willingness to assist go beyond the work environment.

I am grateful to the Federal University of São Carlos, the Graduate Program in Chemical Engineering, the Department of Chemical Engineering, and the Center for Research in Advanced Materials and Energy for providing the necessary infrastructure that enabled the development of this work. I would also like to thank the National Council for Scientific and Technological Development (CNPq – Grant Number 140412/2020-4) and the Coordination for the Improvement of Higher Education Personnel (CAPES – Finance Code 001) for their financial support.

"It is necessary to dream, but with the condition of believing in our dreams. To examine real life carefully, to confront our observation with our dreams, and to perform our fantasy scrupulously."

V. I. Ulyanov

Resumo

Em escoamentos carregados de partículas, é essencial modelar a interação fluido-partícula. Porém, a depender de efeitos como atração e atrito entre partículas, propriedades superficiais e colisões, as partículas podem se aglomerar, formando novas partículas de formatos irregulares. Tal fenômeno tem sua importância, visto que sua geometria altera diretamente a dinâmica do escoamento. Uma maneira de avaliar a forma como a partícula interfere no escoamento é utilizando a força de arraste. No desenvolvimento teórico de equipamentos, tal força é levada em consideração, sendo representada pelo coeficiente de arraste e é altamente dependendente de duas variáveis: geometria da partícula e velocidade do escoamento. Na literatura, são observadas diversas correlações, obtidas tanto experimentalmente quanto numericamente, utilizando técnicas de fluidodinâmica computacional (CFD). A vantagem do uso de métodos numéricos se dá na facilidade de se variar a velocidade do escoamento, bem como no cálculo do coeficiente de arraste a partir dos campos de pressão. Porém, a maioria destes utilizam métodos de formulação transiente, obtendo resultados com elevados níveis de detalhamento, mas de alto custo computacional, que aumenta exponencialmente quanto maior o número de Reynolds. Deste modo, tais modelos são obtidos, em geral, para valores de Reynolds inferiores a 300 e extrapolados para valores elevados ao serem implementados em códigos de CFD. Assim, neste estudo foram propostas tanto uma maneira alternativa de abordar o problema, utilizando simulações de formulação estacionária, reduzindo o custo computacional, quanto uma nova correlação de coeficiente de arraste simples e unificada, capaz de abranger amplas faixas de escoamento, do laminar ao turbulento, aplicável a partículas irregulares, e de fácil implementação em códigos de CFD. Utilizando-se de CFD com validação experimental, foi possível obter a curva característica de coeficiente de arraste ao longo de uma ampla faixa de números de Reynolds ($0{,}1 \leq Re \leq 3500$) para aglomerados de esferas, que representavam partículas de formatos irregulares. Ao simular individualmente o escoamento de um fluido ao redor de tais aglomerados, variando as geometrias e velocidade do escoamento, foi possível propor a nova correlação de cálculo de coeficiente de arraste capaz de se ajustar às curvas características obtidas. Em linhas gerais, os resultados obtidos mostraram que o uso de uma formulação estacionário é capaz de obter bons resultados, desde que a malha seja corretamente refinada e o modelo de turbulência seja capaz de representar corretamente o escoamento. A nova correlação, aliada ao uso do achatamento como parâmetro de caracterização geométrica, mostrou-se eficaz em representar a curva de arraste, apresentando desvios máximo, mínimo e médio de 10,78 %, -7,62 % e 3,79 %, respectivamente, em relação aos resultados simulados, e 14,36 %, -12,36 % e 9,6 % em relação aos resultados experimentais.

Palavras-chave: Material particulado, Aglomerados de partículas, Partículas de formatos irregulares, Coeficiente de arraste, Fluidodinâmica computacional

Abstract

In particle-laden flows, it is essential to model the fluid-particle interaction. However, depending on effects such as friction and attraction, surface properties, and collisions, particles can agglomerate, generating new irregularly-shaped particles. Such phenomenon is relevant since the geometry directly interferes with the flow dynamics. One way to evaluate how the particle will interfere is through the drag force. In the theoretical development of equipment, this force is taken into account and represented by the drag coefficient and is highly dependent on two variables: particle geometry and flow velocity. In the literature, several correlations are observed, obtained both in the experimental field or numerical field, using computational fluid dynamics (CFD). The advantage of using CFD lies in the ease of varying the flow velocity and in obtaining the drag coefficient from the pressure and velocity fields. However, most of these methods employ transient formulations, resulting in highly detailed but computationally expensive outcomes. This cost increases exponentially as the Reynolds number of the flow increases, making the study of turbulent flows infeasible. Consequently, these models are generally obtained for Reynolds numbers below 300 and then extrapolated to higher values when implemented in CFD codes. Thus, this study proposes an alternative approach to the problem by using steady formulation simulations, aiming to reduce computational costs and proposing a new, simple, and unified correlation for the drag coefficient capable of encompassing a wide range of flows, from laminar to turbulent, applicable to irregularly shaped particles and easily implementable in CFD codes. Using CFD simulations with experimental validation, it was possible to obtain the characteristic drag coefficient curve over a wide range of Reynolds numbers ($0.1 \leq \mathrm{Re} \leq 3500$) for agglomerates of spheres representing irregularly-shaped particles. By individually simulating the flow around these agglomerates while varying the geometries and flow velocities, a new correlation for calculating the drag coefficient was proposed, capable of fitting the obtained characteristic curves. In general, the results showed that the use of a steady formulation can yield good results provided that the mesh is properly refined and the turbulence model accurately represents the flow. The new correlation, combined with the use of flatness as a geometric characterization parameter, proved effective in representing the drag curve, with maximum, minimum, and average deviations of 10.78 %, -7.62 %, and 3.79 %, respectively, compared to simulated results, and 14.36 %, -12.36 %, and 9.6 % compared to experimental results.

Keywords: Particulate matter, Particle agglomerates, Irregularly-shaped particles, Drag coefficient, Computational fluid dynamics

List of figures

List of tables

List of symbols

Latin

A, B, C, D	Parameters of the Haider and Levenspiel drag model	$[\,-\,]$
A_{mp}	Maximum projected area de máxima projeção	$[\,m^2\,]$
A_b	Body's area	$[\,m^2\,]$
A_p	Projected area	$[\,m^2\,]$
A_{ps}	Particle surface area	$[\,m^2\,]$
A_{sph}	Surface area of the volume-equivalent sphere	$[\,m^2\,]$
A_{ws}	Windward surface area	$[\,m^2\,]$
$A.R.$	Aspect ratio	$[\,-\,]$
c	Circularity	$[\,-\,]$
c_S	Surface circularity	$[\,-\,]$
C_D	Drag coefficient	$[\,-\,]$
C_D^{corr}	Drag coefficient estimated by correlations	$[\,-\,]$
C_D^{exp}	Drag coefficient obtained experimentally	$[\,-\,]$
C_D^{sim}	Drag coefficient estimated by correlations simulations	$[\,-\,]$
C_1, C_2, C_3, C_4 C_5, C_6, C_7, C_8	Fit parameters of the new drag correlation proposed	$[\,-\,]$
d_A or d_S	Surface-equivalent sphere diameter	$[\,m\,]$
d_{eq} or d_n	Volume-equivalent sphere diameter	$[\,m\,]$
f	Flatness	$[\,-\,]$
F_B	Buoyancy	$[\,N\,]$
F_D	Drag	$[\,N\,]$
F_W	Weight	$[\,N\,]$
$\mathbf{g}$	Gravitational acceleration	$[\,m\,s^{-2}\,]$

k	Turbulence kinetic energy	$[\, m^2\, s^{-2}\,]$
K	Fluctuation kinetic energy	$[\, m^2\, s^{-2}\,]$
k_N	Newton's parameter	$[\, -\,]$
k_S	Stokes' Parameter	$[\, -\,]$
L_x	Streamwise length	$[\, m\,]$
m_p	Particle's mass	$[\, kg\,]$
N	Total data in the sample studied or number of grid points	$[\, -\,]$
P_c	Perimeter of the circle equivalent to the particle maximum projection	$[\, m\,]$
P_D	Dynamic pressure	$[\, kg\ m^{-1} s^{-2}\,]$
P_k	Production of turbulence kinetic energy	$[\, m^2 s^{-2}\,]$
P_{mp}	Maximum projected perimeter	$[\, m\,]$
Re	Reynolds number	$[\, -\,]$
$\widetilde{Re}_{\theta t}$	Transition momentum thickness Reynolds number	$[\, -\,]$
SD	Standard deviation	$[\, \%\,]$
t	Time	$[s]$
$\mathbf{u}$	Velocity vector	$[\, m\, s^{-1}\,]$
u_f	Fluid velocity	$[\, m\, s^{-1}\,]$
u_p	Particle velocity	$[\, m\, s^{-1}\,]$
u_t	Terminal velocity	$[\, m\, s^{-1}\,]$
U_∞	Freestream velocity	$[\, m\, s^{-1}\,]$
V_b or V_p	Volume of the particle in free fall	$[\, m^3\,]$
x	Position vector	$[\, -\,]$
$\hat{x}_i$	Value of the i-th data obtained by correlations	$[\, -\,]$
x_i	Value of the i-th data obtained by simulations	$[\, -\,]$

Greek

γ	Intermittency $[-]$
δ	Relative error or percent deviation $[\%]$
ε	Turbulence dissipation rate $[m^2 s^{-3}]$
ν	Kinematic viscosity $[m^2 s^{-1}]$
ν_t	Turbulent kinematic viscosity $[m^2 s^{-1}]$
$\tilde{\nu}$	Spalart-Allmaras variable $[m^2 s^{-1}]$
μ	Dynamic viscosity $[kg\ m^{-1} s^{-1}]$
ρ_f	Fluid's density $[kg\ m^{-3}]$
ρ_p	Particle's density $[kg\ m^{-3}]$
τ_{ij}	Reynolds stress tensor $[kg\ m^{-1} s^{-1}]$
ϕ	Sphericity $[-]$
ϕ_W	Sphericity of Wadell $[-]$
$\phi_\perp$	Crosswise sphericity $[-]$
$\phi_\parallel$	Lengthwise sphericity $[-]$
Ψ	Generic geometry parameter $[-]$
ω	Specific turbulence dissipation $[s^{-1}]$

Subscript

i	Cartesian coordinate
j	Cartesian coordinate

Mathematical operators

∇	Gradient
$\nabla\cdot$	Divergence
∂	Partial derivative
Σ	Summation sign

List of abbreviations and acronyms

CAD	Computer Aided Design
CFD	Computational Fluid Dynamics
DNS	Direct Numerical Simulation
LBM	Lattice-Boltzmann Method
LES	Large-Eddy Simulation
PISO	Pressure-Implicit with Splitting of Operators
PRESTO !	PREssure STaggering Option
RANS	Reynolds-Averaged Navier-Stokes
RMS	Root-mean-square
RMSE	Root-mean-square error
RSM	Reynolds Stress Model
SIMPLE	Semi-Implicit Method for Pressure-Linked Equations
SST	Shear Stress Transport
URANS	Unsteady Reynolds-Averaged Navier-Stokes

Table of contents

1 Introduction

1.1 Structure of the thesis

The study presented in this thesis was divided into three stages, using the methodology commonly employed in conducting studies that utilize Computational Fluid Dynamics (CFD) as the main tool. These stages are as follows:

1. Study of mathematical formulation and numerical methods;
2. Verification and experimental validation of the results;
3. Study of cases aiming to propose new hypotheses.

Throughout the development of this work, scientific articles were written, which were submitted and/or published in international journals. Thus, in order to make the reading of this text more dynamic, the thesis is presented in chapters as the articles were developed. Therefore, the chapters of this thesis are presented in the following sequence:

- chapter 1 – contextualization and research motivation, including a brief literature review and the study objectives;
- chapter 2 – a brief summary of the numerical methods and experimental methodology used;
- chapter 3 – a literature review and the numerical methodology proposed to reduce the computational effort to estimate the drag coefficient;
- chapter 4 – a literature review, the experimental methodology used and the experimental validation of the numerical approach proposed in chapter 3;
- chapter 5 – a literature review and the proposal of a new correlation to estimate the drag coefficient;
- chapter 6 – main conclusions of the work.

1.2 Context and motivation

In the design of equipment involving particle-laden flows, it is essential to model the interaction between the two phases in order to obtain consistent results, for both laboratory and industrial scales. The interaction forces between fluid and particles are directly related to the characteristics of the particles, such as size, shape, elasticity, and roughness, which play a crucial role in the performance of equipment (WANG; GE; LI, 2008; HARTGE et al., 2009; NIKOLOPOULOS et al., 2010; WANG; WU; WEI, 2017).

Generally, in models simulating such equipment, the drag force is related to the solid fraction of the flow, assuming that particles are homogeneously distributed (WEN; YU, 1966; GIDASPOW, 1994; HILL; KOCH; LADD, 2001a; HILL; KOCH; LADD, 2001b; HOEF; BEETSTRA; KUIPERS, 2004). However, depending on the attraction and friction between the particles, the type of collision, and their physical, surface, and mechanical characteristics, irregular agglomerate formation and distribution can occur, altering the flow dynamics through pressure oscillations (SENIOR; BRERETON, 1992; KUWAGI; TAKANO; HORIO, 2000).

The phenomenon of agglomeration is observed in various situations, whether in natural phenomena such as sedimentation and flocculation of fine agglomerates in rivers and lakes or in equipment used in industrial processes, such as chemical mixing, mineral processing, stirred tanks, dust sintering, and manufacturing processes involving phase changes (TRAN-CONG; GAY; MICHAELIDES, 2004; DEGLON; MEYER, 2006; LANE, 2017; DELACROIX et al., 2021). Therefore, the behavior of particle agglomerates in different arrangements requires attention.

For many cases, a relevant aspect in the design and optimization of processes and equipment is the determination of the particle's terminal velocity. Since this velocity is strongly influenced by the drag coefficient of the body, the study of this topic becomes significant. In turn, drag is dependent on the contact area; thus, agglomerate formation reduces drag and, consequently, reduces pressure drop (CLIFT; GRACE; WEBER, 1978; GERHART; GERHART; HOCHSTEIN, 2016). Therefore, the formation of such arrangements becomes desirable, adding relevance in industrial application on the study of drag.

Fluid dynamics for a wide range of Reynolds numbers is described by the Navier-Stokes equations, which do not have an analytical solution, particularly for cases involving immersed three-dimensional bodies or turbulence. Therefore, empirical or numerical studies are currently necessary to obtain a correlation between the drag coefficient and the Reynolds number. In order to facilitate the understanding of the phenomenon, studies are typically experimental, with Läpple & Shepherd (1940) being pioneers in the field. They published a historical series of 17 works, conducting a study of mean values and presenting a drag coefficient curve for particles over a wide range of Reynolds numbers. The average curve presented, known as the Standard Drag Curve (SDC), continues to be used as a reference in studies on this topic (SCHLICHTING; GERSTEN, 2017).

Recent studies dealing with particle-laden flows consider the particles as perfect spheres, making it possible to estimate the individual drag coefficient through analytical solutions for low Reynolds number values, in the region known as the Stokes regime. In order to obtain estimates that better represent empirical data, equipment has been developed over the decades to describe and quantify particle shape characteristics, such as shape, circularity, roughness, and sphericity (CLIFT; GRACE; WEBER, 1978; GERHART; GERHART; HOCHSTEIN, 2016).

Due to the lack of a general solution, the literature presents various empirical correlations developed to predict the drag coefficient of both spherical and non-spherical particles, associated with different ranges of validation and precision (CLIFT; GRACE; WEBER, 1978; LEITH, 1987; HAIDER; LEVENSPIEL, 1989; GANSER, 1993; HÖLZER; SOMMERFELD, 2008; BAGHERI; BONADONNA, 2016). However, these correlations have some disadvantages. One of the main drawbacks is that early studies were predominantly based on experiments with regularly-shaped particles, such as cubes, cylinders, and disks, which deviate from one of the main characteristics of flow in agglomerates: the chaotic behavior of the flow as it passes through the agglomerates (CLIFT; GRACE; WEBER, 1978).

For the evaluation of the drag coefficient of isolated groups of packed spheres moving through non-Newtonian fluids, Tran-Cong, Gay & Michaelides (2004) conducted a laboratory study, leading to a correlation with a good fit for a limited range of Reynolds numbers and body dimensions. However, this correlation covers most irregularly-shaped particles in practical engineering applications. This work has become a reference in the field due to the innovation of proposing the use of surface circularity as a geometric parameter for correcting the correlation of Clift & Gauvin (1971), as well as the proposal of sphere agglomeration to emulate irregular bodies.

With the increase in computational capabilities, the field of simulation studies continues to expand. In the literature, there are studies employing the lattice-Boltzmann method (LBM), Large-Eddy Simulation (LES), and Direct Numerical Simulation (DNS) to evaluate the drag coefficient of particles. For industrial-scale problems, such approaches are impractical due to the high computational effort, especially for high Reynolds numbers. Simulations are performed in a transient formulation with very small time steps and highly refined grids to respect the Kolmogorov scales (POPE, 2000; HEINZ, 2020). However, in the subgrid-scale field, such approaches are highly useful to understand the influence of turbulence on micro-scale vortices, owing to their high resolution of the study object.

LBM has proven to be a valuable computational fluid dynamics (CFD) method for understanding particle flows due to the simplicity of the algorithm and use of explicit methods. Initial studies using LBM have shown a correlation between the drag coefficient and gas-solid interaction, not only with Reynolds number and solid volume fraction, but also with the geometry of the agglomerate (CHEN; DOOLEN, 1998; HILL; KOCH; LADD, 2001a).

For instance, Beetstra, Hoef & Kuipers (2006) compared experimental data obtained by Tran-Cong, Gay & Michaelides (2004) with results from simulations using the lattice-Boltzmann method under the same conditions, aiming to extend the influence of geometry on fluidized bed disturbances. They concluded that the drag force on each particle also depends on the variation in distance between particles. The results highlighted how neglecting the agglomeration effect can lead to deviations in the simulated behavior of equipment, both in terms of the expected and experimentally obtained values.

However, LBM is primarily applied in the study of gas-particle interactions, leading to errors when attempting to extrapolate equations proposed in such studies to cases involving liquid-particle interactions. Hence, there is a demand for simulation studies using DNS or LES, such as high-resolution works, or simulations that model turbulence, such as Reynolds-Averaged Navier-Stokes (RANS) or Unsteady Reynolds-Averaged Navier-Stokes (URANS) formulations of the Navier-Stokes equations (LUNA et al., 2017).

DNS simulations have proven to be a crucial tool for accurately estimating correlations for transport coefficients in microscales, one of the essential parameters for coarse-grained modeling of fluid-particle systems (DEEN et al., 2012). To understand fluid-particle mass transfer in randomly arranged particle configurations, Mehrabadi, Murphy & Subramaniam (2016), for instance, employed DNS in a homogeneous flow to isolate the phase interaction effect in a particle agglomerates. They developed a gas-solid drag law for particle agglomerates based on the observation that particle agglomerates reduce drag.

A review of literature on drag coefficient models proposed using computational methods and unsteady formulations indicates that these studies are predominantly focused on low Reynolds numbers, mainly for values below 300 (KE et al., 2018). Such models are applied to industrial-scale problems, extrapolating them to situations where the Reynolds number significantly exceeds the proposed flow range.

The use of extrapolation as an initial approximation is a recurring method. However, when aiming for higher precision, this approach can lead to significant deviations, as these models are proposed for a range where the drag coefficient generally does not reach its minimum value. Consider, for example, a classic profile of drag coefficient behavior for a Newtonian fluid flowing around a spherical particle, as shown in Figure 1.

It can be observed that the value continues to decrease until Reynolds numbers around 2000, reaching drag coefficient values up to 50% lower than those observed for

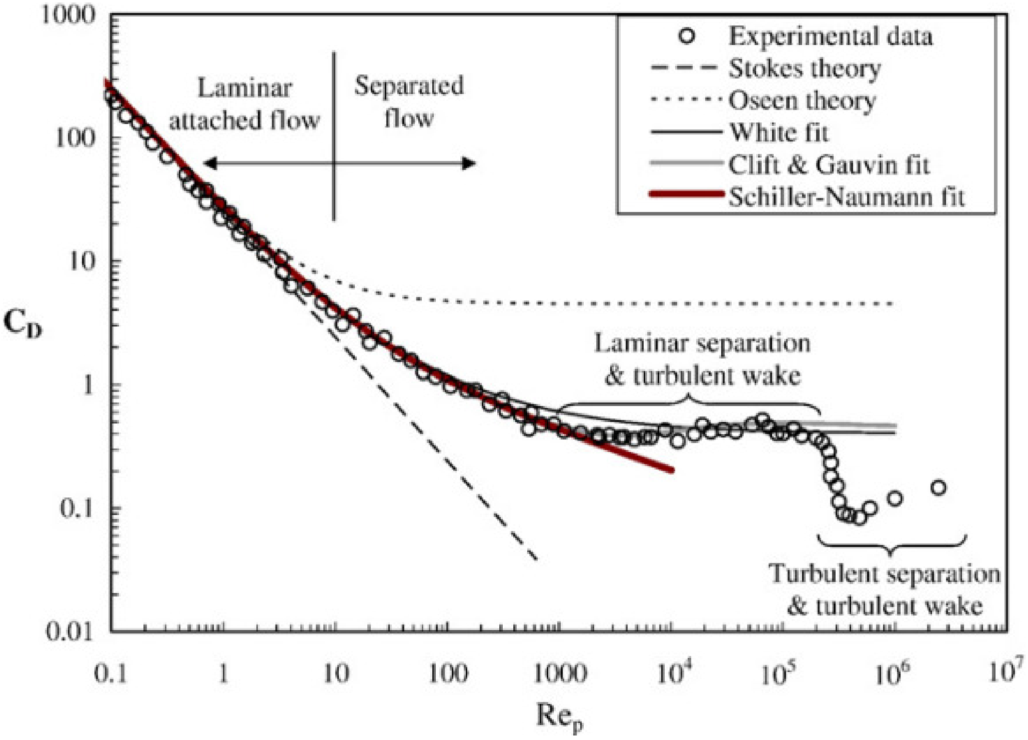

Figure 1 – Example of the behavior of the drag coefficient curve along a wide range of Reynolds numbers. Source: Loth (2008).

values near 300. It is also noticeable that once the minimum value is reached, the coefficient starts to increase again, making it insufficient to model the curve for values limited to 300.

Figure 1 illustrates the drag coefficient behavior observed across a wide range of Reynolds numbers for simple spheres. However, it can be used as an example to present results for all flow profiles of a Newtonian fluid around a particle. As Reynolds number varies, a different velocity field profile is observed. Altogether, six different profile types are observed as the influence of inertial effects on the flow increases. The expected drag coefficient curve for irregular bodies, although maintaining the same general shape, differs in the Reynolds number ranges where the various flow types are observed (BAGHERI; BONADONNA, 2016).

There is no consensus on the exact ranges at which transitions between types of Newtonian fluid flows occur, as the shape of the body alters pressure and velocity fields, as well as vortex formation. This behavior becomes quite evident, especially in the transition to turbulence range, where small perturbations, even due to particle geometry, generate vortices that alter the flow. However, there is a widely accepted approximation in the literature for flow around irregular particles (GOOSSENS, 2019), where profiles are classified into six ranges:

- $Re \leq 20$ – perfect laminar flow

For flows with $Re \leq 20$, the motion is smooth and undisturbed. Despite the predominance of inertial forces over viscous forces, it is still not sufficient for boundary layer detachment to occur, so the fluid tends to flow following the shape of the particle walls.

- $20 \leq \text{Re} \leq 210$ – steady axisymmetric flow regime

  For $\text{Re} \geq 20$, a flow detachment is observed near the stagnation point in the rear region, forming an axially symmetric recirculating zone where the von Kármán vortex street begins to form and continues until Reynolds values close to 200.

- $210 \leq \text{Re} \leq 270$ – steady planar-symmetric flow regime

  As Reynolds numbers increase, there is an increase in the separation angle of the flow, shifting the region where the recirculating zone begins and consequently leading to an elongation of the wake.

- $270 \leq \text{Re} \leq 400$ – unsteady planar-symmetric regime

  In this Reynolds range, a transition to turbulence is observed, where the flow transitions from forming a symmetric and stationary wake to an asymmetric and time-dependent wake.

- $400 \leq \text{Re} \leq 1000$ – unsteady asymmetric flow regime

  Starting from this range, the flow loses its full symmetry and becomes time-dependent. It is possible to clearly observe the formation of large-scale vortices occurring cyclically in an irregular fashion.

- $1000 \leq \text{Re} \leq 380000$ – turbulent wake regime

  For Reynolds numbers above 1000, the flow around the particle is considered turbulent. Starting from values around 2000, the effects of vorticity become evident in the wake region, with smaller and more chaotic scales as Reynolds number increases. For values up to 200,000, it still remains at subcritical condition, where a laminar separation region and a turbulent wake are observed.

Now, if we consider a practical perspective, there exists a connection between the use of empirical correlations and their implementation in CFD codes, which aims at engineering applications involving simulation and optimization of industrial equipment. Taking the main commercial CFD codes as an example, many drag coefficient correlations are already implemented as subroutines. However, these correlations are quite generic and largely applicable to perfect spheres, lacking an application for specific cases where particles have irregular geometries. As a result, such codes allow for the implementation of custom subroutines.

In the Fluent's theory guide, for instance, we will find that most of the correlations follows two classic models for drag coefficient calculation (ANSYS, INC, 2012):

$$C_D = \frac{\Lambda_1}{Re} + \frac{\Lambda_2}{\sqrt{Re}} + \Lambda_3 \tag{1.1}$$

$$C_D = \frac{24}{Re}\left(1 + A \cdot Re^B\right) + \frac{C}{1 + \frac{D}{Re}} \tag{1.2}$$

which, initially, seem to be a simple adjustment of data and straightforward implementation in a code. However, upon consulting the primary source, we see that these models exhibit a certain level of implementation complexity, as the terms Λ or A, B, C, and D are not constants.

The Morsi & Alexander (1972) model, as implemented in the Fluent code, for instance, is based on Equation 1.1. However, the values of Λ are parameters that vary according to the Reynolds range, making the correlation actually a set of 8 equations, dependent on the Reynolds range. Another model implemented in Fluent, designed for irregular particles, is the Haider & Levenspiel (1989) model, which is based on Equation 1.2. However, the terms A, B, C, and D are, in fact, functions that vary with sphericity and Reynolds number.

From this brief contextualization, two questions remain unanswered: is it possible to simulate the drag coefficient in particles using a mathematical modeling that requires less computational resources in order to propose new correlations? And if feasible, is such modeling reliable enough to allow us to propose a unified and simple correlation that is robust enough to encompass flow ranges from fully laminar to fully turbulent?

Therefore, the objective of this study is to investigate these inquiries by evaluating whether a steady formulation, featuring turbulence modeling, can accurately predict the drag coefficient. Additionally, based on a comprehensive review of the literature, the goal is to propose a novel, simple, and unified correlation to calculate the drag coefficient. This correlation should be easily implementable in CFD codes and capable of encompassing a wide range of subcritical flow conditions, specifically $\mathrm{Re} < 2 \cdot 10^5$. The overarching aim is to provide practical engineering applications for equipment involving particle-laden flows with irregularly-shaped agglomerates.

1.3 Objectives

1.3.1 Main Objective

In general lines, the study aims to propose a new correlation capable of estimating the drag coefficient for irregularly-shaped particles that encompass all six flow profiles.

1.3.2 Specific Objectives

To accomplish the primary aim of this study, it was necessary to divide the work into four stages:

- Propose the steady formulation approach to estimate the drag coefficient, as less computational effort formulation without losing quality of numerical results;
- Experimentally obtain the drag coefficient for particle agglomerates to validate simulations using CFD;
- Numerically obtain the drag coefficient for experimental agglomerates across flow ranges between $0.1 \leq \mathrm{Re} \leq 3500$;
- Propose a new unified correlation capable of accurately representing the drag coefficient for all flow profiles around particles.

2 Methods

The work was divided into two stages. Initially, a computational less expensive approach to simulate the flow around particle agglomerates was proposed. Thus, a numerical methodology was initially introduced through CFD study. In this initial stage, hypothetical geometries were proposed, serving as tests for the simulations. The second stage involves the study under real, experimentally observed conditions, aiming to validate the numerical methodology. Therefore, configurations of sphere agglomerates were proposed to represent irregularly-shaped particles.

2.1 Numerical methods and convergence criteria

In general terms, the numerical methods employed in the simulations are presented in Table 1. As various turbulence models were tested in this study, the type of spatial discretization varies according to the model used. Since these models involve the Reynolds-Averaged Navier-Stokes equations (RANS), they all share a similar modeling approach. Large-Eddy Simulations (LES) were also conducted as an evaluation criterion for the transient model's ability to estimate drag coefficients. The methods used in LES simulations are further detailed in subsection 5.3.2.

Table 1 – General setup of the numerical methods used.

Numerical methods		
Formulation	Steady	
	Transient	First Order Implicit
Pressure-velocity Coupling	PISO	
Spatial discretization	Gradient	Least-Square Cell-Based
	Pressure	*PRESTO* !
	Momentum	Second Order Upwind
Turbulence closure equations	Spalart-Allmaras RNG k-epsilon SST k-omega Langtry-Menter Reynolds Stress Model	Second Order Upwind

For all the cases studied, regardless of the turbulence model, the convergence criterion used was a root-mean-square (RMS) error of cell residuals lower than 10^{-9} for both continuity and the variables modeled by the closure equations of the turbulence model employed. The details regarding the geometry, mesh, and boundary conditions of the computational domain are presented in the methods sections of the chapters containing the articles (subsection 3.2.1, subsection 4.2.2, and subsection 5.2.1).

2.2 Experimental methods

Three geometries of agglomerates consisting of Acrylonitrile Butadiene Styrene (ABS) spheres were proposed, and using super glue, the spheres were agglomerated into a stable configuration.

To determine the drag coefficient of the agglomerate, the terminal velocity method for a submerged body was employed. In order to calculate the drag coefficient over a wide range of Reynolds numbers, water-glycerin solutions were utilized, varying the volume fraction of glycerin from 0 to 1. The viscosities of the fluids were measured using a Ford viscosity cup from the brand Tech Vision Ltda., with tests conducted in triplicate. Density measurements were performed using specific gravity densimeters for ranges between 0.9 and 1.3 g/cm^3, always considering the experimental uncertainties provided by the manufacturers.

In order to eliminate bubbles during the agglomerate's free fall, the agglomerates were immersed and randomly released in free fall in the solution multiple times before starting tests with a new fluid. The agglomerates were stored in a beaker containing a sample of the solution used in the experimental setup of the conducting essays.

To prevent any interference in the results when switching fluids, the agglomerates were washed multiple times using distilled water and left to dry on paper towels overnight. Subsequently, the bubble elimination procedure was repeated for the new fluid.

Using a high-speed camera, the agglomerates were recorded in free fall using a SONY RX-110 IV camera at a resolution of 3840 x 2160 pixels and a frame rate of 960 frames per second. Consequently, multiple essays were conducted to obtain as many data points as possible for each tested condition.

Using the *Tracker 6.10* software, it was possible to determine the terminal velocity of each essay, as well as the agglomerate's falling angle. Therefore, essays in which the agglomerate displayed falling angles below 89° or above 91° at any moment during the fall were discarded.

In order to reduce experiment uncertainty, the values from the 7 experiments that were closest to a normal fall to the bottom plane of the tank were adopted. Subsequently, Tukey's fence for outlier removal was applied, to improve the accuracy of the results (TUKEY, 1977).

The methodology employed in conducting the experiments is further detailed in subsection 5.2.4, which presents a scheme of the experimental setup, sphere characteristics, as well as the arrangement in which they were bonded to form the agglomerates, the flow direction, and details of the laboratory's ambient conditions.

3 Proposition of the modelling

This chapter is dedicated to presenting the first part of the thesis: analyze the steady formulation as an alternative way to study the drag coefficient in particle agglomerates that requires less computational effort. The study in this chapter resulted in an article entitled *Numerical study of turbulence on drag coefficient determination for particle agglomerates*, published in the journal *Chemical Industry & Chemical Engineering Quarterly*, (available at: 10.2298/CICEQ221206021O).

The focus of this stage was to evaluate an alternative approach to the study of drag coefficient calculation, aiming for a reduction in computational cost. In the field of numerical simulations, the most common way to calculate the drag coefficient is through the use of unsteady formulations. Recurrent use is observed for simulations such as LES, DNS, and lattice-Boltzmann (KE et al., 2018), which, with a high level of flow detail, can obtain highly accurate results for pressure and velocity fields, and consequently, high precision for the drag coefficient.

However, two problems are observed in the unsteady approach: high computational cost, which increases with increasing turbulence intensity due to the generation of smaller vortices (CHOI; MOIN, 2012), limiting the models to flows with Reynolds numbers generally below 300; and low geometric complexity, given the difficulty of generating homogeneous meshes around complex bodies.

The mesh generation limitation does not apply to the lattice-Boltzmann method. Still, to accurately represent the flow from the smallest vorticity scales, the method requires time steps of magnitude $\mathcal{O}$(-6) (DIETZEL; SOMMERFELD, 2013), thereby maintaining the flow restriction to Reynolds values below 100 (KE et al., 2018).

The limitation due to high computational cost results in a condition where studies being conducted provide only a few simulation-obtained data points and are restricted to a very limited range of Reynolds numbers, where correlations are extrapolated, compromising the reliability of the results obtained. Thus, the proposal of this stage is, as an initial study, to assess the ability of a steady-state formulation to provide reliable results in the calculation of drag coefficient for particle agglomerates, once the correct turbulence model is employed.

To achieve this, Reynolds-Averaged Navier-Stokes (RANS) turbulence models were tested based on the criterion of using wall functions to model the regions around the agglomerate surfaces. Therefore, the RNG k-ε and Reynolds Stress Model with the standard wall function in Fluent 14.5 (ANSYS, INC, 2012) were chosen, along with the Spalart-Allmaras, SST k-ω, and Langtry-Menter models, as they do not use wall functions.

It was observed that the turbulence models followed a trend of results similar to the behavior of the drag coefficient curve over a range of Reynolds numbers. When compared with literature correlations for calculating drag coefficient in agglomerates, it was noticed that, in general, the results followed the curve predicted by the Tran-Cong, Gay & Michaelides (2004) model. This trend was statistically confirmed using the root-mean-square error method.

It was also observed that turbulence models without wall functions generally better represented the behavior of the drag coefficient curve along the Reynolds number, with the Spalart-Allmaras and SST k-ω models being the closest to the curve predicted by the Tran-Cong, Gay & Michaelides (2004) model.

3.1 Introduction

In the design of equipment involving particle-laden flows, it is essential to correctly model the interaction between the two phases to obtain consistent results. The forces of fluid-particle interaction are directly related to the characteristics of the particles, such as size, shape, elasticity, and roughness, which are determining in the performance of equipment such as the fluidized bed (WANG; GE; LI, 2008; HARTGE et al., 2009; NIKOLOPOULOS et al., 2010; WANG; WU; WEI, 2017). Usually, in models that simulate fluidized bed reactors, the drag force is related to the porosity of the bed, assuming that the particles are distributed homogeneously (GIDASPOW, 1994; HILL; KOCH; LADD, 2001a; HILL; KOCH; LADD, 2001b; HOEF; BEETSTRA; KUIPERS, 2004). However, depending on their physical, superficial, and mechanical characteristics, the collision, attraction, and friction between the particles can lead to the formation and irregular distribution of agglomerates, therefore altering the flow dynamics through pressure oscillations (SENIOR; BRERETON, 1992; KUWAGI; TAKANO; HORIO, 2000).

Indeed, the behaviour of particle agglomeration in different arrangements deserves attention, as it occurs in almost all forms, whether naturally or artificially. One can find such kind of irregularly shaped particles in many applications, such as sedimentation and flocculation of fine particle aggregates in rivers and lakes, chemical mixing, mineral processing, stirred tanks, powder sintering, and manufacturing with phase change processes (TRAN-CONG; GAY; MICHAELIDES, 2004; DEGLON; MEYER, 2006; LANE, 2017). For several of these processes, determining the terminal velocity of the particle is an important stage for the design and optimization of processes and equipment. Since this velocity is straightly dependent on the drag coefficient of the body, such kind of study is important to simulate the movement of such particles.

Due to the lack of an analytical solution, the literature presents several empirical correlations designed to predict the drag coefficient of spherical and non-spherical particles associated with different ranges of validity and precision (CLIFT; GRACE; WEBER, 1978; LEITH, 1987; HAIDER; LEVENSPIEL, 1989; GANSER, 1993; HÖLZER; SOMMERFELD, 2008; BAGHERI; BONADONNA, 2016). To obtain predictions that better represent the empirical observations, shape descriptors have been developed in recent decades to quantify aspects such as shape, circularity, roughness, and sphericity. However, the correlations present some disadvantages, such as the fact that the first studies are, mainly, based on experiments with regularly-shaped particles such as cubes, cylinders, and disks, which reduces the level of detail and accuracy in the description of the local scale phenomena (BEETSTRA; HOEF; KUIPERS, 2006; DEEN et al., 2012).

For the evaluation of the drag coefficient of isolated groups of ordered packed spheres moving through Newtonian fluids, Tran-Cong, Gay & Michaelides (2004) conducted laboratory measurements, leading to a correlation with good agreement over a limited range of Reynolds numbers and body dimensions, but covering most of the irregularly shaped particles in engineering applications. Beetstra, Hoef & Kuipers (2006) compared these experimental data with lattice-Boltzmann simulations for the same conditions, aiming to expand the field of the influence of the geometry on the disturbance of fluidized beds, stating that, indeed, the drag force on each particle is strongly dependent on the inter-particle distance variation. The results showed how the omission of the agglomeration effect can cause deviations between the simulated behaviour of equipment and experimental results.

Literature presents studies using the lattice-Boltzmann method (LBM) and Direct Numerical Simulation (DNS) to evaluate the drag coefficient in particles. For industrial-scale problems, these approaches are considered impractical, due to the high computational effort, mainly for high Reynolds numbers, since the simulations must be carried out in a transient formulation with small timesteps and the mesh must be fine enough, to respect the Kolmogorov scales (POPE, 2000; HEINZ, 2020). However, in the field of sub-grid scale, they are very useful to understand the influence of turbulence in small-scale vortices. The LBM showed to be a useful method for CFD to understand the flow in particles, due to the algorithm simplicity and explicit methods (CHEN; DOOLEN, 1998). Since the method presents a high resolution of the domain, the studies present better accuracy, as observed in studies such as Dietzel & Sommerfeld (2013), that used the LBM to investigate complex geometry with a high discretization around the agglomerate and obtained deviations lower than 10% for lower values of Reynolds, where deviations are generally by the order of 20% (DIETZEL; SOMMERFELD, 2013).

DNS showed to be an important tool to estimate with accuracy correlations for the micro-scale transport coefficients, one of the essential parameters for coarse-grained models of fluid-particle systems (DEEN et al., 2012). To understand the fluid-particle mass transfer in random arrays of particles, Mehrabadi, Murphy & Subramaniam (2016) performed DNS in a homogeneous flow, aiming to isolate the effect of interphase interactions on a particle agglomerate, developing a gas-solid drag law for clustered particles based on the conclusion that particle clusters lead to a drag reduction. Another recent example of this method is the study of Chen, Chen & Fu (2022), where the drag and lift in particle agglomerates were studied for different orientations and sizes of particles and presented deviations between 2 and 4%. However, due to the constraints of the method, the study focused on understanding the hydrodynamic on agglomerates for a range of Reynolds below 100, where highly dependent on the projected area (DIETZEL; SOMMERFELD, 2013).

In contrast to the large number of empirical correlations to predict the drag coefficient of irregular particles, there is a scarcity of studies in which specific correlations have been proposed to determine drag forces acting on particle agglomerates. The literature in the computational field using the unsteady formulation, such as LES and DNS, focuses on analyzing simple bodies – such as regularly-shaped single bodies –, due to the difficulty in generating uniform meshes around complex bodies, as well as limited to low Reynolds flows, generally below 250, due to the computational demands associated with higher Reynolds numbers (POPE, 2000). The use of LBM eliminates the difficulty of mesh generation, so we observe studies on more complex and arbitrary bodies (DIETZEL; SOMMERFELD, 2013), with an agglomeration of several spheres, but the method is still limited for low Reynolds flows, since the forces acting on walls inside the flow are directly calculated in the smaller scales (CHEN; DOOLEN, 1998; BEETSTRA; HOEF; KUIPERS, 2006; DEEN et al., 2012; DIETZEL; SOMMERFELD, 2013; MEHRABADI; MURPHY; SUBRAMANIAM, 2016; CHEN; CHEN; FU, 2022).

Because of the lack of studies for higher Reynolds flows, and since the high computational cost needed to perform transient simulations, we focus on proposing a methodology, using the steady formulation, to simplify the problem of calculating the drag coefficient in complex bodies, which allowed the investigation of the flow for a wide range of Reynolds numbers. Since turbulence plays an important role in the flow profile as we increase the velocity of the fluid, we focused on how its modelling interferes with the drag estimation in particle agglomerates. So, the present paper evaluates the drag coefficient of three different conformations of irregularly shaped particle agglomerates, composed of spherical particles, surrounded by a water flow, varying the turbulence model tested. The models were compared using steady RANS turbulence models to investigate their robustness to predict the drag acting in particle agglomerates for different conformations, to reduce computational costs of unsteady simulations, such as URANS, LES, DNS or LBM.

3.2 Methods

This study was carried out in the theoretical field, using CFD simulations to obtain the flow profile of water around particle agglomerates. The drag coefficient of the particles was calculated by CFD simulations, using five different turbulence models. The results were compared with five empirical correlations for estimation of the drag coefficient in irregularly-shaped particles present in literature, to find which is robust enough to represent the trend of the results of drag coefficient in particle agglomerates obtained by simulations.

The drag coefficient for spheres, in the theoretical field, is simple to calculate, since it depends on a balance of forces. This balance leads to Equation 3.1

$$C_D = -\frac{F_D}{\frac{1}{2}\rho_f A \left| u_p - u_f \right| \left(u_p - u_f \right)} \tag{3.1}$$

where F_D is the drag force. The drag depends on the fluid, particle and flow characteristics, i.e. fluid density and velocity, ρ_f and u_f, respectively, and the particle velocity and reference area, u_p and A, respectively. The particle in the domain of the present study is fixed, leading to a particle velocity equal to zero, so the fluid flow profile and the drag coefficient are given exclusively by the behaviour of the fluid flow around the particle.

To determine which correlation better follows the trend observed in the drag coefficient obtained by CFD, we must define some criteria to compare the simulations with the correlations. The first consideration was the analysis and comparison of the flow profile for each of the five turbulence models with the behaviour expected by the literature. This step is important to understand if the results obtained for the drag coefficient are reliable.

Since a quantitative analysis is crucial, we also chose to evaluate the percent deviation between simulations and correlations, estimated by the Equation 3.2.

$$\delta = 100 \cdot \frac{C_D^{corr} - C_D^{sim}}{C_D^{corr}} \tag{3.2}$$

where C_D^{corr} and C_D^{sim} are the drag coefficients obtained by the correlation and the simulation respectively. Another quantitative analysis considered was the root-mean-square error, *RMSE*, given by

$$RMSE = \sqrt{\frac{\sum_{i=1}^{N} \left(\hat{x}_i - x_i\right)^2}{N}} \tag{3.3}$$

where $\hat{x}_i$ is the value of the i^{th} data of a parameter estimated by the correlation, x_i is the value of the i^{th} data of the parameter obtained by simulation – i.e. the drag coefficient – and N is the total data in the sample studied.

3.2.1 Numerical simulations

The numerical simulations were carried out using the software ANSYS 14.5. The computational domain and numerical meshes of the particle agglomerates in this study were generated using the software ANSYS Design Modeler and Meshing 14.5. The software ANSYS Fluent 14.5 was used to solve the model equations, and to analyze the fluid flow profile and the drag coefficient we used the software CFD-Post.

3.2.1.1 Design and mesh generation

Simulations were carried out for three different computational domains, varying the geometry of the agglomerates, containing three, four, and five particles, where the radius of each particle in the agglomerate measures 0.5 cm. The domain generated corresponds to a parallelepiped with a height and width of 0.1 m and a length of 0.2 m.

Aiming the generation of well-structured meshes, the domain was divided into two cubes, as presented in Figure 2. The cube on the left side, close to the inlet, was subdivided into seven smaller parts, for better control of the quality of the elements around the agglomerate of spheres. Six of them are pyramidal-shaped, connected to an inner cube, surrounding the agglomerate of spheres, and positioned in the center of the major cube. For the second cube, on the right side and close to the outlet, there was no need to divide into smaller parts. Figure 2 also shows a cut of the lateral view of the computational domain using the agglomerate of five spheres as an example, while Figure 3 shows the isometric view of the geometry of the three agglomerates.

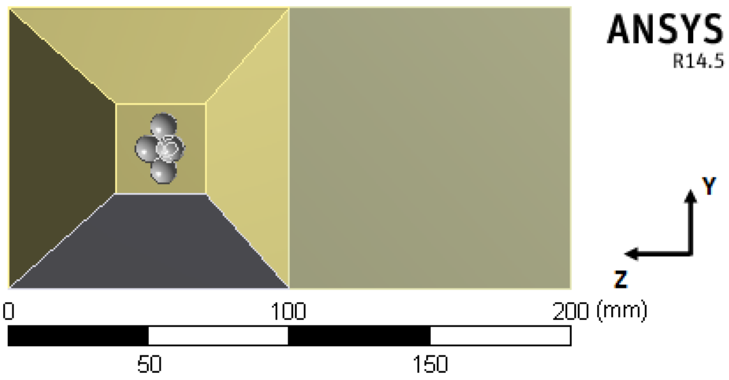

Figure 2 – Example of the lateral view of the interior of the computational domains simulated.

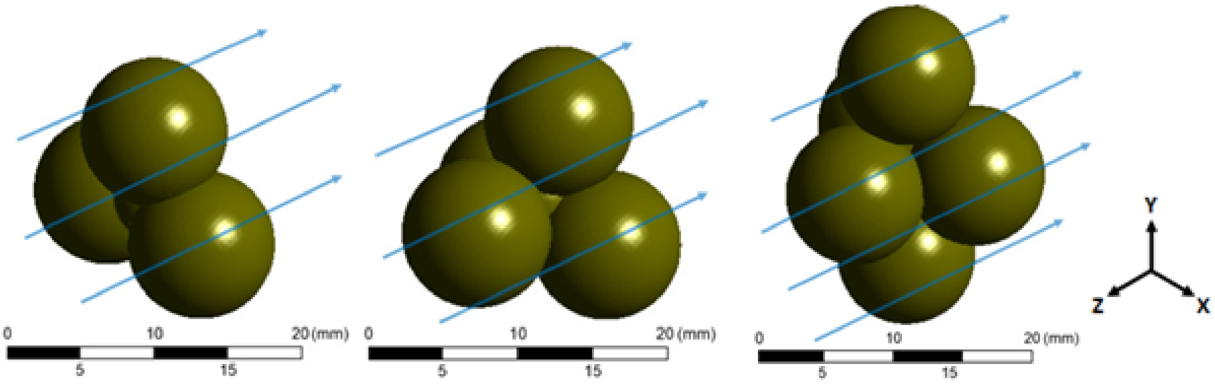

Figure 3 – From left to right: Isometric view of the particle agglomeration of three, four and five particles and a scheme of the flow direction.

3.2.1.2 Meshes statistics

Before running simulations, it is important to analyze the quality of the mesh, by verifying the elements according to their shape and criteria for several mesh quality parameters. In this study, we chose to evaluate its aspect ratio, orthogonality, and skewness. To obtain easier convergence stability and better accuracy, it is ideal to have elements exclusively hexahedral. However, due to the complexity of the geometry of the agglomerates, hybrid meshes were generated. These meshes contain elements with shapes referred to as tetrahedral, six-node wedge, five-node pyramid, and hexahedral.

To avoid distorting the mean values and standard deviations, the values are presented separately according to two regions: the inner cube around the agglomerate (Figure 2), referred to as Subdomain, and the whole computational domain, referred to as Total domain. Table 2 shows the values of minimum, maximum, mean, and standard deviation of the three parameters for the tested meshes, detailed for the subdomain and the total domain.

Table 2 – Mesh quality for the three agglomerates studied.

Mesh quality parameter		Subdomain			Total domain		
		3 spheres	4 spheres	5 spheres	3 spheres	4 spheres	5 spheres
Aspect ratio	Minimum	1	1	1	1	1	1
	Maximum	32.12	24.58	299.98	32.12	24.58	299.98
	Mean	1.1233	1.1856	1.1869	1.0613	1.0694	1.0760
	SD (%)	0.4025	0.4758	0.5467	0.2835	0.3062	0.3491
Orthogonality	Minimum	0.2115	0.1516	0.0324	0.2095	0.1516	0.0324
	Maximum	1	1	1	1	1	1
	Mean	0.9622	0.9441	0.9440	0.9866	0.9839	0.9820
	SD (%)	0.0805	0.0929	0.0945	0.0517	0.0563	0.0601
Skewness	Minimum	0	0	0	0	0	0
	Maximum	0.9753	0.9929	0.9866	0.9820	0.9966	0.9986
	Mean	0.0412	0.0623	0.0629	0.0177	0.0219	0.0243
	SD (%)	0.1198	0.1422	0.1143	0.078	0.0879	0.0935

The minimum value possible for the aspect ratio is 1, where the quality is considered excellent for values lower than 20 (ANSYS, INC, 2012; FERZIGER; PERIĆ, 2002). For both total domain and subdomain, the maximum values obtained were above 20, however, their average values are lower than 1.2 with standard deviations lower than 0.48%. Analyzing the aspect ratio of the three meshes, presented in Table 3, we find a high number of elements with values below 5, so that they are considered excellent for this criterion.

The orthogonality varies from 0 to 1, where values above 0.8 are considered excellent (ANSYS, INC, 2012; FERZIGER; PERIĆ, 2002). Even though some elements present poor quality, the mean value for each proposed domain was above 0.94, with a standard deviation lower than 0.1%, where elements with orthogonality above 0.8 correspond to at least 94% of the elements, as seen in Table 3. This occurs due to the high quantity of hexahedrons, which tend to have higher orthogonality. This effect is also present in skewness. Analyzing the skewness, where elements have excellent quality for values between 0 to 0.2 and good quality for values between 0.2 and 0.4, we observe that the mean values do not exceed 0.07 and the standard deviations do not exceed 0.12% for any mesh. The low value is a direct result of the high quantity of hexahedrons with good and excellent quality.

Pyramidal shapes, such as tetrahedrons and five-node pyramids are expected to have lower orthogonality and higher skewness (FERZIGER; PERIĆ, 2002). Table 3 shows that the influence of such shapes to the quality of the meshes was not significant, as consequence of the low number of pyramidal elements – representing less than 2.5% of the elements of the subdomain and less than 0.5% of the total domain for all meshes.

It is relevant to emphasize the predominance of hexahedral elements for both subdomain and total domain in all meshes. The agglomerate of three spheres presented percentages of hexahedral elements above 83% in the subdomain and 93% in the total domain. In the meshes of agglomerates of four and five spheres, these percentages were above 92% in the subdomain and 95% in the total domain. Also, analyzing the meshes statistics for three main parameters, the elements have good or excellent quality, so the meshes are expected to behave with convergence stability and obtain accurate results.

3.2.1.3 The governing equations

The time-averaged conservation equations for the steady incompressible isothermal turbulent flow in the three-dimensional model, neglecting body force, can be expressed by the equations of continuity and motion (POPE, 2000).

The closure equations for the RANS approach depend on the turbulence model used. In this study, we investigated the effects of five turbulence models. The models are classified according to the number of transport equations used to close the modelling of the problem. The models tested are the one-equation based Spalart-Allmaras, the two-equation based RNG k-ε and SST k-ω, the four-equation based Langtry-Menter, and the six-equation Reynolds stress model. The modelling of its closure equations and coefficients are better

Table 3 – Percentage of elements of the meshes attending to the criteria of the quality coefficients.

			Aspect ratio	Orthogonality	Skewness
Region	Agglomerate	Number of elements	Below 5 (%)	Above 0.8 (%)	Below 0.4 (%)
Subdomain	3 spheres	1240970	99.99	96.24	96.39
	4 spheres	1064255	99.96	94.25	94.59
	5 spheres	1328015	99.97	94.21	94.41
Total domain	3 spheres	5234907	99.99	98.67	98.64
	4 spheres	5001753	99.99	97.89	98.17
	5 spheres	5220320	99.98	97.98	97.87

detailed in the literature (LAUNDER; REECE; RODI, 1975; SPALART; ALLMARAS, 1992; YAKHOT et al., 1992; MENTER, 1994; LANGTRY; MENTER, 2009).

3.2.1.4 Simulation setup

The fluid properties were set up for an isothermal operation condition of 25 °C, obtaining water density and viscosity of 998.2 kg/m^3 and 1.003·10^{-3} Pa·s, respectively. As a boundary condition, the inlet velocity of the water was set as an injection normal to the inlet surface. Since the drag experienced by particles flowing in a Newtonian fluid can be divided in six main flow regimes according to its Reynolds number, we varied the velocities of the flow to obtain Reynolds numbers between 1 and 1500, to assure that we will observe how the turbulence model interferes on the estimation of the drag coefficient in all the regimes, from laminar to turbulent wake flow regimes (LOTH, 2008; GOOSSENS, 2019). The velocities varied from $5 \cdot 10^{-5}$ to 0.10501 m/s, as presented in Table 4, according to the agglomerate, to obtain the range of Reynolds numbers proposed, calculated by Equation 3.4.

$$Re = \frac{\rho \cdot u \cdot d_{eq}}{\mu} \tag{3.4}$$

where ρ, u, and μ are the density, relative velocity, and viscosity of the fluid, and d_{eq} is the diameter of the sphere equivalent to the agglomerate, i.e. with the same volume. At the higher Reynolds number, we also carried out unsteady simulations, to compare the difference between the drag coefficients. Despite presenting the unsteady turbulent wake profile, the drag coefficient obtained did not present significant deviations, so, to reduce computational efforts, we chose the steady simulations. The boundary conditions were set to the no-slip condition for the sphere walls and specified-shear for the domain walls.

Table 4 – Inlet velocity of the flow for the Reynolds numbers tested.

Reynolds	Velocity [m/s]		
[-]	3 spheres	4 spheres	5 spheres
1	0.000070	0.000064	0.000059
5	0.000350	0.000318	0.000295
10	0.000700	0.000636	0.000590
30	0.002100	0.001907	0.001770
50	0.003500	0.003178	0.002950
80	0.005600	0.005085	0.004720
100	0.007000	0.006356	0.005900
300	0.021002	0.019069	0.017702
500	0.035003	0.031781	0.029503
800	0.056005	0.050849	0.047205
1000	0.070007	0.063562	0.059006
1300	0.091009	0.082631	0.076708
1500	0.105010	0.095343	0.088509

Despite the SIMPLE-based algorithms present lower computational effort (DOORMAAL; RAITHBY, 1983), we chose the PISO algorithm, since it presents greater stability, requiring less iterations, generating a faster convergence, and, as consequence, less processing time (VERSTEEG; MALALASEKERA, 2007; TUKOVIĆ; PERIĆ; JASAK, 2018).

The spatial discretization was set to the least-squares cell-based method for gradients, *PRESTO*! scheme for pressure and second-order upwind scheme for energy, momentum, and turbulence equations, to solve the problem of underestimation of turbulent kinetic energy and its dissipation rate, as suggested in previous studies (DEGLON; MEYER, 2006; LANE, 2017).

3.2.1.5 Turbulence closure models

The choice of the turbulence models was based on their characteristics and ability to solve specific problems presented by the complex geometry of the meshes generated. Since one of the focuses in the present study stands on analyzing the drag coefficient in an agglomerate of particles, predicting the flow in the boundary layer is essential. The Spalart-Allmaras model, a one-equation based model, fits in this type of flow since it was developed to study the flow in the boundary layers of airfoils (SPALART; ALLMARAS, 1992). Two other models that were also developed to represent this zone are the transition models SST k-ω and the Langtry-Menter k-ω (POPE, 2000). The first one is a two-equation based model that solves the equation of the turbulent kinetic energy, k, for the flow far from the wall and, for the boundary layer, weights the influence of the turbulent kinetic turbulence and the specific turbulence dissipation rate, ω, using blending functions. The second is based on the k-ω, however, implements two transport equations, one to solve the intermittency, γ, and one to solve the transition momentum-thickness Reynolds number, $\widetilde{Re}_{\theta t}$, to better represent profiles with strong adverse pressure gradients (MENTER, 1994; LANGTRY; MENTER, 2009; WILCOX, 2004).

We also tested turbulence models that were developed to represent wide ranges of Reynolds numbers. The k-ε model was developed to solve several engineering in a wide range of Reynolds numbers, with a low computational cost (LAUNDER; SHARMA, 1974). This model has the characteristic of modelling the near-wall region and solve the transport equation for the outer region of the boundary layer. We chose to use the RNG k-ε, an improvement of the k-ε developed to solve problems where the flow presents a highly swirling profile (YAKHOT et al., 1992). Another model tested in this study, with similar characteristics, but more robust was the Reynolds stress model. The main difference in this seven-equation-based model that leads to its robustness is the addition of six transport equations, one for each of the independent Reynolds stress, to the solution for the dissipation equation, ε, and its anisotropic treatment (LAUNDER; REECE; RODI, 1975). The following items enumerated are reserved for the modelling of the transport equations of each turbulence model presented.

i. Spalart-Allmaras model

The Spalart-Allmaras is a one-equation model which solves the transport equation for a viscosity-like variable $\tilde{\nu}$, also referred as the Spalart-Allmaras variable. The model is given by the Equation 3.5

$$\frac{\partial \tilde{\nu}}{\partial t} + \frac{\partial \left(u_j \tilde{\nu}\right)}{\partial x_j} = \frac{1}{\sigma} \frac{\partial}{\partial x_j} \left[\left(\nu + \tilde{\nu}\right) \frac{\partial \tilde{\nu}}{\partial x_j} \right] + \frac{c_{b2}}{\sigma} \frac{\partial \tilde{\nu}}{\partial x_j} \frac{\partial \tilde{\nu}}{\partial x_j} + c_{b1} \tilde{S} \tilde{\nu} - c_{w1} f_w \left(\frac{\tilde{\nu}}{d} \right)^2 \tag{3.5}$$

where $\tilde{S}$ is the production of turbulent viscosity, c_{b1}, c_{b2}, c_{w1}, f_w and σ are closure coefficients and auxiliary relations of the model, better described by Spalart &

Allmaras (1992).

ii. RNG k-ε model

The RNG k-ε model uses the renormalization group theory to improve the Standard k-ε model, which models the turbulence kinetic energy, k, and the turbulence dissipation rate, ε, given by Equations 3.6 and 3.7, respectively,

$$\frac{\partial k}{\partial t}+\frac{\partial\left(u_i k\right)}{\partial x_i}=\frac{\partial}{\partial x_j}\left[\left(\nu+\frac{\nu_t}{\sigma_k}\right)\frac{\partial k}{\partial x_j}\right]+P_k-\varepsilon \tag{3.6}$$

$$\frac{\partial \varepsilon}{\partial t}+\frac{\partial\left(u_i \varepsilon\right)}{\partial x_i}=\frac{\partial}{\partial x_j}\left[\left(\nu+\frac{\nu_t}{\sigma_\varepsilon}\right)\frac{\partial \varepsilon}{\partial x_j}\right]+C_{1\varepsilon}\frac{\varepsilon}{k}P_k-C_{2\varepsilon}^{*}\frac{\varepsilon^2}{k} \tag{3.7}$$

where P_k is the production term of the turbulent kinetic energy (YAKHOT et al., 1992).

iii. SST k-ω model

The SST k-ω model implements modifications for low-Reynolds number effects, compressibility, and shear flow spreading. The model is based on modelling transport equations for turbulence kinetic energy and the specific dissipation rate, given by the Equations 3.8 and 3.9, respectively.

$$\frac{\partial k}{\partial t}+\frac{\partial\left(u_j k\right)}{\partial x_j}=\frac{\partial}{\partial x_j}\left[\left(\nu+\sigma_k\nu_t\right)\frac{\partial k}{\partial x_j}\right]+P_k-\beta^{*}k\omega \tag{3.8}$$

$$\begin{aligned}\frac{\partial \omega}{\partial t}+\frac{\partial\left(u_j \omega\right)}{\partial x_j}=\frac{\partial}{\partial x_j}\left[\left(\nu+\sigma_\omega\nu_t\right)\frac{\partial \omega}{\partial x_j}\right]+\alpha S^2-\beta\omega^2+\\ 2\left(1-F_1\right)\sigma_{\omega 2}\frac{1}{\omega}\frac{\partial k}{\partial x_i}\frac{\partial \omega}{\partial x_i}\end{aligned} \tag{3.9}$$

where F_1 is the blending function, α, β and σ refers to closure coefficients of the model (MENTER, 1994).

iv. Langtry-Menter SST k-ω model

Modelled similarly to the SST k-ω model, presented previously, the Langtry-Menter model implements two transport equations, to solve the intermittency and the turbulent transition Reynolds number, given by Equations 3.10 and 3.11, respectively.

$$\frac{\partial \gamma}{\partial t}+\frac{\partial\left(u_j \gamma\right)}{\partial x_j}=\frac{\partial}{\partial x_j}\left[\left(\nu+\frac{\nu_t}{\sigma_f}\right)\frac{\partial \gamma}{\partial x_j}\right]+P_{\gamma 1}-E_{\gamma 1}+P_{\gamma 2}-E_{\gamma 2} \tag{3.10}$$

$$\frac{\partial \widetilde{Re}_{\theta t}}{\partial t}+\frac{\partial\left(u_j \widetilde{Re}_{\theta t}\right)}{\partial x_j}=\frac{\partial}{\partial x_j}\left[\sigma_{\theta t}\left(\nu+\nu_t\right)\frac{\partial \widetilde{Re}_{\theta t}}{\partial x_j}\right]+P_{\theta t} \tag{3.11}$$

where $P_{\gamma 1}$ and $E_{\gamma 1}$ are the transition sources, $P_{\gamma 2}$ and $E_{\gamma 2}$ are the destruction sources and $P_{\theta t}$ is a source term (LANGTRY; MENTER, 2009).

v. Reynolds Stress model

The RSM consists on modelling the Reynolds stresses, represented by the tensor τ, and the turbulence dissipation rate, ε (POPE, 2000). The exact transport equation of the Reynolds stresses, in tensorial notation, is given by Equation 3.12

$$\begin{aligned}\frac{\partial \tau_{ij}}{\partial t} + \overline{u_k}\frac{\partial \tau_{ij}}{\partial x_k} = \frac{\partial}{\partial x_k}\left(\frac{\nu_t}{\sigma_k}\frac{\partial}{\partial x_k}\tau_{ij}\right) - \left[\tau_{ik}\frac{\partial \overline{u_j}}{\partial x_k} + \tau_{jk}\frac{\partial \overline{u_i}}{\partial x_k}\right] - \\ C_1\frac{\varepsilon}{K}\left[\tau_{ij} - \frac{2}{3}\delta_{ij}K\right] - C_2\left[P_{ij} - \frac{2}{3}\delta_{ij}P\right] - \frac{2}{3}\delta_{ij}\varepsilon \end{aligned} \tag{3.12}$$

where the turbulence production terms P_{ij} are given by

$$P_{ij} = -\left[\tau_{ik}\frac{\partial \overline{u_j}}{\partial x_k} + \tau_{jk}\frac{\partial \overline{u_i}}{\partial x_k}\right] \tag{3.13}$$

with P being the fluctuation kinetic energy production and ν_t the turbulent kinematic viscosity.

The transport equation for turbulence dissipation rate, ε, is given by

$$\frac{\partial \varepsilon}{\partial t} + \overline{u_j}\frac{\partial \varepsilon}{\partial x_j} = \frac{\partial}{\partial x_j}\left[\left(\nu + \frac{\nu_t}{\sigma_\varepsilon}\right)\frac{\partial \varepsilon}{\partial x_j}\right] - C_{\varepsilon 1}\frac{\varepsilon}{K}\tau_{ij}\frac{\partial \overline{u_i}}{\partial x_j} - C_{\varepsilon 2}\frac{\varepsilon^2}{K} \tag{3.14}$$

where $K = \frac{1}{2}\overline{u_i' u_i'}$ is the fluctuation kinetic energy (LAUNDER; REECE; RODI, 1975).

3.2.2 Drag coefficient correlation modelling

For several applications in industry, the drag force is the main acting force on a particle in the opposite direction of the particle motion.

To estimate the drag coefficient, studies generally take into account the most influential parameters, i.e. the particle Reynolds number, shape, orientation, particle-to-fluid density ratio. Also, parameters considered secondary, such as secondary motions, turbulence and particle/fluid acceleration, are the focus of studies (TRAN-CONG; GAY; MICHAELIDES, 2004; HAIDER; LEVENSPIEL, 1989; GANSER, 1993; BEETSTRA; HOEF; KUIPERS, 2006; ISAACS; THODOS, 1967; CLIFT; GAUVIN, 1971; MARCHILDON; GAUVIN, 1979; CHHABRA; AGARWAL; SINHA, 1999).

The present study took into account five correlations observed in the literature that consider only the main parameters, as follow. Four of them consider the Reynolds number and shape parameters, such as the sphericity, circularity and flatness of the agglomerate (TRAN-CONG; GAY; MICHAELIDES, 2004; HAIDER; LEVENSPIEL, 1989; GANSER, 1993; BAGHERI; BONADONNA, 2016), while one of them uses the orientation of the agglomerate to estimate two different shape parameters (HÖLZER; SOMMERFELD, 2008).

3.2.2.1 Haider & Levenspiel model

The study of Haider & Levenspiel (1989) was the first to propose that the drag coefficient is a function of the Reynolds number and sphericity for both spherical and nonspherical particles. Also, the Reynolds number should be calculated using an equivalent diameter, d_{eq}, corresponding to the diameter of a sphere with the same volume of the particle tested. They proposed that drag correlations could be written as

$$C_D = \frac{24}{Re}\left(1 + A \cdot Re^B\right) + \frac{C}{1 + \frac{D}{Re}} \tag{3.15}$$

where A, B, C and D are parameters given as function of the sphericity ϕ, and is applicable for $Re < 2.5 \cdot 10^4$ for isometric particles (HAIDER; LEVENSPIEL, 1989) such as the proposed in the present study.

3.2.2.2 Ganser model

The model proposed by Ganser (1993) adapts the Haider & Levenspiel model, introducing two other shape-dependent parameters: the Newton's and Stokes' parameters, k_N and k_S, respectively and is given by Equation 3.16

$$C_D = \left(24 \cdot \frac{k_S}{Re}\right)\left[1 + 0.1118\left(Re \cdot \frac{k_N}{k_S}\right)^{0.6567}\right] + \frac{0.4305 \cdot k_N}{1 + \frac{3305}{Re\ ^{k_N/k_S}}} \tag{3.16}$$

where k_N and k_S are functions of the sphericity, ϕ, and the model is applicable for Re $< 3 \cdot 10^5$ if k_N and k_S are known. Literature presents several proposals to estimate these parameters, such as the Tran-Cong, Gay & Michaelides (2004), Hölzer & Sommerfeld (2008) and Bagheri & Bonadonna (2016), tested in this study and presented in sections 3.2.2.3 to 3.2.2.5, respectively.

3.2.2.3 Tran-Cong model

The model proposed by Tran-Cong, Gay & Michaelides (2004) considers that the drag coefficient is a function not only of the Reynolds number, but also the ratio between the surface-equivalent-sphere diameter, d_A, and the volume-equivalent-sphere diameter, d_{eq}, referred as flatness, and the circularity, c. The correlation is given by Equation 3.17.

$$C_D = \frac{24}{Re}\frac{d_A}{d_{eq}}\left[1 + \frac{0.15}{\sqrt{c}}\left(\frac{d_A}{d_{eq}}Re\right)^{0.687}\right] + \frac{0.42\left({d_A}/{d_{eq}}\right)^2}{\sqrt{c}\left[1 + 4.25 \cdot 10^4\left({d_A}/{d_{eq}}\ Re\right)^{-1.16}\right]} \tag{3.17}$$

for the ranges of variables $0.15 < Re < 1500$, $0.80 < {d_A}/{d_{eq}} < 1.50$ and $0.4 < c < 1.0$ (TRAN-CONG; GAY; MICHAELIDES, 2004).

3.2.2.4 Hölzer & Sommerfeld model

The drag coefficient can also be modeled using the theoretical and experimental correlation for drag in the Stokes region (LEITH, 1987), as the one proposed by Hölzer &

Sommerfeld (2008). Their model has its base on the proposal of Leith (1987) and Ganser (1993) for C_D in the Stokes region, including shape and orientation-dependent terms, and Reynolds number of the particle. The correlation is given by Equation 3.18

$$C_D = \frac{8}{Re}\frac{1}{\sqrt{\phi_{||}}} + \frac{16}{Re}\frac{1}{\sqrt{\phi}} + \frac{3}{\sqrt{Re}}\frac{1}{\phi^{3/4}} + 0.421^{0.4(-\log\ \phi)^{0.2}}\frac{1}{\phi_{\perp}} \tag{3.18}$$

where the sphericity, ϕ, represents the ratio between the surface area of the volume-equivalent-sphere and that of the particle, the crosswise sphericity, $\phi_{\perp}$, is the ratio between the cross-sectional area of the volume-equivalent-sphere and the projected cross-sectional area of the particle and the lengthwise sphericity, $\phi_{||}$, is the ratio between the cross-sectional area of the volume-equivalent-sphere and the difference between half the surface area and the mean projected longitudinal cross-sectional area of the particle. The correlation is applicable over the entire range of Reynolds numbers up to the critical Reynolds number (HÖLZER; SOMMERFELD, 2008).

3.2.2.5 Bagheri & Bonadonna model

This model is also derived from the Ganser model, however, accounts for more accurate and easier shape descriptors, rather than sphericity (BAGHERI; BONADONNA, 2016). Here, the form factors, F_S and F_N are functions of the volume-equivalent-sphere, and three size parameters, which are the longest, the intermediate and the shortest lengths of the particle, L, I and S, respectively. The correlation is given by Equation 3.19

$$C_D = \frac{24}{Re}k_S\left[1 + 0.125\left(Re\frac{k_N}{k_S}\right)^{2/3}\right] + \frac{0.46 \cdot k_N}{1 + \frac{5330}{(Re\ ^{k_N}/_{k_S})}} \tag{3.19}$$

where the drag corrections, k_N and k_S, are functions of the form factors, F_N and F_S.

3.3 Results and discussion

3.3.1 Grid refinement near the agglomerate walls

To analyze if the turbulence models are applicable, it is important to evaluate the y^+, since the flow near the walls is a relevant region in the study of the drag coefficient. Turbulence models that do not use wall functions need better refinement near walls since its y^+ shall be lower than 1 (WILCOX, 2004), whereas turbulence models that use wall-function, the value depends on the type of function treatment. For values as low as 3 it is recommended to use the Enhanced-Wall functions (ANSYS, INC, 2012). Since the value of y^+ increases as the velocity of the flow increases, it is necessary to analyze only the highest velocity, i.e. for Reynolds number of 1500.

Simulations presented good results. In general, the y^+ were below 1 for over 99.5% of the elements in the walls of the agglomerates. Worst values were obtained by the RNG k-ε simulations, where the percentage of elements below 1 varied between 97 and 98%. The values confirm that the meshes are fine enough near the agglomerates and it is reasonable to use the Enhanced-Wall functions for the RSM and RNG k-ε turbulence models and fine enough to use k-ω-based models and the Spalart-Allmaras model.

However, wall functions are approximations for zones near the walls, leading the RSM and RNG k-ε turbulence models to lower efficiency on representing the flow surrounding the agglomerate as well as models without wall functions. Also, it is expected that RSM and RNG k-ε turbulence models correctly represent the flow far from the agglomerates, like the models without wall functions.

3.3.2 Statistical analysis of results – Comparison between simulations and empirical correlations

In Figure 7 we observe three models that present promising curves where simulations are correlated: the Haider and Levenspiel model, the Bagheri and Bonadonna model and the Tran-Cong model. However, it is important to statistically confirm which model better fits the results obtained in the simulation. The criterion used was the method known as the root-mean-square error (RMSE), calculated by Equation 3.3 and which values are presented in Table 5.

Table 5 – Root-mean-square error of the turbulence models compared to drag coefficient models.

Agglomerate	Drag coefficient model	Turbulence model				
		RSM	RNG k-ε	SST k-ω	Langtry-Menter	Spalart-Allmaras
3 spheres	Haider & Levenspiel	1.818	1.513	1.557	1.539	1.240
	Ganser	2.604	2.306	2.328	2.319	2.001
	Tran-Cong et al.	2.435	2.150	2.150	2.148	1.819
	Hölzer & Sommerfeld	2.389	2.089	2.112	2.103	1.781
	Bagheri & Bonadonna	2.409	2.116	2.154	2.138	1.856
4 spheres	Haider & Levenspiel	0.724	0.664	0.770	0.921	0.722
	Ganser	1.094	1.064	1.117	1.380	1.038
	Tran-Cong et al.	0.317	0.338	0.311	0.249	0.370
	Hölzer & Sommerfeld	0.804	0.784	0.821	1.128	0.738
	Bagheri & Bonadonna	0.545	0.538	0.557	0.347	0.615
5 spheres	Haider & Levenspiel	1.694	1.639	1.741	1.714	1.527
	Ganser	2.444	2.394	2.484	2.467	2.244
	Tran-Cong et al.	1.061	1.046	1.080	1.078	0.836
	Hölzer & Sommerfeld	1.970	1.944	1.994	1.984	1.737
	Bagheri & Bonadonna	1.051	0.994	1.101	1.081	0.906

Here, we observe that, in most cases, the Tran-Cong model presents lower RMSE for the agglomerates of four and five spheres. An exception is observed for the agglomerate of three spheres, where the Haider and Levenspiel model presented the lower RMSE for all turbulence models tested.

Now, still analyzing Figure 7 we observe lower deviations of the Haider and Levenspiel model for Reynolds numbers between 1 and 100. For this range, the drag coefficient presents higher values, which interferes the most in the RMSE, compared to the drag values for Reynolds above 100. This behavior generates the distortion that leads to statistical inferring that the Haider and Levenspiel model can better represent the drag coefficient in the agglomerate of 3 spheres. Now, considering the range between 1 and 1500, the plot shows that the Tran-Cong model presents the best agreement with simulation data, while the Haider and Levenspiel presents good agreement only for lower Reynolds numbers.

3.3.3 Analysis of the turbulence models

To understand the influence of the turbulence models on the drag coefficient prediction, we first observed the behaviour of the streamlines of the flow surrounding the agglomerate to determine which one better represent three relevant regions of the flow: the boundary layer, the flow far from the walls of the particle and the wake region in the rear of the agglomerates. To infer if the simulation results are consistent, we compared with correlations of the literature, to observe if simulations follow a trend. At last, we compared the results of the turbulence models with the correlation that better represented the trend of the simulations, to find which turbulence model presents lower deviations from the predicted by the correlation.

Before analyzing the drag results, it is relevant to observe if the flow profile corresponds to the expectations from the literature. Militzer et al. (1989) stated that the aspect ratio of a particle substantially interferes on where the separation begins and on the size of the recirculation wake. According to them, particles with similar aspect ratios present similar flow profile. The flow profile past a sphere is well-known and, since the particle agglomerates are composed of spheres, it is expected that the flow profile behaves similarly (OUCHENE, 2020). To compare the velocity profiles, we chose the inlet velocity to reach Re = 1000, where the flow is turbulent and the vortex street in the rear of the agglomerate is considered fully turbulent (BAGHERI; BONADONNA, 2016; GOOSSENS, 2019; OUCHENE, 2020). Figures 4 to 6 present the velocity streamlines for agglomerates of three, four and five particles, respectively, according to the turbulence models. Comparing the models with wall functions, due to its anisotropic treatment, the RSM is more capable of representing the velocity in the rear of the particle agglomerates in the wake region than the RNG k-ε. However, both of them do not represent the profile as well as the turbulence models without wall functions. Such behaviour confirms the expectation since they model the boundary layer zone to represent it, instead of solving the transport equations around the particle.

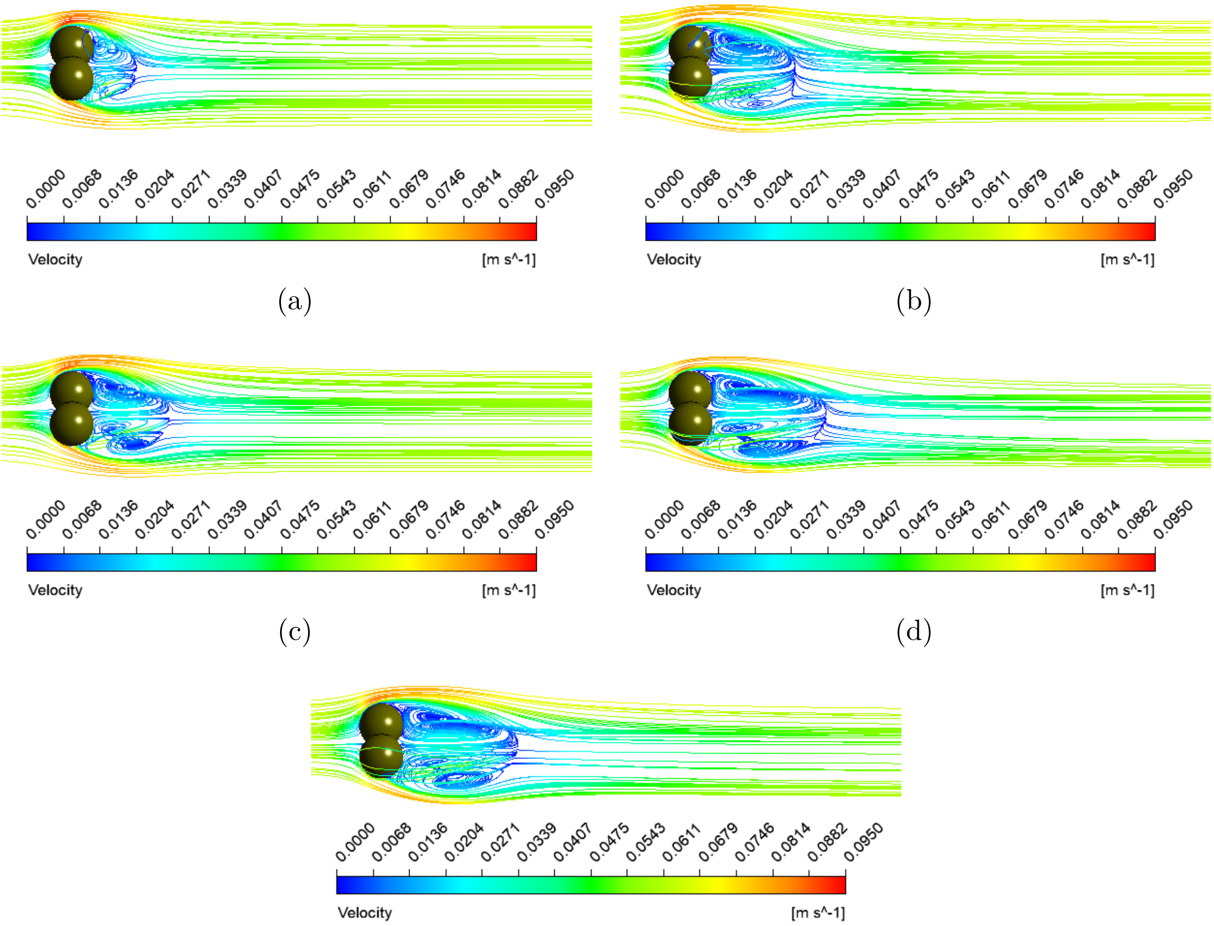

(a) (b) (c) (d) (e)

Figure 4 – From left to right and top to bottom: velocity streamlines for Re = 1000 in the agglomerate of three particles using the RNG k-ε, RSM, Langtry-Menter, Spalart-Allmaras and SST k-ω turbulence models.

The velocity streamlines obtained by the SST k-ω model, seen Figures 4e, 5e and 6e, better represent the flow profile near the agglomerate walls, i.e. the viscous effects ahead the particle becoming less important than the inertial effects (BAGHERI; BONADONNA, 2016; GERHART; GERHART; HOCHSTEIN, 2016). Such behaviour leads to a separation of the flow from the particle at the so-called separation location and the fluid's inertia is large enough so that the fluid cannot follow the path around the rear of the particle. This effect results in a separation bubble after the particle (OUCHENE, 2020), in a region that the boundary layer thickens rapidly in rising pressure, generating a backflow.

In the moderate Reynolds number range, e.g. the tested in this study, as the Reynolds number increases, the backflow profile increases in the rear of the particle to regions far from the particle. The SST k-ω model better represented the recirculating profile in the rear of the agglomerates for all the particle agglomerates. However, for larger Reynolds numbers, by the order of Re = 10^5, the separation is not so clear, since it occurs together with the wake region (GERHART; GERHART; HOCHSTEIN, 2016). As

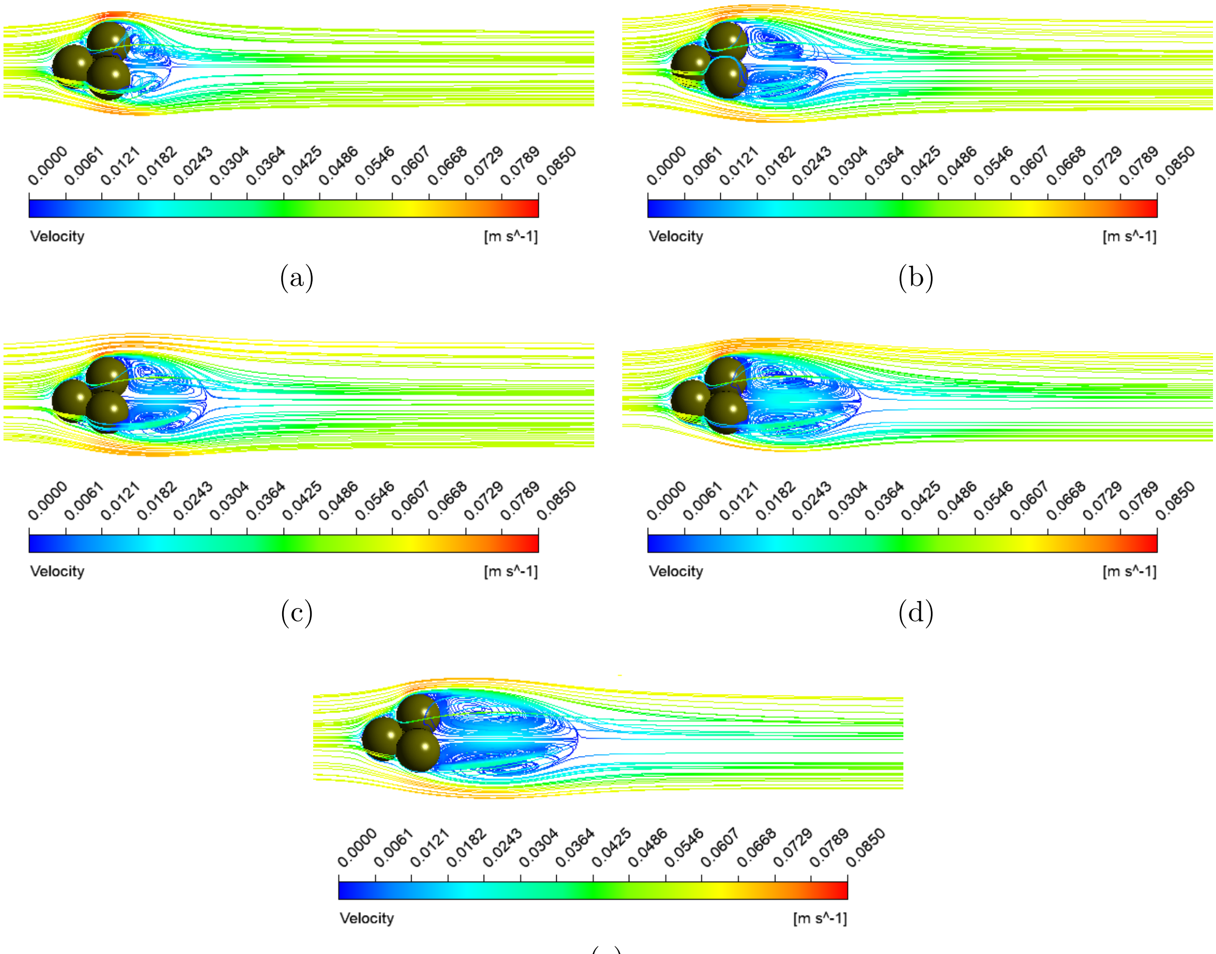

(a)

(b)

(c)

(d)

(e)

Figure 5 – From left to right and top to bottom: velocity streamlines for Re = 1000 in the agglomerate of four particles using the RNG k-ε, RSM, Langtry-Menter, Spalart-Allmaras and SST k-ω turbulence models.

consequence, the results of the drag coefficient estimated by simulations using such model tends to obtain, in general, lower deviations from the empirical model of drag coefficient, as presented in Figure 8.

To find a correlation that better represents the trends of the drag coefficient estimated by simulations, we compared the results of the five turbulence models tested with five drag coefficient correlations present in the literature (TRAN-CONG; GAY; MICHAELIDES, 2004; HAIDER; LEVENSPIEL, 1989; GANSER, 1993; HÖLZER; SOMMERFELD, 2008; BAGHERI; BONADONNA, 2016). The comparisons are presented in Figure 7.

In a first analysis, one can infer that the simulations are better correlated to the Tran-Cong, Gay & Michaelides (2004) model for the three agglomerates along the range of Reynolds numbers tested. An exception occurs in the agglomerate of three particles, as seen Figure 7a, where the Haider & Levenspiel (1989) model has a slightly better representation for Reynolds numbers lower than 10 and a significant better representation

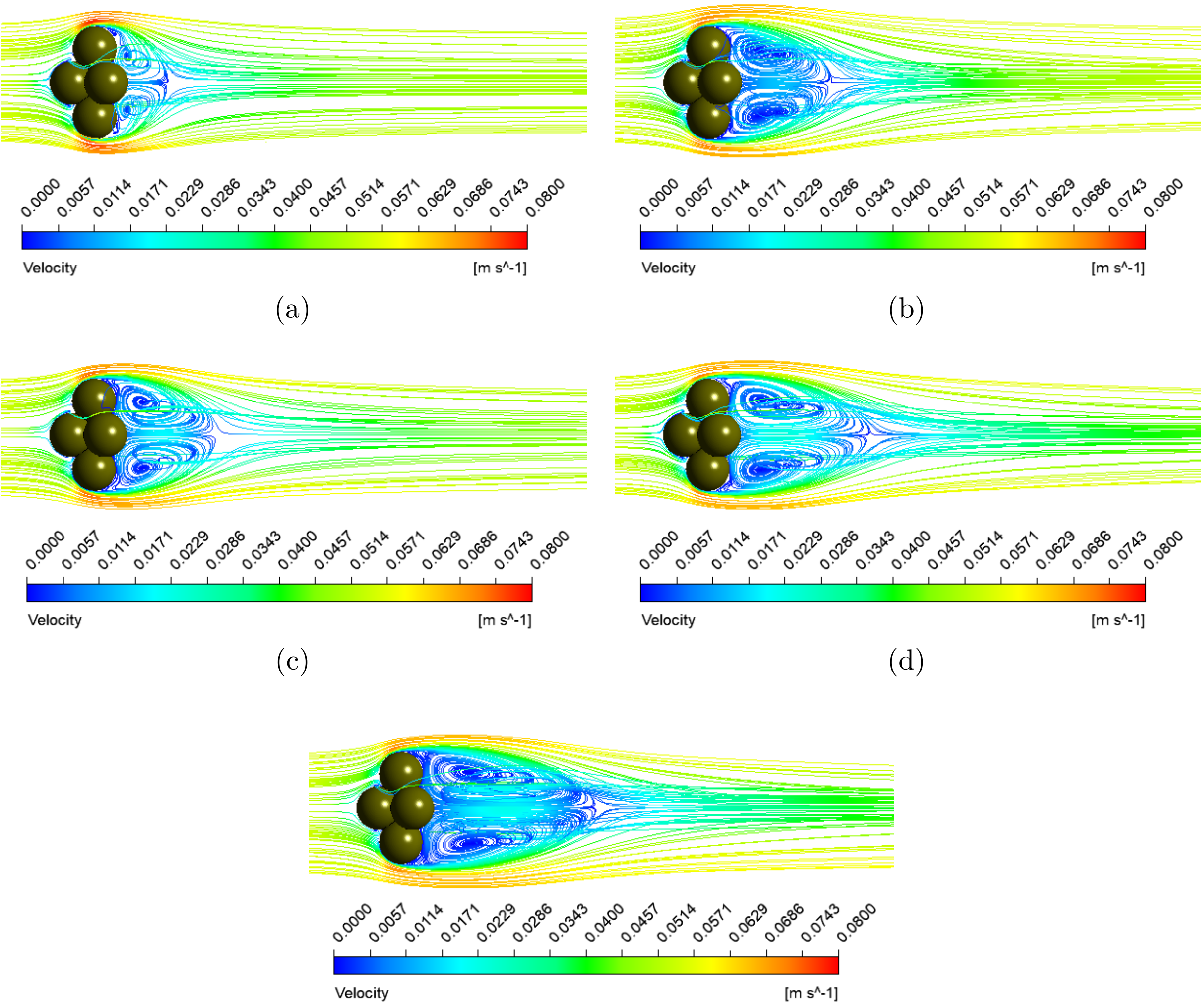

(a) (b) (c) (d) (e)

Figure 6 – From left to right and top to bottom: velocity streamlines for Re = 1000 in the agglomerate of five particles using the RNG k-ε, RSM, Langtry-Menter, Spalart-Allmaras and SST k-ω turbulence models.

for Reynolds numbers between 10 and 100. Since the range of Reynolds numbers is wide, the logarithm scale distorts the perception of the deviations.

To reduce the distortion, the relative deviations along the Reynolds number were plotted for the Tran-Cong, Gay & Michaelides (2004) model, to analyze if the model indeed represents the simulations, and find the turbulence model that presents lower deviations from the correlation. Analyzing the plot of the deviations for the agglomerate of three particles (Figure 8a), the range from 1 to 100 is not so distant from the error of 12% observed in the literature (TRAN-CONG; GAY; MICHAELIDES, 2004). Also, considering the wide range of Reynolds numbers to which the models are applicable, deviations between ± 25% are considered low.

For lower velocities, the flow still follows the curvature of the particle and, consequently, the path around the rear of the particle, for all turbulence models, presented

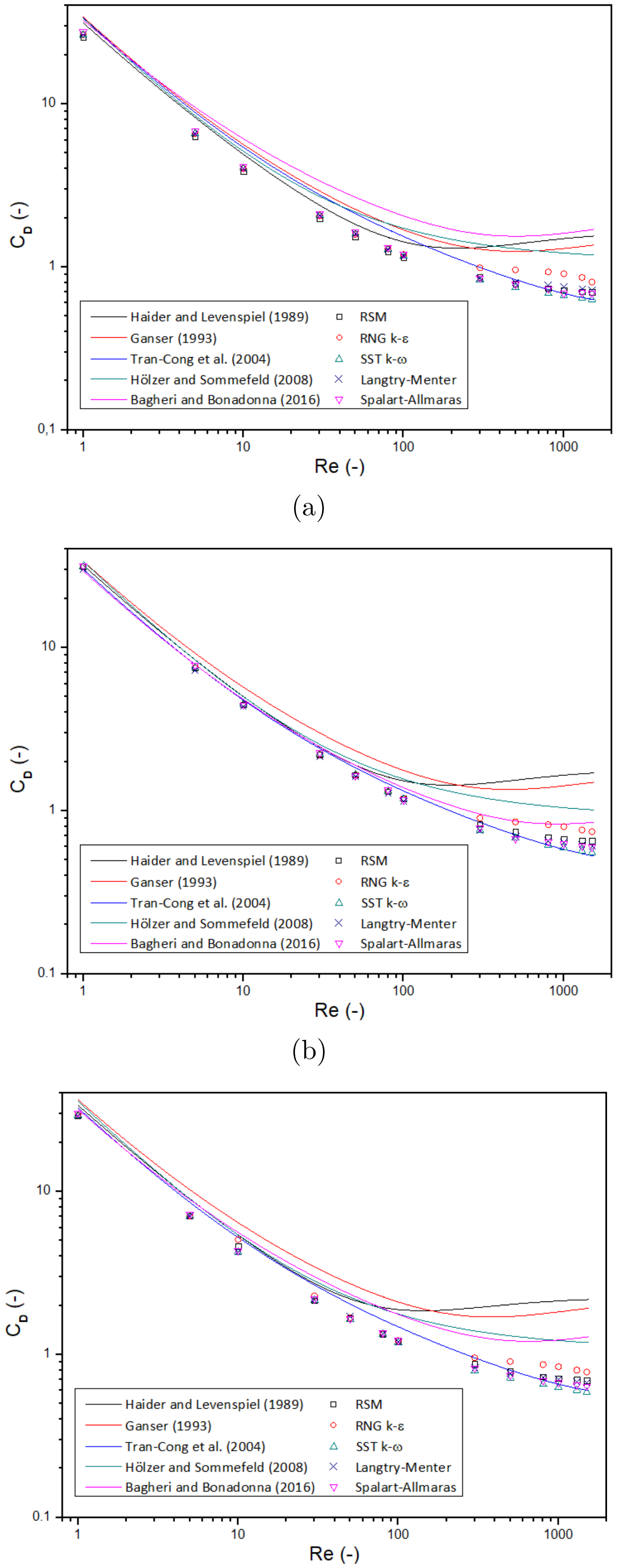

(a)

(b)

(c)

Figure 7 – Comparison between predictions of the experimental drag models tested and the simulations data using different turbulence models for agglomerates of: (a) three particles, (b) four particles, and (c) five particles.

a similar flow profile, leading to similar values for the drag coefficient. As the velocity increases, the edge of the boundary layer gets far from the particle, the boundary layer separation location gets far from the stagnation point and the turbulence models that use wall functions present difficulties on representing the backflow and wake regions after the particles. Consequently, the RNG k-ε and RSM do not follow the trends observed by the other three turbulence models. The RSM is closer to the trends observed due to its robustness, compared to the RNG k-ε, but in Figures 4 to 6 we observe that the RSM also does not represent so well the velocity profile expected.

Figure 8 shows the deviation of the drag coefficient obtained by simulations compared to the correlation of Tran-Cong, Gay & Michaelides (2004) for the agglomerates in the applicable range of Reynolds number of the model. The figure shows a trend for all agglomerates, where the deviation slight and negatively increases as the Reynolds number increases in the range of low Reynolds numbers, from 1 to 100, and for the moderate Reynolds numbers range, from 100 to 1500, the deviation slope is positive and higher.

For Reynolds numbers between 1 and 100, turbulence models presented similar deviations for each of the three agglomerates studied, since it corresponds to the laminar regime presenting unseparated flow. The variation between the models is a consequence of the different values of the closure constants present in each turbulence model. The deviations begin to diverge for Re $\geq$ 300, where the flow is in the transition to turbulence region and the vortices are becoming present. Figure 8 shows that the values obtained are lower than the predicted by equations, by the magnitude of -25%, -10% and -18% for the agglomerates of three, four and five particles, respectively.

As the velocity increases, the gradient of the deviations is positive. However, the slope of the curves for Spalart-Allmaras and SST k-ω models are smoother and, for Reynolds numbers above 1000, the deviations for the SST k-ω presents a trend to converge to a value between ± 5%, according to the agglomerate studied. This is explained by the increase of kinetic turbulence, so turbulence models that better capture effects in the boundary layer and the outer layer can better estimate the drag force acting in the agglomerate. The streamlines presented in Figures 4 to 6 show that the SST k-ω better represents these effects, followed by the Spalart-Allmaras model, confirming the ability of these model to estimate the drag coefficient in particle agglomerates.

For Reynolds numbers between 10 and 100 the deviations are constant or close to constant – in the case of the agglomerate of four particles. This corresponds to the range where the von Kármán vortex street starts to appear in a laminar flow, depending on the shape of the body and the kinematic viscosity of the fluid. The deviations varied from -13 to -28% in the agglomerate of three particles, -6 to -14% in the agglomerate of four particles and -13 to -20% in the agglomerate of five particles. However, simulations with Reynolds numbers below 10 results in drag coefficients closer to the estimated by the

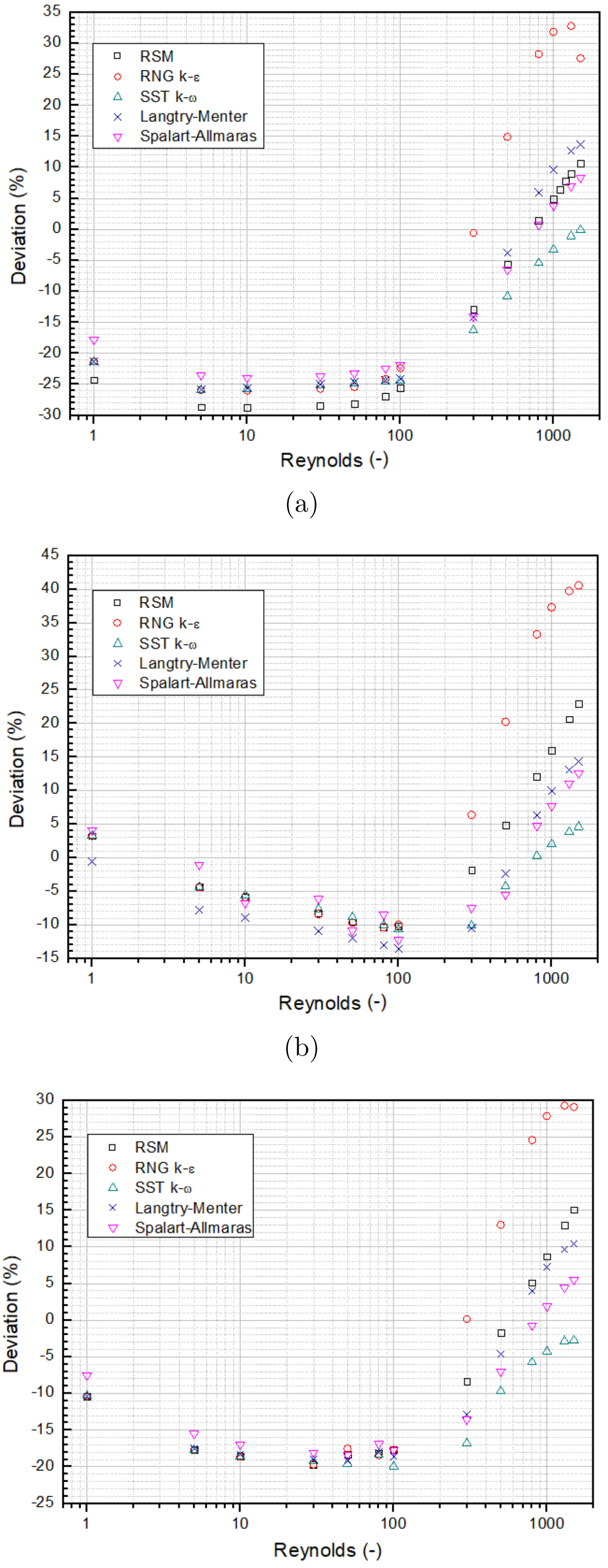

(a)

(b)

(c)

Figure 8 – From left to right and top to bottom: deviations of simulated data from the Tran-Cong model for the agglomerate of three, four and five particles.

correlation.

The symmetry of the agglomerate is a very important variable to consider in the analysis. In numerical simulations, symmetric geometries are easier to generate meshes with good refinement quality in the boundary layer separation region, leading to better results, reducing errors of pressure and velocity fields, mainly near walls, where the drag and lift are computed. The capacity to predict the flow profile and the adverse pressure gradient is correlated with the geometry since the interference of the effect between the spheres of each agglomerate of particles is reduced as the symmetry of the agglomerate increases. Physically, it means that symmetric geometries tend to generate symmetric streamlines, which are easier to be calculated by turbulence models. Such behaviour is well presented in Figure 8, where the agglomerate of four particles has lower deviations, since its symmetry is closer to a single sphere – the most symmetrical shape for spheric particle agglomerates – followed by the agglomerate of five and three particles.

Still analyzing the geometry of the agglomerates, it is possible to see that they generate curvature in the streamlines as we increase the velocity, which directly affects the turbulence and, consequently, the flow profile. The curvature effect can highly decrease the Reynolds stress normal to the wall as the ratio between the boundary layer thickness and the radius increases. Such decrease reaches up to 50% for a ratio of 0.03 (THOMPSON; WHITELAW, 1985). The simulations confirmed the expectations of better results when the curvature effects are considered, by using the Spalart-Allmaras and both SST k-ω-based models (DAVIDSON, 1995).

Since the geometry in the agglomerate of four particles is closer to a single sphere, the deviations are lower for the turbulence models that do not use wall functions. Turbulence models such as the RSM and RNG k-ε are accurate to compute the field far from the agglomerate, however, the near-wall regions and boundary layers are not correctly presented, with difficulties to represent the adverse pressure gradient of the agglomerate in a greater area, lacking the quality to compute the drag coefficient, increasing the deviation. This is related to the fact the wall-functions effects are more influential in the turbulence model than the curvature effects present in a sphere so that the pressure and velocity fields are not well represented near the walls as in the others turbulence models.

The results of this study demonstrate that the utilization of the steady formulation approach yields accurate estimations of the drag coefficient. Furthermore, it is evident that the turbulence model plays a crucial role in effectively modeling the problem, not only for estimating the drag coefficient, but also for accurately predicting the flow profile in regions characterized by separation and recirculating wakes, particularly in flows with higher Reynolds numbers. The implementation of RANS turbulence models that calculate the flow field near the particles instead of relying on wall-function modeling exhibited robustness in representing the presented problem. Moreover, these models exhibited a closer agreement with experimental correlations for drag estimation in particle agglomerates.

The simplifications proposed in this study offer a significant advantage, primarily through the reduction of computational time required to obtain results. Consequently, this reduction allows for an increased number of simulations to be conducted, facilitating a more detailed presentation of the drag coefficient curve and enabling the proposal of new correlations. By incorporating these findings into future research, it is possible to advance the understanding of drag coefficient estimation and develop improved correlations for industrial-scale problems.

3.4 Conclusions

The present study carried out steady simulations of three irregularly-shaped particle agglomerates, composed of spherical particles, surrounded by water. The drag coefficient at different inlet conditions were obtained for five different turbulence models and compared with five correlations in the literature to predict the drag coefficient in agglomerates to understand which numerical setup better represents the flow. The methodology proposed presented good agreement with experimental correlations of drag coefficient estimation, showing to be useful to reduce the time and computational efforts required to numerically obtain the drag acting in particle agglomerates and robustness to estimate the drag coefficient in higher Reynolds numbers. Main observations were

1. Steady RANS turbulence models showed good agreement with the literature to estimate the drag coefficient on particle agglomerates, without the drawback of high computational cost seen in unsteady simulations, such as URANS, LES, DNS or LBM.
2. The turbulence closure equations present lower influence in the evaluation of flow fields for $1 \leq \mathrm{Re} \leq 100$, so the drag coefficients estimated for each turbulence model are very similar.
3. The flow profile is better represented using turbulence models with no wall functions. Both Spalart-Allmaras and SST k-ω models were able to represent the flow near the particle agglomerates and far from its walls, however, the second one showed to be more robust.
4. The use of steady formulation with SST k-ω turbulence model is able to represent the flow for a wide range of Reynolds numbers with less computational effort.
5. Despite presenting a best agreement with the Tran-Cong model, the numerical results presented relative deviations by magnitude of -20%, mainly for lower Reynolds

numbers, representing a good agreement, since the average error of the empirical correlation is 10%.

6. Reduced computational costs makes it possible to obtain more data, so that further studies can focus on elaborating new accurate correlations to, eventually, be scaled-up for industry-scale problems.
7. The numerical methodology proposed showed to be useful for initial test and for experimental validation.

4 Experimental validation of the modelling

This chapter is dedicated to presenting the second part of this thesis: experimentally validate the new approach proposed in the previous chapter. The study in this chapter resulted in an article, entitled *Drag coefficient on particle agglomerates: A CFD study with experimental validation*, published in the journal *Journal of the Brazilian Society of Mechanical Sciences and Engineering* (available at: 10.1007/s40430-023-04366-9).

In this chapter, an experimental methodology is presented to obtain the terminal velocity of real particle agglomerates to assess the robustness of the methodology proposed in Chapter 3, comparing numerically obtained results with results experimentally obtained in the laboratory. To achieve this, three arrangements of Acrylonitrile Butadiene Styrene (ABS) sphere agglomerates were proposed, containing three, four, and five spheres.

The agglomerates consist of ABS spheres glued together with super glue in the most stable arrangement and in three different arrangements, aiming to obtain the drag coefficient for irregularly-shaped particles from the terminal velocity. The method of obtaining terminal velocity is the most recurrent in the literature, used since the XVII century when Sir Isaac Newton measured the terminal velocity of spheres: a body submersed in a fluid is released in free fall, and its velocity is measured (FAN; SU; YANG, 2022).

In the case of this study, which aims to propose a unified correlation capable of estimating the drag coefficient for particles flowing from a fully laminar to a fully turbulent range, validation of the flow is necessary for Reynolds numbers ranging from below 1 to above 1000. Thus, for this article, the terminal velocity was measured from tests conducted in glycerin-water solutions ranging from 0 to 100% water.

Therefore, the water fraction in the glycerin solution was varied into four concentrations, so that the particle agglomerates exhibited Reynolds numbers ranging from 0.1 to 3500. So, the numerical methodology was put to test under 12 different conditions, where one of them showed a higher deviation, underestimating the value by -19%.

4.1 Introduction

In industrial processes particle-laden flows, such as pipeline transportation of biomass feedstock, mineral processing, powder sintering, fluidized bed reactors, and stirred tanks (DEGLON; MEYER, 2006; LANE, 2017) it is recurring the effect of agglomeration of particles. Such effect occurs due to collision, attraction and friction, and generates a specific kind of irregularly-shaped particle known as particle agglomerate. A consequence of the formation of these agglomerates is the modification of the behavior of the flow dynamics, which is directly affected by the particle properties and characteristics - e.g. density, roughness, diameter, and shape - and, consequently, interferes in fundamental variables to the design of these equipment (SENIOR; BRERETON, 1992; KUWAGI; TAKANO; HORIO, 2000).

The drag force experienced by the particles as consequence of a variation in motion generated by the particle-fluid interaction is directly affected by these characteristics. This force, given by the surface integral of both normal and shear stresses acting in the particles, is used to calculate a dimensionless quantity known as drag coefficient. The drag coefficient of spherical particles is a function of dimensionless fluid dynamics numbers, such as the Mach number, the Reynolds number, and Knudsen number. In cases of irregularly-shaped particles, such as particle agglomerates, some parameters related to the body, such as its shape and orientation, have to be taken into account. For incompressible fluids where only inertia and friction are observed the dependent variables to estimate the drag coefficient in particle reduces to two: the Reynolds number and a shape parameter (BEETSTRA; HOEF; KUIPERS, 2006; DEEN et al., 2012; GOOSSENS, 2019).

Despite some properties of the particulate material, such as the elasticity, density, and roughness of the particle agglomerate, directly interfere in the behavior of the flow, two parameters not related to the material must be taken into account: size and shape (WANG; GE; LI, 2008; NIKOLOPOULOS et al., 2010; WANG; WU; WEI, 2017). In fact, these parameters exert the most influence on how the fluid behaves around the particle, so it is important to focus on these parameters by studying the particle agglomeration for different arrangements to predict the drag acting on them, as a relevant variable for the design and optimization of processes equipment (TRAN-CONG; GAY; MICHAELIDES, 2004; DEGLON; MEYER, 2006).

Since the drag force acting in a body is strongly related to the velocity, the most used method to evaluate it is to experimentally estimate the drag coefficient by measuring the body's terminal velocity. A recurring method to obtain it is to release the body into free-fall, to estimate the terminal velocity of particles, and consider the area of the windward surface as the projected area of the agglomerate to obtain the drag coefficient (HAIDER; LEVENSPIEL, 1989; GANSER, 1993; TRAN-CONG; GAY; MICHAELIDES, 2004; HÖLZER; SOMMERFELD, 2008; BAGHERI; BONADONNA, 2016).

The study of particle agglomerates in the theoretical field presents difficulties, mostly related to its complex geometry, which makes it infeasible to obtain analytical equations to estimate the drag coefficient, so that, literature presents several empirical studies in this field (BAGHERI; BONADONNA, 2016). The experimental field also experiences difficulties related to the complexity of the geometry, as it is difficult to accurately measure the area of the windward surface of agglomerates. In order to simplify the problem, experimental studies focused on the analysis of regularly-shaped geometries, such as cones and cylinders (MARCHILDON; CLAMEN; GAUVIN, 1964; JAYAWEERA; MASON, 1965; LASSO; WEIDMAN, 1986), cubes and disks (MCKAY; MURPHY; HILLIS, 1988; WILLMARTH; HAWKS; HARVEY, 1964), polyhedrons (PETTYJOHN; CHRISTIANSEN, 1948; HAIDER; LEVENSPIEL, 1989), or parallelepipeds (HEISS; COULL, 1952), with lower details for the shape.

Another solution observed in the literature is to prepare particle agglomerates, using spheres and super glue, to emulate irregularly-shaped particles (LASSO; WEIDMAN, 1986). By hand-making the particle, one can better control the shape of the particle, to improve the details of the study of the geometry influence (TRAN-CONG; GAY; MICHAELIDES, 2004). However, as the number of spheres in the agglomerate increases, the complexity to calculate the area of the windward surface of the agglomerate increases (HAIDER; LEVENSPIEL, 1989; TRAN-CONG; GAY; MICHAELIDES, 2004; BEETSTRA; HOEF; KUIPERS, 2006; DEEN et al., 2012; BAGHERI; BONADONNA, 2016). So, measuring the area is still a difficulty in the experimental field and, up to now, most of the studies simplify the problem by considering the agglomerate as a single sphere with the same volume as the agglomerate and estimating its projected area using the equivalent-volume diameter (LASSO; WEIDMAN, 1986; HAIDER; LEVENSPIEL, 1989; GANSER, 1993; TRAN-CONG; GAY; MICHAELIDES, 2004; HÖLZER; SOMMERFELD, 2008; WANG; GE; LI, 2008; BAGHERI; BONADONNA, 2016; WANG; WU; WEI, 2017; FAN; SU; YANG, 2022; ROOSTAEE; VAEZI, 2022).

These approaches lead to deviations from the phenomena studied and lower accuracy. However, in a computational fluid dynamics approach, the use of CAD software makes it easier to accurately estimate the projected area of a sketch of the agglomerate. So that, the use of computational fluid dynamics can strengthen the level of details of the shape in the study, being a powerful tool to extrapolate the information, once the model is experimentally validated for complex geometries (DEEN et al., 2012).

Such behavior is also applicable to non-spherical and irregularly-shaped particles, such as the agglomerate of spheres (LOTH, 2008). So, in this study, we aim to validate simulations of the drag coefficient on three different conformations of particle agglomerates with experimental assays in four different flow regimes: the perfect laminar and Stokes' regime, the unsteady asymmetric flow and the turbulent wake regime. The terminal velocities of the agglomerates were measured in four different fluids: water and three different glycerin solutions, varying the concentration to obtain different viscosities and, consequently, different flow regimes. The experiments were used to compare with computational fluid dynamics (CFD) simulations, aiming to validate the simulations and assess their capability to estimate the drag coefficient in particle agglomerates. Once the simulations are experimentally validated, CFD can be used as a powerful tool to study the drag in several conformations and to propose new drag correlations for complex bodies, such as irregularly-shaped particles.

4.2 Methods

The study was carried out in two fields: experimental and numerical. In the first one we performed assays to obtain the density and viscosity of the fluids tested and the particle agglomerates' terminal velocities for each fluid. Then, we performed simulations at the experimental conditions observed to compare the results and observe if the simulations are capable to represent the flow and correctly estimate the drag coefficient.

4.2.1 Experimental setup

The experiments were performed in an acrylic tank with dimensions (20x30x50) cm filled with 28 L of fluid at 25 °C. To vary the Reynolds number of the flow and obtain different flow regimes, the terminal velocities of the particle agglomerates were experimentally obtained in four fluids: water and three different glycerin-water solutions (0.40, 0.80, and 1.0 volume fraction of glycerin).

Figure 9 shows a scheme of the experimental apparatus. The particle agglomerate, initially immersed in the fluid, is released using a lever. To avoid the generation of bubbles due to presence of air in the wholes between the spheres, which interfere the flow, the agglomerates were immersed in the fluid for 4 h and randomly released several times. To avoid the effect of disturbances of the fluid, the agglomerate was fixed in the lever in the position to be released for 10 min, to ensure that the fluid was initially steady.

The experiment was performed for three different conformations of particle agglomerates, as presented in a CAD representation in Figure 10, composed by spheres of Acrylonitrile Butadiene Styrene (ABS) with diameter of 5.95 mm and density of 1822 kg/m^3, to obtain their terminal velocities. The agglomerates were released on its most stable conformation, to avoid oscillations due to fluctuations of the turbulent flow, reducing measurement errors.

As a consequence of fluctuations, the agglomerate oscillates during the free fall, leading to variations in the velocity. So, using a high-speed camera and aided by the software *Tracker 6.10.0*, we could measure the velocity of the particle agglomerate and its

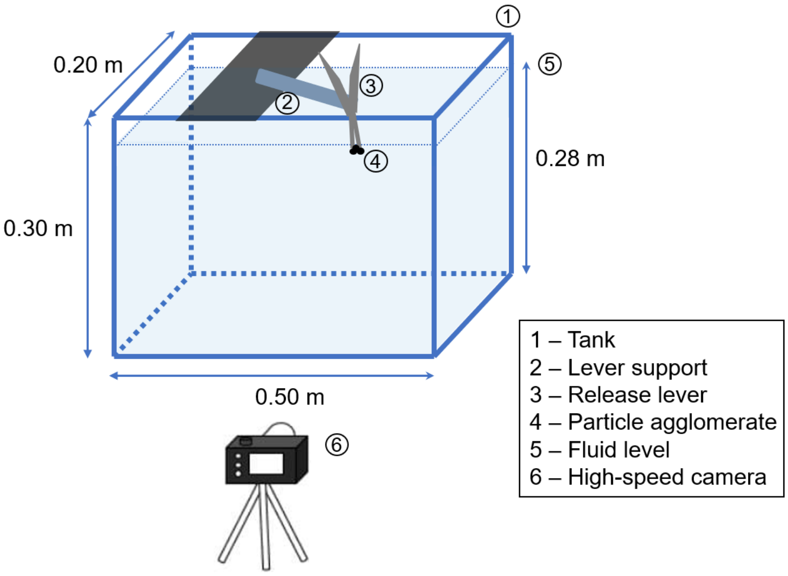

Figure 9 – Scheme of the experimental apparatus.

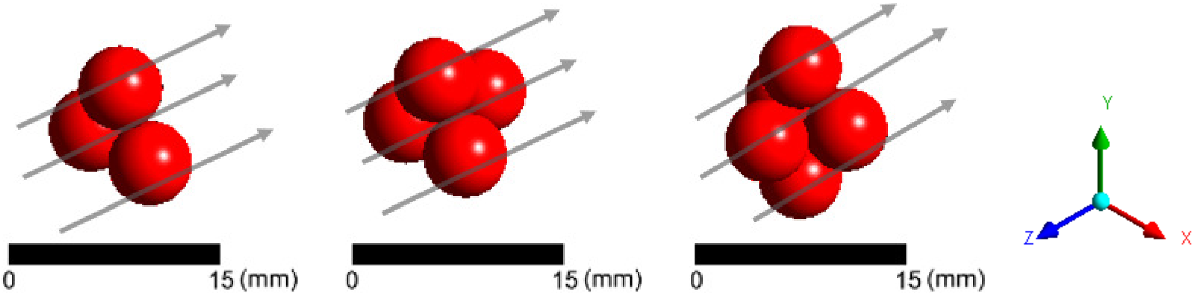

Figure 10 – Isometric view of the three conformations of the particle agglomerates studied and a scheme of the flow direction.

angle during the free fall. We considered only the assays falling in the angle close to the normal, so, assays out of the range between 89 and 91° were discarded. Once we observe that the acceleration is close to zero mm/s^2 (generally with less than 1 cm of free fall), we consider that the agglomerate reached the terminal velocity and take an average of the velocities during the free fall.

For both terminal velocities and fluid properties the assays were performed seven times, in order to reduce experimental errors. Densities and viscosities were obtained with densimeters and Ford viscosity cup, adopting the uncertainty given by the manufacturer. Table 6 shows the density and dynamic viscosity of the fluids, ρ_f and μ, respectively and its corresponding experimental uncertainty.

4.2.1.1 Experimental drag estimation

The experimental determination of the drag coefficient in a body in free fall comes from a balance of forces acting on it: the weight, F_W, drag, F_D and buoyancy, F_B, forces. A scheme of a body in free fall is shown in Figure 11 to better represent the forces.

Table 6 – Properties of the fluids obtained experimentally.

Fluid	ρ_f (kg/m^3)	μ (Pa · s) x 10^3
Water	998 ± 1	1.003 ± 0.030
Glycerin 1	1118 ± 1	4.260 ± 0.128
Glycerin 2	1234 ± 2	111.069 ± 3.332
Glycerin 3	1257 ± 2	585.498 ± 17.565

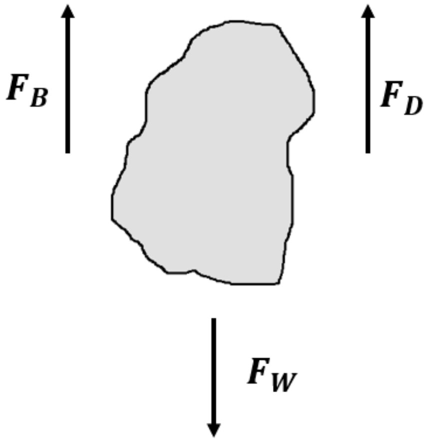

Figure 11 – Scheme of a generic body in free fall and the forces acting on it.

Once the body reaches the terminal velocity, the sum of the forces is zero and the balance is given by the Equation 4.1 (CIMBALA; ÇENGEL, 2000).

$$F_W = F_D + F_B \tag{4.1}$$

which can be expanded as

$$\rho_p \cdot V_b \cdot g = \frac{1}{2} \cdot C_D \cdot A_P \cdot \rho_f \cdot u_t^2 + V_b \cdot \rho_f \cdot g \tag{4.2}$$

where ρ_p and ρ_f are, respectively, the densities of the particle and the fluid, V_b is the volume of the body, A_P is the projected area, g is the gravity and u_t is the terminal velocity of the body, obtained experimentally (see subsection 4.2.1).

Now, isolating the drag coefficient, we obtain

$$C_D^{exp} = \frac{\rho_p - \rho_f}{\rho_f} \cdot \frac{V_b}{A_P} \cdot \frac{2g}{u_t^2} \tag{4.3}$$

where C_D^{exp} is the experimentally-obtained drag coefficient.

4.2.2 Numerical simulations

In the numerical part of the study, simulations were carried out to predict the drag coefficient for four different conditions of fluid flows surrounding three different particle agglomerates. The computational domain and numerical meshes were generated using the ANSYS 14.5 packages Design Modeler and Meshing, respectively. To solve the model equations we used ANSYS Fluent 14.5, and the analysis of the fluid flow was carried out in the software CFD-Post.

4.2.2.1 Design and mesh generation

Simulations were carried out for three different computational domains, varying the geometry of the agglomerates containing three, four and five particles of 5.95 mm of diameter, such as in the experimental step. Differently from the experimental setup, where the particle falls in a static fluid, in CFD simulations the agglomerates were statically set in a position and the fluid flows around it. The domain corresponds to a parallelepiped with a height and width of 40 mm and a length of 180 mm, to ensure that the flow profile before, near, and after the agglomerate is fully developed.

To better control the quality of the elements near the walls of the particles, the domains were divided into a cube-shaped subdomain, near the inlet, surrounding the particle agglomerate. Figure 12 shows a cut of the lateral view of the computational domain of four spheres as an example of the domains simulated and the setup of its boundaries.

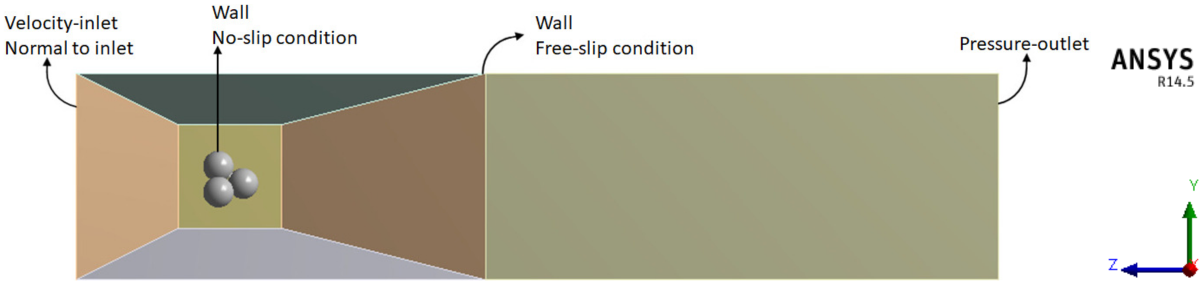

Figure 12 – Example of the lateral view of the interior of the computational domains simulated.

To better observe the refinement of the meshes, we present as example the finest mesh tested for the domain shown in Figure 12. Figure 13 presents the lateral cut of the mesh in the center of the domain, while Figure 14 presents an isometric view of the mesh surrounding the particle agglomerate.

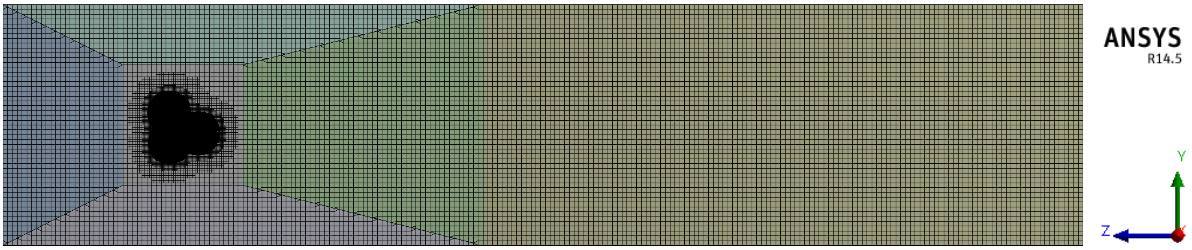

Figure 13 – Example of a lateral view of the finest mesh generated for the particle agglomerate of four spheres.

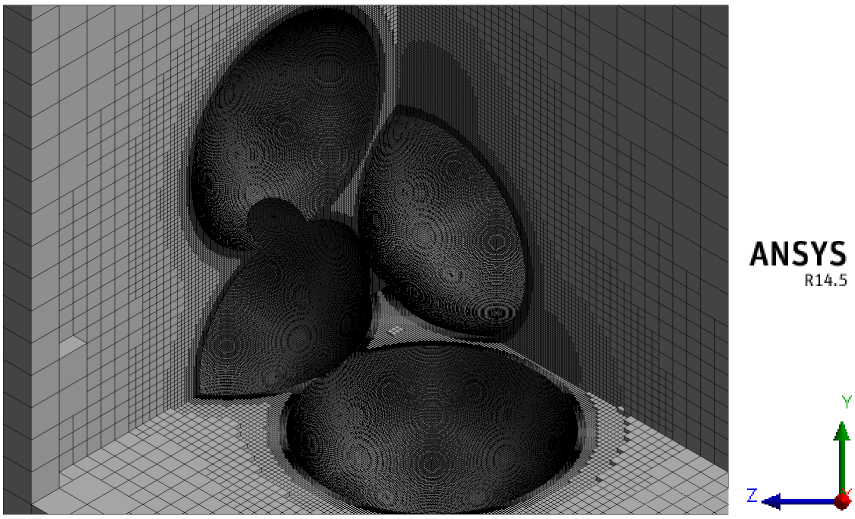

Figure 14 – Example of an isometric view of the mesh surrounding the particle agglomerate of four spheres.

Before comparing the experimental and simulated results, we carried out a grid independence study, better detailed in the subsection 4.4.1.1.

4.2.2.2 Numerical setup

Simulations were carried out in a steady-state formulation of isothermal fluids at 25 °C. As boundary condition, the inlet velocities were set as an injection normal to the surface using the fluid properties and terminal velocities presented in Tables 6 and 8, respectively.

Despite SIMPLE-based algorithms present low computational effort, we chose the PISO algorithm, due to its greater stability, requiring less number of iterations and faster convergence, leading to less processing time (DOORMAAL; RAITHBY, 1983; TUKOVIĆ; PERIĆ; JASAK, 2018). The spatial discretization was set to the least-square cell-based method for gradients, *PRESTO*! scheme for pressure and second-order upwind scheme for energy, momentum and turbulence closure equations, to solve the problem of underestimation of turbulent kinetic energy and its dissipation rate, as suggested in previous studies (DEGLON; MEYER, 2006; LANE, 2017).

4.2.2.3 Numerical drag estimation

For CFD simulations, we calculate the drag coefficient, C_D^{sim}, using its definition. The drag force can be specified as (CIMBALA; ÇENGEL, 2000)

$$F_D \propto P_D A_b \tag{4.4}$$

where A_b is the body's area – generally simplified as the projected area, A_P, of the body studied –, where the fluid exerts a dynamic pressure, P_D. The Equation 4.4 can be re-written by expanding the dynamic pressure due to the kinetic energy of the fluid experiencing relative flow velocity u, obtaining

$$F_D \propto \frac{1}{2} \cdot \rho_f \cdot u^2 \cdot A_P \tag{4.5}$$

In order to change the proportionality to equality, we must include a proportionality constant, in this case, the drag coefficient, C_D, leading to

$$F_D = C_D \cdot \frac{1}{2} \cdot \rho_f \cdot u^2 \cdot A_P \tag{4.6}$$

As the drag obtained by CFD is a theoretical value, we can assume

$$C_D^{sim} = C_D = \frac{F_D}{\frac{1}{2} \cdot \rho_f \cdot A_P \cdot u^2} \tag{4.7}$$

where the drag force is obtained by the pressure fields obtained by CFD simulations.

4.3 Mathematical modelling

4.3.1 The governing equations

The time-averaged conservation equations for the three-dimensional, incompressible, isothermal, and steady flow in this study is modelled by the Navier-Stokes equations (POPE, 2000), as follows

$$\nabla \cdot \mathbf{u} = 0 \tag{4.8}$$

$$\rho \left(\mathbf{u} \cdot \nabla \mathbf{u}\right) = -\nabla p + \mu \nabla^2 \mathbf{u} + \rho \mathbf{g} \tag{4.9}$$

The closure equations for the Reynolds-Averaged Navier-Stokes equations depends on the turbulence model. In this study, we chose the SST k-ω model, which solves the transport equations for the turbulence kinetic energy and the specific dissipation rate, given by Equation 4.10 and Equation 4.11, respectively

$$\frac{\partial \left(u_j k\right)}{\partial x_j} = \frac{\partial}{\partial x_j} \left[\left(\nu + \sigma_k \nu_t\right) \frac{\partial k}{\partial x_j}\right] + P_k - \beta^* k \omega \tag{4.10}$$

$$\frac{\partial \left(u_j \omega\right)}{\partial x_j} = \frac{\partial}{\partial x_j} \left[\left(\nu + \sigma_\omega \nu_t\right) \frac{\partial \omega}{\partial x_j}\right] + 2\left(1 - F_1\right) \sigma_{\omega 2} \frac{1}{\omega} \frac{\partial k}{\partial x_i} \frac{\partial \omega}{\partial x_i} + \alpha S^2 - \beta \omega^2 \tag{4.11}$$

where F_1 is the blending function, α, β and σ are closure coefficients of the model (MENTER, 1994; WILCOX, 2004).

4.4 Results

The validation of the simulation was performed by comparing the drag coefficient obtained experimentally, by the measure of the terminal velocity of the particle agglomerate, and simulations at the same conditions of the experiments.

4.4.1 Numerical results

Before comparing results, it is important to analyse if the results obtained by simulations are reliable. So, we first analyse if the mesh is fine enough to obtain the converged result and the accuracy of the mesh used.

4.4.1.1 Grid independence study

To assure that the results obtained by simulations are grid independent, we tested three different sizes of meshes for each particle agglomerate, using the same pattern of refinement for each geometry. To observe the meshes convergence, we chose the results of drag obtained for the highest Reynolds number. The trend is presented in the Figure 15, showing that the increase of the refinement results in a convergence to the value of the variable tested for each geometry. It is possible to observe that no further refinement is necessary, since the increase of the number of elements between the intermediate to the finest mesh increased the computational effort without significant gain of precision – lower than 0.9%. So, we chose to use the meshes of 5679637, 7176887 and 8673271 elements for the agglomerates of three, four and five spheres, respectively.

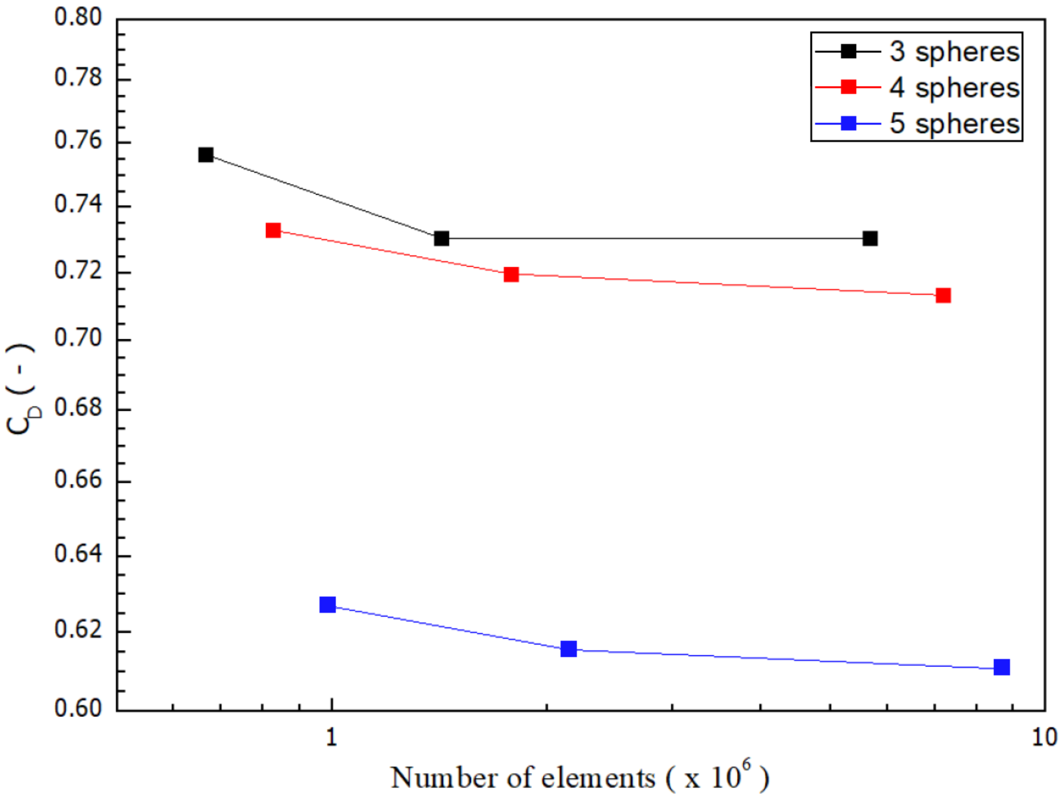

Figure 15 – Grid independence test for the drag coefficient of the particle agglomerates for simulations performed at terminal velocity in water.

4.4.1.2 Mesh quality

It is also relevant to evaluate the mesh accuracy, by analysing some mesh quality parameters. In this study, we chose to evaluate the aspect ratio, the orthogonality and the skewness. The average value of each quality parameter for each particle agglomerate is presented in Table 7.

Table 7 – Mesh quality for the three particle agglomerates studied.

Agglomerate	Number of elements	Statistic variable	Aspect ratio	Orthogonality	Skewness
3 spheres	5679637	Average	1.165	0.950	0.056
		SD (%)	0.570	0.088	0.134
4 spheres	7176887	Average	1.171	0.949	0.058
		SD (%)	0.452	0.089	0.137
5 spheres	8673271	Average	1.176	0.948	0.060
		SD (%)	0.458	0.090	0.139

The minimum value for the aspect ratio is 1 and the element is considered excellent for values lower than 20, while orthogonality and skewness varies from 0 to 1, where the element is considered excellent for values higher than 0.8 for orthogonality and lower than 0.2 for skewness (FERZIGER; PERIĆ, 2002). As presented in Table 7, each mesh presented average values lower than 1.18 for the aspect ratio, higher than 0.94 for the orthogonality and lower than 0.06 for the skewness. So, quality of the elements of the meshes can be considered excellent, assuring a better convergence.

4.4.2 Comparison of results

The experimentally measured terminal velocity for the agglomerates of three, four and five spheres, $u_{t,3}$, $u_{t,4}$ and $u_{t,5}$, and their corresponding experimental uncertainties are presented in Table 8, while Table 9 shows the drag coefficient obtained for both numerical and experimental assays and the corresponding relative deviation between them. The results show lower deviations for lower Reynolds numbers. Since laminar flows do not develop eddies around the walls of the agglomerate, the particle tends to stay in the initial orientation of the release, with a stable fall, i.e. without oscillating (GRAF, 1971). So, experimentally, it is easier to perform the assay in the same orientation of the design performed in simulations for lower Reynolds.

It is relevant to emphasize that the most accurate way to study the phenomena in the flow studied, i.e. the drag coefficient and the velocity field, is using the Direct Numerical Simulation (DNS). The method eliminates the difficulty of modelling turbulence by resolving the whole range of spatial and temporal scales of turbulence. However, this method presents two major difficulties: the generation of uniform meshes around complex bodies and the high computational effort. For wall-bounded problems, the formula

Table 8 – Experimentally measured terminal velocities for each particle agglomerate for the four fluids studied.

Fluid	$u_{t,3}$ (cm/s)	$u_{t,4}$ (cm/s)	$u_{t,5}$ (cm/s)
Water	30.004 ± 0.108	31.045 ± 0.267	32.487 ± 0.082
Glycerin 1	22.702 ± 0.168	27.118 ± 0.125	25.504 ± 0.113
Glycerin 2	8.513 ± 0.040	9.735 ± 0.047	10.661 ± 0.054
Glycerin 3	2.130 ± 0.023	2.858 ± 0.024	3.145 ± 0.049

Table 9 – Comparative between experimental (C_D^{exp}) and CFD (C_D^{sim}) results.

Agglomerate	Fluid	Reynolds [-]	C_D^{exp} [-]	C_D^{sim} [-]	δ [%]
3 spheres	Glycerin 3	0.39	77.075	79.335	2.932
	Glycerin 2	8.09	5.158	5.172	0.271
	Glycerin 1	511.27	0.951	0.884	-7.016
	Water	2570.20	0.709	0.733	3.389
4 spheres	Glycerin 3	0.57	56.253	61.444	9.229
	Glycerin 2	10.08	5.286	4.802	-9.154
	Glycerin 1	672.2	0.875	0.836	-4.543
	Water	2918.19	0.819	0.714	-12.732
5 spheres	Glycerin 3	0.68	44.337	50.524	13.955
	Glycerin 2	12.04	4.101	4.079	-0.522
	Glycerin 1	680.99	0.944	0.882	-6.604
	Water	3289.49	0.763	0.611	-19.923

$N = \left({U_\infty L_x}/{\nu}\right)^{37/14}$ – where U_∞ is the freestream velocity, L_x is the streamwise length, and ν is the kinematic viscosity – is accurate to estimate the magnitude of grid points to resolve the Kolmogorov length scale (CHOI; MOIN, 2012). Despite being proposed for a flow in flat-plate, the formula is useful to observe that for the cases of the agglomerates in Glycerin 1 and Water, presented in Table 9, the meshes would need a magnitude of $\mathcal{O}(8)$ elements to correctly calculate the smaller scales.

Particles settling under turbulent wake regime, i.e. Re $\geq$ 1000, present different orientations during the free fall, as a consequence of the oscillations, leading to different drag coefficients. Such oscillatory behavior is related to the eddies observed in the flow, reducing the stability, due to the irregular vortex loops that eliminate the planar symmetry for complex bodies (GOOSSENS, 1987), such as the agglomerates of four and five spheres. The effect of oscillations during the free fall is not considered in simulations, as the orientation of the particle in free fall in CFD was fixed in the most stable conformation. Experimentally, we consider the drag coefficient of each assay based on an averaged-terminal velocity to obtain an average of the drag coefficient.

The agglomerate of three spheres has less areas to generate the eddies, reducing the instability generated by the oscillations, leading to lower deviations between experimental and simulation data. The opposite is observed in the agglomerates with four and five spheres: the increase of the area generates more eddies and, consequently, presents a most complex wake region in the rear of agglomerate, as seen in Figure 16. As consequence the oscillations increase the instability, making it difficult to obtain accurate experimental results, leading to greater deviations. Such behavior is confirmed by the results presented in Table 9, where agglomerates with four and five spheres falling in water presented the higher deviations, however, they were lower than 20%, which can be considered good for validation of the simulations.

The drag experienced by a sphere flowing in a Newtonian fluid can be divided in seven main flow regimes - that were also observed in literature for irregularly-shaped particles -, classified according to the Reynolds number (GOOSSENS, 2019). The perfect laminar flow, where $\mathrm{Re} \leq 20$, has a particular condition, known as Stokes' regime. By omitting the non-linear inertial term, Stokes analytically obtained the relation called Stokes' law, experimentally validated for $\mathrm{Re} \leq 1$ (LOTH, 2008). Analyzing the Table 9, we observe that both the laminar and the Stoke' regime were obtained and simulations presented low deviations from the experimental data. The agglomerate of five spheres presented the higher deviation, reaching 13.95%, mainly due to experimental difficulties, such as releasing the agglomerate in the correct angle.

For $20 \leq \mathrm{Re} \leq 210$ the flow is known as steady axisymmetric flow regime, where the flow separates from the sphere close to the rear stagnation point and a recirculating wake occurs in the rear of the sphere in an axisymmetric vortex ring. As the Reynolds number increases the flow reaches the transition region, that varies from $210 \leq \mathrm{Re} \leq 400$ and present two different profiles. In the first one, the separation angle and the length of the wake increases until reach the steady planar-symmetric flow, observed in the range $210 \leq \mathrm{Re} \leq 270$, consisting of two streamwise vortical tails with equal strength and opposite sign. For $270 \leq \mathrm{Re} \leq 400$ it is observed the unsteady planar-symmetric regime, where occurs a transition between a steady and time-dependent symmetric wake.

However, due to the difficulties of the mathematical modelling of the transition flow we chose to avoid experiments in this regime and perform them in two regimes that present larger influence of turbulence. The first one occurs for $400 \leq \mathrm{Re} \leq 1000$, presenting an unsteady asymmetric flow and the second, for $1000 \leq \mathrm{Re} \leq 380000$, presenting the fully turbulent wake regime. The main characteristics observed are the lost of a planar symmetry due to the irregular vortex loops and, as the Reynolds number increases, the drag coefficient tends to converge to a constant value (LÄPPLE; SHEPHERD, 1940). In these regimes we observe less than 10% of deviation between simulations and experiments, but a higher deviation is observed in the fully turbulent flow of the agglomerates of four and five spheres, due to the difficulties of reducing the oscillations.

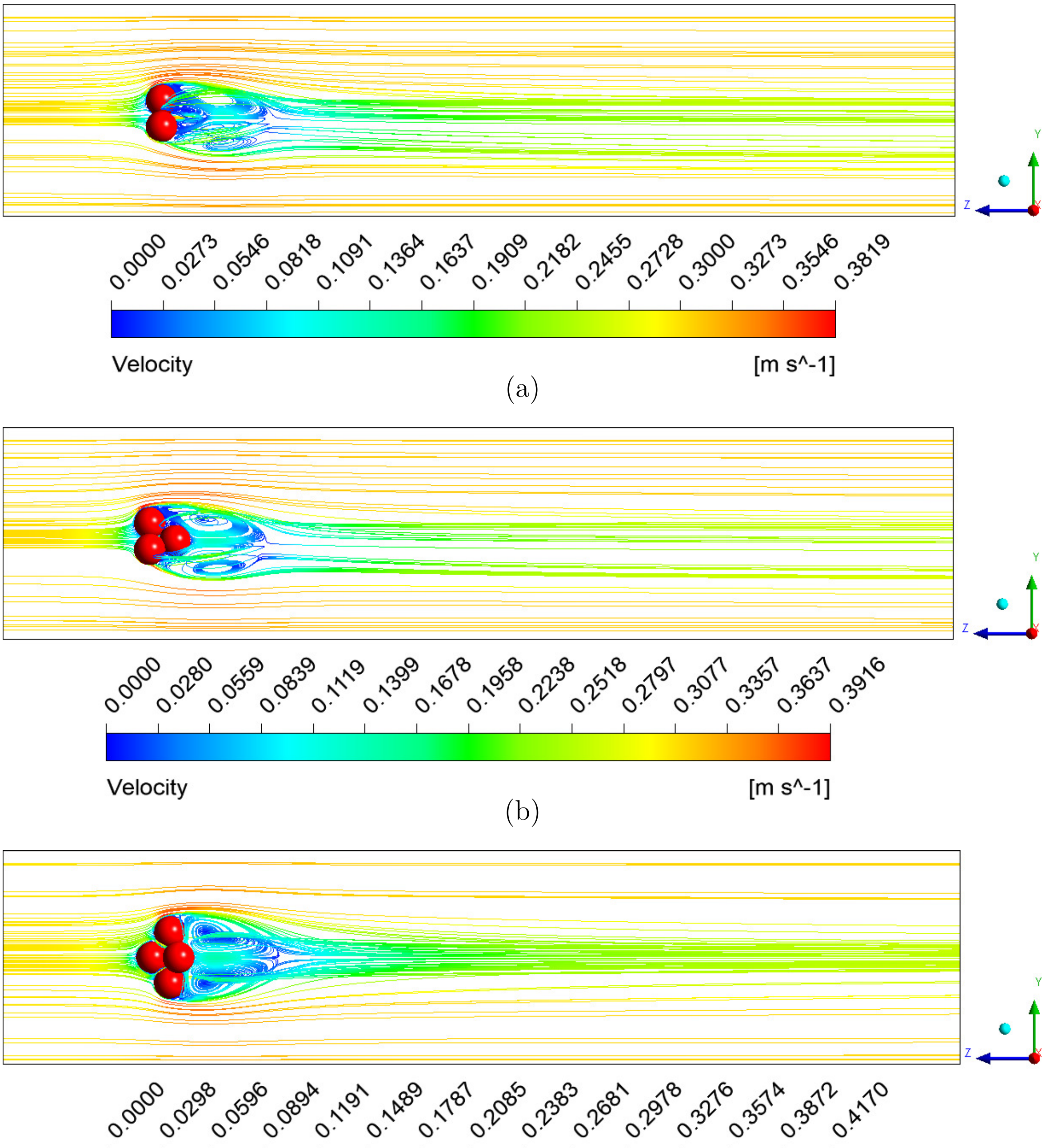

(a)

(b)

(c)

Figure 16 – From top to bottom: streamlines of the flow of water surrounding the agglomerates of three, four and five particles.

4.5 Conclusions

In the present study we performed experiments to estimate the drag coefficient of three conformations of particle agglomerates, composed of spherical particles. The drag coefficient was calculated using the terminal velocity of the agglomerates in free fall using different fluids to vary the Reynolds number. The results obtained were used to validate CFD simulations carried out in a steady state. Main observations were

1. Simulations presented a good agreement with experimental results. For lower terminal velocities the flow presented less fluctuations, generating less oscillations on the agglomerate during the fall, leading to lower deviations.
2. Despite presenting higher deviations flowing in water, results were lower than 20%.
3. The angle of the symmetry plane of the agglomerate with three spheres during the free-fall presents the most stable conformation, compared with the other agglomerates. Fluctuations due to the wake region in the rear, as a consequence of the turbulent flow, generated less oscillations, leading to the lower deviations observed for particles falling in the water.
4. The free-fall of agglomerates with four and five particles did not present the same stability of the agglomerate of three spheres, due to its asymmetric shape.
5. Results show that CFD simulations were able to not only reproduce with fidelity the flow but also to determine the drag coefficient in particle agglomerates, showing to be a feasible tool to propose new correlations to estimate the drag acting in complex bodies.

5 Proposal of the new drag coefficient correlation

This chapter is dedicated to presenting the third part of this thesis: propose a new correlation for prediction of drag coefficient on particle agglomerates using CFD.

In this stage, the study of the drag coefficient is conducted on real particle agglomerates using both numerical and experimental approaches. The experimental methodology presented in Chapter 4 is employed to obtain another terminal velocity value for each agglomerate, aiming to validate the simulations for another one of the six flow profiles described in Chapter 1. To once again confirm the efficiency of the numerical methodology proposed in Chapter 3, the experimental results were compared with results obtained through LES simulations, which, among the commonly used transient models in the literature, has the lowest computational cost and greater stability.

The challenge in proposing a unified equation in this type of problem arises from the wide range of flow conditions, encompassing various flow profiles, and the drag curve exhibiting four different behaviors: a rapid linear decay, a rapid nonlinear decay, a smooth and nonlinear rise, and finally, a nearly constant value.

Another significant challenge is the variation in drag coefficient values across the Reynolds range, spanning from fully laminar to fully turbulent flows. In the context of this study, where Reynolds numbers range from 0.1 to 3500, the drag coefficient varies approximately between 0.5 and 400, with the curve showing non-monotonic behavior for values above 2000.

If we consider the proposed correlation as an individual case study of a particle, treating it as an academic investigation, the flatness and sphericity of the agglomerates presented, in general, lower deviations from the ideal curve, with values between the range of ± 10%. However, since the flatness was applicable over a broader range of geometric parameter values, the fit using flatness proves more useful for potential engineering applications.

The other parameters yielded good results but with deviations within the ± 20% range. An exception was observed in the fit for circularity, which encountered some difficulty in representing turbulent flows in clusters of three and four spheres, showing deviations beyond the ± 20% range.

Nevertheless, if we approach the work from an engineering perspective, extrapolating to applications in industrial equipment, where deviations of approximately ± 20% are often accepted, the correlation exhibited good results for the six tested geometric parameters.

Thus, it is feasible to implement a simple subroutine, where the user can input the particle's flatness, and the CFD code uses the input value in the proposed correlation for flatness. Alternatively, a more complex, yet easily implementable, subroutine could allow the user to provide the values of all six geometric parameters, and the code itself selects the most appropriate correlation for the simulated case.

5.1 Introduction

In particle-laden flows, such as mineral processing, powder sintering, stirred tanks, Venturi scrubber, cyclone separator, pipeline transportation, fluidized bed reactors, or multi-phase chemical reactors, it is essential to understand the interaction between the phases before modelling the flow. The forces related to this interaction mainly depend on the characteristics of particles, such as size, shape, roughness, and elasticity, which determine the equipment's performance (TRAN-CONG; GAY; MICHAELIDES, 2004; NIKOLOPOULOS et al., 2010; WANG; WU; WEI, 2017; OLIVEIRA; GUERRA; LOPES, 2019; DELACROIX et al., 2021; XIA et al., 2023). However, another interaction also relevant occurs between the particles, where three major effects are observed: collision, attraction, and friction. These effects produce a secondary effect known as particle agglomeration, which generates irregularly-shaped particles and changes their physical characteristics, such as diameter, roughness, and shape. These changes interfere in the flow through velocity and pressure fluctuations, in a phenomenon known as turbulence modulation and, consequently, in relevant variables in the design and optimization of industrial equipment (SENIOR; BRERETON, 1992; KUWAGI; TAKANO; HORIO, 2000; DEGLON; MEYER, 2006; WANG; GE; LI, 2008; HARTGE et al., 2009; LANE, 2017; ZHAO et al., 2021; LIN et al., 2022).

The particle-fluid interaction generates the drag, a force experienced by particles due to the dynamic pressure exerted by the fluid, which varies according to the flow velocity. The force is given by the surface integral of the stresses acting on the particle, so it is dependent not only on the motion but also on the shape of the particle (CIMBALA; ÇENGEL, 2000). For simple bodies, such as single sphere, and low Reynolds, it is simple to obtain an analytical solution. For Reynolds numbers up to 1 the Stokes' law is the analytical solution, which by taking the inertia terms in the Navier-Stokes equations, was extended, increasing the applicability of the solution to Reynolds numbers up to 5 (GERHART; GERHART; HOCHSTEIN, 2016).

However, at higher Reynolds or complex geometries, it does not present an analytical solution or becomes infeasible to obtain it. Since the drag force is strongly related to the velocity, the most common solution is to obtain the drag coefficient, by experimentally measuring the terminal velocity of the particle. This methodology is widely used, and numerous experimental correlations are obtained from it for various ranges of subcritical flow and tested for several types of geometries (ISAACS; THODOS, 1967; CLIFT; GAUVIN, 1971; CLIFT; GRACE; WEBER, 1978; MARCHILDON; GAUVIN, 1979; GOOSSENS, 1987; LEITH, 1987; HAIDER; LEVENSPIEL, 1989; GANSER, 1993; CHHABRA; AGARWAL; SINHA, 1999; TRAN-CONG; GAY; MICHAELIDES, 2004; LOTH, 2008; BAGHERI; BONADONNA, 2016). This method is based on the fact that, at terminal velocity, the gravitational, drag, and buoyancy forces are in equilibrium, leading to:

$$m_p \cdot g = F_D + \rho_f \cdot gV_p \tag{5.1}$$

where m_p, g, F_D, ρ_f and V_p are the particle mass, gravitational acceleration, drag force, and particle volume, respectively, and the drag force is given by

$$F_D = \frac{1}{2} \cdot \rho_f \cdot C_D \cdot A_{ws} \cdot u_t^2 \tag{5.2}$$

where A_{ws} and u_t^2 are the windward surface area and the terminal velocity, respectively.

The studies of the drag coefficient are divided in two, according to the shape of the particle: spherical and non-spherical particles, where non-spherical particles can assume regular or irregular shapes. Regular shapes are easier to describe and, along time, many studies focused on understand the physics of flow around the simple bodies - i.e. spheres, disks, cones, parallelepipeds, polyhedrons, or cubes (HEISS; COULL, 1952; MARCHILDON; CLAMEN; GAUVIN, 1964; JAYAWEERA; MASON, 1965; LASSO; WEIDMAN, 1986; MCKAY; MURPHY; HILLIS, 1988; HAIDER; LEVENSPIEL, 1989; GANSER, 1993; CHHABRA; AGARWAL; SINHA, 1999; BEETSTRA; HOEF; KUIPERS, 2006; HÖLZER; SOMMERFELD, 2008; BAGHERI; BONADONNA, 2016; KE et al., 2018) - and estimate the drag force acting on it, proposing correlations in the numerical or experimental fields.

However, irregularly-shaped particles present several difficulties to be studied for both fields. In the experimental field we have the problem of difficulties to measure the windward surface area of the particle. To avoid this difficulty, most of studies approach is to assume that the windward surface is the same of the projected area of an equivalent-volume sphere (FAN; SU; YANG, 2022), leading to equation

$$C_D = \frac{4gd_{eq}\left(\rho_p - \rho_f\right)}{3\rho_f u_t^2} \tag{5.3}$$

where d_{eq} is the diameter of the sphere with the same volume of the irregularly-shaped particle studied. On the other hand, for CFD simulations we have difficulties such as generating stable and homogeneous meshes and the high computational costs (HOEF; BEETSTRA; KUIPERS, 2004; BEETSTRA; HOEF; KUIPERS, 2006; HÖLZER; SOMMERFELD, 2008; RICHTER; NIKRITYUK, 2012; KRAVETS et al., 2019; FAN; SU; YANG, 2022).

Since the present study is in the numerical field, we can use another method to obtain the drag coefficient, which is to calculate the actual windward surface area. By combining Eq. (5.1) and (5.2), we obtain

$$C_D = \frac{2V_p g\left(\rho_p - \rho_f\right)}{A_{ws}\rho_f u_t^2} \tag{5.4}$$

where the windward surface area can be estimated using a CAD software.

In the numerical field, we observe that most of studies use DNS (WEN; JOG, 2005; RICHTER; NIKRITYUK, 2012; RICHTER; NIKRITYUK, 2013; HE; TAFTI; NAGENDRA, 2017) or LBM (HILL; KOCH; LADD, 2001a; HILL; KOCH; LADD, 2001b; HOEF; BEETSTRA; KUIPERS, 2004; BEETSTRA; HOEF; KUIPERS, 2006; HÖLZER; SOMMERFELD, 2008; KE et al., 2018) and, in some cases, LES (JONES; CLARKE, 2008; MOHAMMAD et al., 2018). Due to their high resolution, the results obtained are very accurate. However, these methods require high number of grid points of the meshes, unsteady formulation and low time-step, which leads to a high computational cost and limits the studies to low Reynolds numbers, generally for Re ≤ 300 (KE et al., 2018), so that the correlation is extrapolated for higher values and becoming less accurate for turbulent flows (DIETZEL; SOMMERFELD, 2013; CHENG, 2009; KALMAN; MATANA, 2022; ROOSTAEE; VAEZI, 2022). Using such methodology, the correlations are not modeled for three relevant flow regimes: the unsteady planar-symmetric regime ($270 \leq$ Re ≤ 400), the unsteady asymmetric flow regime ($400 \leq$ Re ≤ 1000) and the turbulent wake regime ($1000 \leq$ Re ≤ 200000) (GOOSSENS, 2019; FAN; SU; YANG, 2022). In contrast, empirical correlations present a wider range, but are more complex to implement in CFD codes, since the correlations are, generally, piecewise functions, which can lead to numerical instabilities in the transition between the sub-functions. Also, they present lower accuracy for turbulent flows, from 60% (BAGHERI; BONADONNA, 2016) or 180%(CHHABRA; AGARWAL; SINHA, 1999) up to 400% (HAIDER; LEVENSPIEL, 1989; GANSER, 1993).

Aiming to propose a new, simple and unified drag correlation for irregularly-shaped particles, applicable for a wide range of Reynolds numbers and particle shapes, in this study we conducted CFD simulations with experimental validations. To assess the applicability of the numerical formulation proposed across a wide range of Reynolds numbers, steady simulations were performed using the SST k-ω turbulence model, as proposed in previous studies (OLIVEIRA; ZANATA; LOPES, 2023; OLIVEIRA; LOPES, 2023), and the results were compared with turbulent flows utilizing Large Eddy Simulation as well as the experimental data. Once the formulation was validated, steady simulations were carried out within the Reynolds number range of 0.1 to 3500, and a new drag correlation was proposed to effectively represent the observed numerical results and, finally compared to experimental data, for validation.

5.2 Methodology

The study was carried out in two fields: experimental assays and numerical simulations. The first part consists on measuring the terminal velocity of three different particle agglomerates in five fluids, to validate the simulations. Once the model is validated, we can use it to simulate the flow for several inlet velocities and propose a new correlation to estimate the drag coefficient.

5.2.1 Numerical simulations

The numerical simulations were carried out using the software ANSYS 14.5. The computational domains and numerical meshes were generated using the software Design Modeler and Meshing 14.5, respectively. The code Fluent 14.5 was used to solve the model equations to analyze the fluid dynamics and estimate the drag force acting on the particles.

5.2.1.1 Domain and mesh generation

Simulations were carried out in three different computational domains, according to the agglomerate studied. The domain is composed of a major parallelepiped with height and width of 40 mm and a length of 180 mm, to assure that the velocity profile of the fluid surrounding the agglomerates and at their rear are fully developed. Figure 17 shows an example of the lateral view of the interior of the computational domain and the boundary conditions of the simulations, while Figures 18 and 19 show, respectively, the lateral and zoomed isometric views of the mesh, to show the high level of detail of the flow surrounding the particle agglomerate.

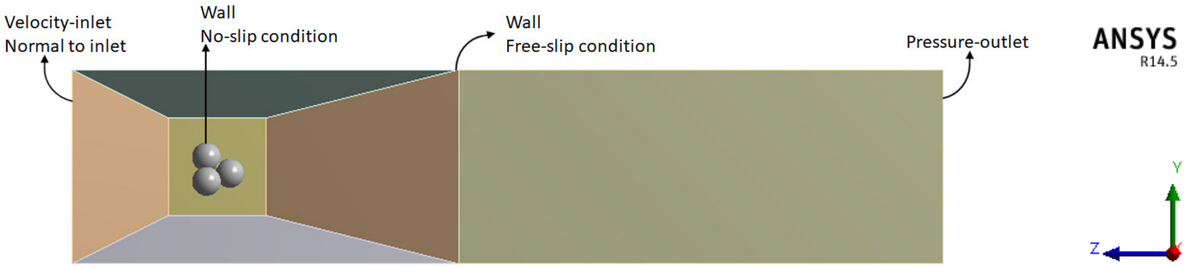

Figure 17 – Example of the lateral view of the interior of the computational domains simulated.

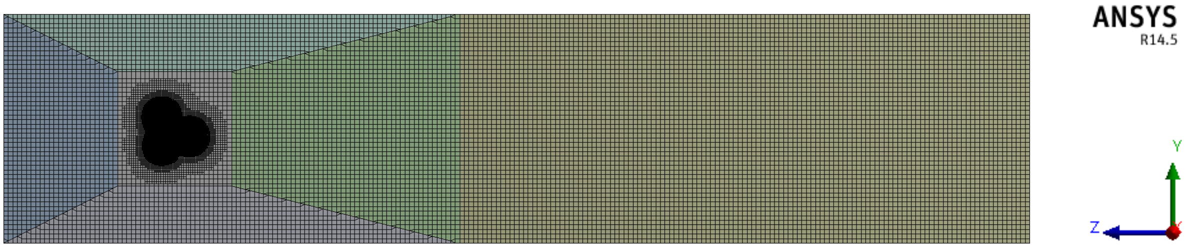

Figure 18 – Example of a lateral view of the finest mesh generated for the particle agglomerate of four spheres.

5.2.2 Mathematical modelling – model setup and governing equations

The present study's focus is the fluid flow past on particle agglomerates at a constant temperature of 25 °C. The time-averaged conservation equations for the three-dimensional, incompressible, isothermal, and steady flow in this study are modelled by the

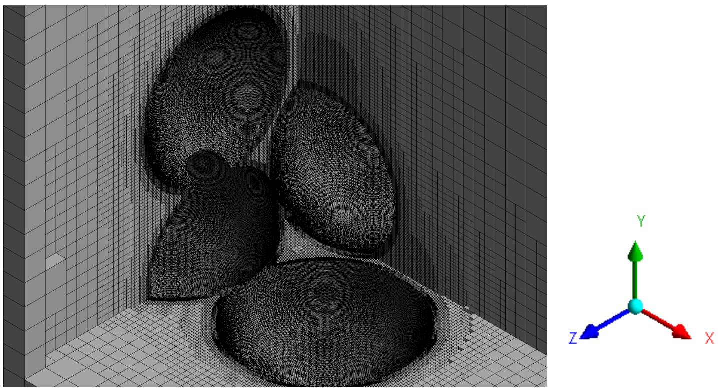

Figure 19 – Example of an isometric view of the finest mesh surrounding the particle agglomerate of four spheres.

Navier-Stokes equations (POPE, 2000), as follows

$$\frac{\partial \overline{u_i}}{\partial x_i} = 0 \tag{5.5}$$

$$\frac{\partial \overline{u_i}}{\partial t} + \overline{u_j}\frac{\partial \overline{u_i}}{\partial x_j} = -\frac{1}{\rho}\frac{\partial \overline{p}}{\partial x_i} + \nu\frac{\partial^2 \overline{u_i}}{\partial x_j \partial x_j} - \frac{\partial \tau_{ij}}{\partial x_j} \tag{5.6}$$

The closure equations for the Reynolds-Averaged Navier-Stokes equations depends on the turbulence model. In this study, we chose the SST k-ω model, which solves the transport equations for the turbulence kinetic energy and the specific dissipation rate, given by Eqs. (5.7) and (5.8), respectively

$$\frac{\partial k}{\partial t} + \frac{\partial (u_j k)}{\partial x_j} = \frac{\partial}{\partial x_j}\left[(\nu + \sigma_k \nu_t)\frac{\partial k}{\partial x_j}\right] + P_k - \beta^* k\omega \tag{5.7}$$

$$\frac{\partial \omega}{\partial t} + \frac{\partial (u_j \omega)}{\partial x_j} = \frac{\partial}{\partial x_j}\left[(\nu + \sigma_\omega \nu_t)\frac{\partial \omega}{\partial x_j}\right] + 2(1 - F_1)\,\sigma_{\omega 2}\frac{1}{\omega}\frac{\partial k}{\partial x_i}\frac{\partial \omega}{\partial x_i} + \alpha S^2 - \beta\omega^2 \tag{5.8}$$

where F_1 is the blending function, α, β and σ are closure coefficients of the model (MENTER, 1994; WILCOX, 2004).

5.2.3 Simulation setup

For validation, the simulations were carried out using the fluids' properties and terminal velocities previously presented in Table 11, while the simulations to propose a new correlation were carried out considering the water properties (see Table 11) varying the inlet velocity, as presented in Table 10, to obtain the drag coefficient curve.

For higher values of Reynolds, the flow presents a time-dependent profile, so a pseudo-transient under-relaxation scheme was applied using the PISO pressure-velocity coupling algorithm. The spatial discretization was set to the least-squares cell-based method for gradients and second-order upwind scheme for energy, momentum, pressure, and turbulence. The convergence criterion for advancing in time was that the RMS

Table 10 – Inlet velocity of the flow for the Reynolds numbers tested.

Reynolds	Velocity [cm/s]		
[-]	3 spheres	4 spheres	5 spheres
0.1	0.0012	0.0011	0.0010
1	0.0117	0.0106	0.0099
5	0.0585	0.0532	0.0494
10	0.1171	0.1064	0.0988
25	0.2927	0.2660	0.2469
50	0.5855	0.5319	0.4938
75	0.8782	0.7979	0.7407
100	1.1709	1.0638	0.9876
250	2.9273	2.6596	2.4690
500	5.8546	5.3192	4.9379
750	8.7819	7.9789	7.4069
1000	11.7092	10.6385	9.8759
1250	14.6365	13.2981	12.3449
1500	17.5637	15.9577	14.8138
2000	23.4183	21.2769	19.7518
2500	29.2729	26.5962	24.6897
3000	35.1275	31.9154	29.6277
3500	40.9821	37.2347	34.5656

residuals were less than 10^{-9}. For lower values of Reynolds, the time-dependent term does not interfere in the flow profile, so we used the steady-state formulation to reduce computational costs.

5.2.4 Experimental methods

The first part of the study consists of experimentally obtaining the terminal velocity of the particle agglomerates to calculate the drag coefficient. The particle agglomerates were made from spheres of Acrylonitrile Butadiene Styrene (ABS) with a diameter of 5.95 mm and density of 1822 kg/m^3. The particles were glued together in three different conformations and released at the most stable angle, as presented in the scheme in Figure 20, to reduce the oscillations due to fluctuations of turbulent flows, which increases measurement errors.

5.2.4.1 Experimental procedures

The experiment was carried out in an acrylic tank of dimensions (20x30x50) cm filled with 28 L of fluid at 25 °C. To obtain different terminal velocities and, consequently, different flow regimes, the experiment was repeated in five different fluids: water and four different glycerin-water solutions. Figure 21 shows a scheme of the experimental apparatus.

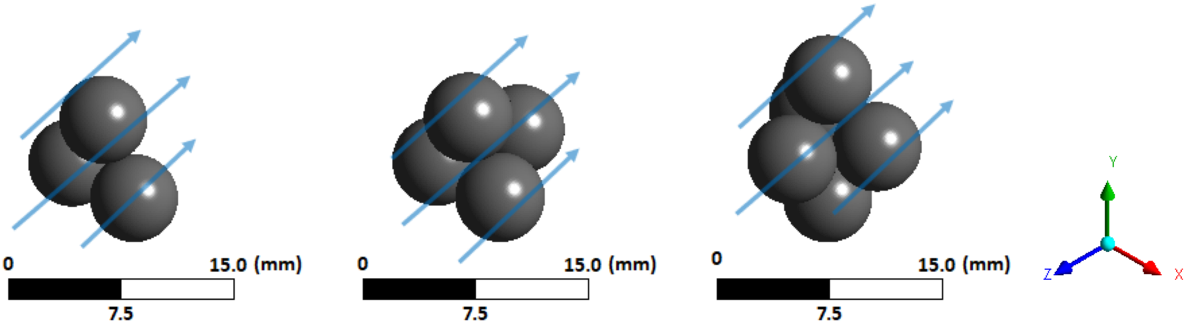

Figure 20 – Isometric view of the three conformations of the particle agglomerates studied and a scheme of the flow direction.

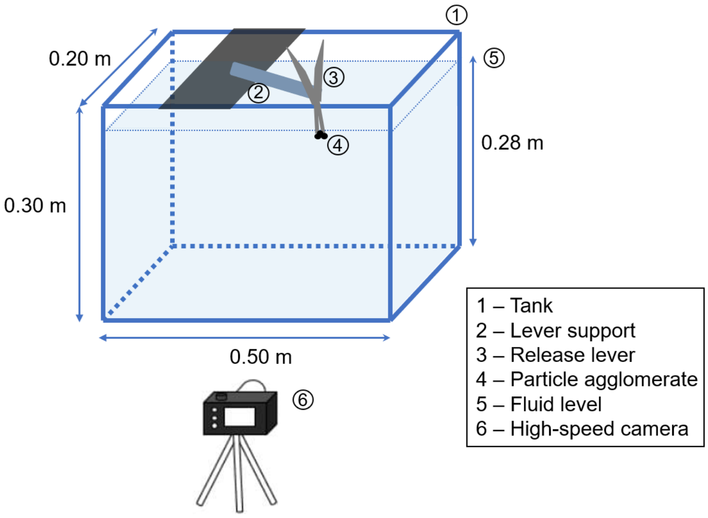

Figure 21 – Scheme of the experimental apparatus.

The preparation for the assays to obtain the terminal velocities were conducted according to the following procedures:

1. **Bubble elimination** – To avoid the generation of bubbles during the fall, the agglomerates were stored in the apparatus filled with the fluid. Before performing the assays, the agglomerates were randomly released several times in the fluid, to ensure that the air inside the holes were eliminated.

2. **Disturbance elimination** – To reduce the effects of the recurring disturbances in the fluid, e.g. waves generated when fixing the particle in the lever, present in fluids with low viscosity, the agglomerate was fixed in the lever, immersed in the fluid in the position to be released, for 10 minutes, to ensure that the fluid becomes steady.

3. **Ambient conditions** – The experiments were performed at atmospheric pressure and a steady room temperature of 25 °C controlled by air conditioning, to ensure that the properties of the fluids remained constant during the assays. Also, a thermometer was immersed in the fluid, to confirm that the temperature was steady.

4. **Tracking setup** – Particles were tracked by recording their fall using a SONY RX-110 IV camera set to 3840 x 2160 pixels per frame and a recording rate of 960 frames per second. To reduce measurement errors, the camera's angle was adjusted using a digital level. To facilitate the recording, a LED spotlight was placed on the left of the lever and a blue card stock was fixed as a background of the tank.

Once the criteria were attended, the assays were performed. The camera was fixed on a tripod in front of the tank. A ruler was fixed and aligned with the lever, to use as a scale during the measure. To reduce the amount of frames recorded before reaching the terminal velocity and before reaching the region where the fluid slows down the particle, the camera was focused on capturing 15 cm of fall after 5 cm of fall.

5.2.4.2 Statistical methods

Using the software *Tracker 6.0.10* we could not only obtain the terminal velocity, but also the angle of inclination of the particle during the free-fall and discard data obtained from assays falling out of the range of 89 and 91°. To reduce the experimental uncertainties, both terminal velocities and fluid properties were measured seven times. Using Tukey's fences for outlier removal (TUKEY, 1977), we observed no outlier points and good accuracy of the assays. Densities were obtained with densimeters, adopting the manufacturer's uncertainty. Table 11 shows the fluids properties and the terminal velocities of the agglomerates with their corresponding experimental uncertainties.

Once we observe that the acceleration is close to zero mm/s^2 - generally with less than 1 cm of free fall -, we consider that the agglomerate reached the terminal velocity and take an average during the free fall. For less viscous fluids, we observe higher Reynolds numbers and, as a consequence of the fluctuations, the agglomerate oscillates along the free fall, leading to variation of the terminal velocity and drag coefficient.

5.2.5 Drag correlation equations

Literature presents several equations used as base to formulate new correlations to estimate the drag coefficient. Most of them are applicable for simple bodies, but very effective, once adaptations are made, such as implementing geometry shape descriptors. Clift, Grace & Weber (1978) proposed a correlation widely used as base for important studies along time, such as Haider & Levenspiel (1989), Ganser (1993), Loth (2008) or Bagheri & Bonadonna (2016). However, we opted to use a simpler model, also frequently adapted in the literature (MORSI; ALEXANDER, 1972; YOW; PITT; SALMAN, 2005; HÖLZER; SOMMERFELD, 2008; RICHTER; NIKRITYUK, 2012; KALMAN; MATANA, 2022), proposed by Kaskas (1964).

Table 11 – From left to right: density and viscosity of the fluids and terminal velocities of particle agglomerates of three, four and five spheres.

Fluid	ρ_f (kg/m^3)	μ (Pa · s x 10^3)	u_{t-3} (cm/s)	u_{t-4} (cm/s)	u_{t-5} (cm/s)
Water	998 ± 1	1.003 ± 0.030	30.0035 ± 0.1079	31.0451 ± 0.2674	32.4866 ± 0.0820
Glycerin 1	1118 ± 1	4.260 ± 0.128	22.7017 ± 0.1681	27.1184 ± 0.1250	25.5036 ± 0.1126
Glycerin 2	1176 ± 1	20.935 ± 0.077	19.3505 ± 0.0267	23.3580 ± 0.0432	23.2619 ± 0.0789
Glycerin 3	1234 ± 2	111.069 ± 3.332	8.5127 ± 0.0402	9.7351 ± 0.0471	10.6612 ± 0.0538
Glycerin 4	1257 ± 2	585.498 ± 17.565	2.1304 ± 0.0226	2.8580 ± 0.0235	3.1447 ± 0.0490

5.2.5.1 Formulation of a new drag correlation

Kaskas (1964) proposed a simple and accurate equation to estimate the drag coefficient:

$$C_D = \frac{\Lambda_1}{Re} + \frac{\Lambda_2}{\sqrt{Re}} + \Lambda_3 \tag{5.9}$$

where Λ_1, Λ_2 and Λ_3 are parameters obtained by regression. This equation has been widely used as an initial test to propose correlations, due to its simplicity and robustness. Khan & Richardson (1987) presented a review showing that this correlation presents good agreement for spherical particles for $0.1 \leq \text{Re} \leq 10000$.

However, the drag is strongly dependent on the shape of the particle, so, the parameters of the regression are, in fact, shape-dependent and such variable must be included in the equation. After analyzing studies taking into account the sphericity, Yow, Pitt & Salman (2005) proposed an improvement given by

$$C_D = \frac{C_1}{Re} + \frac{C_2}{\sqrt{Re}} + C_3 \tag{5.10}$$

where C_1, C_2 and C_3 are parameters calculated by fitting correlations given as functions of the sphericity.

Since the drag is shape-dependent, Richter & Nikrityuk (2012) proposed that, in fact, the correlation could be improved as

$$C_D = \frac{C_1}{Re}\Psi^{C_2} + \frac{C_3}{\sqrt{Re}}\Psi^{C_4} + C_5\ \Psi^{C_6} \tag{5.11}$$

where C_1 to C_6 are fitted by regression and Ψ is a generic shape descriptor. After analyzing five shape descriptors. the best fit was obtained using the aspect ratio, leading to

$$C_D = \frac{C_1}{Re}AR^{C_2} + \frac{C_3}{\sqrt{Re}}AR^{C_4} + C_5\ AR^{C_6} \tag{5.12}$$

Despite presenting good results, the equation presented by Richter & Nikrityuk (2012) was proposed for a restricted range of low Reynolds flows ($10 \leq \text{Re} \leq 250$). However, the study was relevant, since it presented an improved generic equation (Eq. 5.11).

5.2.5.2 New drag correlation

The proposal in this study is to present a new drag correlation for irregularly-shaped particles applicable for a wide range of Reynolds numbers. The correlation is based on the Eq. 5.11, which can be simplified as the following series,

$$C_D = \sum_{i=1}^{N} \frac{C_{2i-1}}{Re^{(3-i)/2}}\ \Psi^{C_{2i}} \tag{5.13}$$

which, for $N = 3$, is well validated for low Reynolds numbers (KE et al., 2018).

The behavior of the drag coefficient curve as a function of the Reynolds number is well known. At subcritical conditions, the flow is divided into three regions: Stoke's regime, the intermediate regime, and Newton's regime. For Stokes' regime (Re $\leq$ 1), we observe a linear decrease as the Reynolds number increases. In the intermediate regime, its behavior shows a non-linear decrease of the drag coefficient as the Reynolds number increases until, for Reynolds close to 2000, it reaches a minimum. As soon as the drag coefficient reaches its minimum, we observe Newton's regime, where the increase of velocity slightly increases the drag coefficient until it reaches a maximum – by the order of 20% higher than of the minimum – and becomes constant, i.e., independent of the Reynolds number.

Now, a trivial solution to present a new correlation is expand the Eq. 5.13 to the fourth term, which leads to

$$C_D = \frac{C_1}{Re}\Psi^{C_2} + \frac{C_3}{\sqrt{Re}}\Psi^{C_4} + C_5\ \Psi^{C_6} + C_7\ \Psi^{C_8}\sqrt{Re} \tag{5.14}$$

which is a potential solution to represent the turbulent region.

However, if we analyze the fourth term in the right-hand side of Eq. 5.14, we observe that the function rapidly varies, since the term $\sqrt{Re}$ rapidly increases as the Reynolds number increases. So, according to the signal of the fitting parameter C_7, the correlation presented in Eq. 5.14 will increasingly underestimate or overestimate the drag at the turbulent range.

So, we propose that the new correlation shall present a closure function to describe the curve, instead of simply expanding the series, as follow

$$C_D = \frac{C_1}{Re}\Psi^{C_2} + \frac{C_3}{\sqrt{Re}}\Psi^{C_4} + C_5\ \Psi^{C_6} + f(\Psi, Re) \tag{5.15}$$

where the term $f\,(\Psi, Re)$ corresponds to a closure function to fit the values in the turbulent region. To solve the problem of rapidly underestimation/overestimation, we chose to use the natural logarithm function, which presents a rapid increase for lower values of Reynolds numbers but slightly increases for higher values, obtaining the following correlation

$$C_D = \frac{C_1}{Re}\Psi^{C_2} + \frac{C_3}{\sqrt{Re}}\Psi^{C_4} + C_5\ \Psi^{C_6} + C_7\Psi^{C_8}\ln Re \tag{5.16}$$

where Ψ is a geometric parameter and the constants C_1 to C_8 are obtained by regressions aiming to minimize the residuals of the errors between the simulation's results and the fitted equation's results.

5.2.5.3 Shape parameters

For non-spherical particles, several shape parameters can be used in particle characterization. Literature presents several methods to obtain shape parameters of non-spherical particles, generally using size parameters (CLIFT; GRACE; WEBER, 1978). One of the most relevant size parameter, defined by Wadell (1932), is the nominal diameter, corresponding to the volume-equivalent-sphere diameter, given by Eq. (5.17)

$$d_n = \sqrt[3]{6V_p/\pi} \tag{5.17}$$

where V_p is the total volume of the non-spherical particle studied. This size parameter is widely used in the characterization of particles and bubbles, for both estimation of some shape factors and, mainly, to estimate the Reynolds number of the particle (CLIFT; GRACE; WEBER, 1978).

Another size parameter widely used, with a similar definition, is the surface-equivalent-sphere diameter, based on the projected area of the particle, given by Eq. (5.18)

$$d_A = \sqrt{4A_p/\pi} \tag{5.18}$$

where A_p is the projected area of the non-spherical particle.

Defining these size parameters is crucial since most of the shape parameters used to characterize the particles are dependent on some size parameter.

I. Sphericity

The sphericity is a geometric parameter used to estimate how spherical an object is. The literature presents several ways to calculate it, however, the definition proposed by Wadell (1932) is one of the most used. It is proposed that the sphericity is given by the ratio between the surface area of the volume-equivalent-sphere and the actual surface area of the particle, as presented by Eq. (5.19)

$$\phi_W = A_{sph}/A_{ps} \tag{5.19}$$

where A_{sph} is the surface area of the volume-equivalent sphere and A_{ps} is the particle surface area. In the present study, the values varied from 0.59 to 0.71.

II. Circularity

Studying the shape of particles, Dellino & LaVolpe (1996) showed that circularity is effective to characterize the roundness of particles. For the present study, such property is relevant, since the more round the particle, the more the flow around it behaves like a single sphere and it can explain the deviations in the drag curve for the new correlation. The circularity is a parameter dependent on the maximum projected perimeter and the perimeter of the circle equivalent to the particle's maximum projection area, as follows

$$c = \frac{P_{mp}}{P_c} = \frac{P_{mp}}{\sqrt{4\pi A_{mp}}} \tag{5.20}$$

where P_{mp} is the maximum projected perimeter, P_c is the perimeter of the circle equivalent to the particle maximum projection area and A_{mp} is the maximum projection area. In the present study, the values varied from 1.23 to 1.52.

III. Surface circularity

The surface circularity, as observed in Tran-Cong, Gay & Michaelides (2004), is given by the ratio between the perimeter of the surface-area equivalent sphere and the maximum projection perimeter, as given by Eq. (5.21)

$$c_s = {}^{\pi d_S}\!/_{P_{mp}} \tag{5.21}$$

where d_S is the surface-area-equivalent sphere's diameter and P_{mp} is the maximum projection perimeter. In the present study, the values varied from 1.30 to 1.84.

IV. Flatness

Heiss & Coull (1952) showed that flatness can be represented by a simple ratio between the surface-area-equivalent-sphere's diameter and the volume-equivalent-sphere's diameter, as follows

$$f = {}^{d_S}\!/_{d_n} \tag{5.22}$$

where d_S can be obtained by CAD software, while d_n is obtained by Eq. (5.17). This parameter is a useful correction factor when experimental results diverge from theoretical if estimated using the area-equivalent-sphere diameter to calculate the drag coefficient (TRAN-CONG; GAY; MICHAELIDES, 2004). In the present study, the values varied from 1.08 to 1.29.

V. Shape factor

Despite presenting good results, literature shows that the sphericity presents some difficulties to describe particles with a very irregular contour that interferes with the flow profile. Büttner et al. (2002) observed that circularity is a parameter sensible to such irregularities. So, to insert an equilibrium to sphericity, the shape factor was proposed as follows

$$\psi = {}^{\phi_W}\!/_{c} \tag{5.23}$$

aiming to better describe irregular particles using a simple and compact descriptor (DELLINO et al., 2005). In the present study, the values varied from 0.45 to 0.54.

VI. Aspect ratio

We use the aspect ratio as the ratio between the minimum and maximum distance of the particle agglomerate in the XYZ axis.

$$A.R. = {}^{min(X,Y,Z)}\!/_{max(X,Y,Z)} \tag{5.24}$$

considering the centroid of the agglomerate fixed at the origin and the agglomerates disposed as presented in Figure 20. In this proposal, the values varied from 0.50 to 0.91.

5.3 Results and discussion

This study was carried out in two fields: experimental and CFD simulations. Experiments were used to validate the simulations and the new correlation proposed by fitting the CFD results.

5.3.1 Grid independence analysis

A grid independence study was performed for the drag coefficient, to assure that the obtained results are grid independent. Three levels of grid density were tested for each particle agglomerate, varying from 665609 to 8673271 cells, as presented in Table 12, for the inlet velocity corresponding to a Reynolds number of 1000 for each the agglomerate.

Table 12 – Details of the meshes for the independence study for drag coefficient of terminal velocity in water.

Agglomerate	Number of elements	C_D^{sim} (-)	Relative difference [a] (%)	Relative difference [b] (%)
3 spheres	665609	0.7565	- 4.4339	- 0.0054
	1421504	0.7307		
	5679637	0.7306		
4 spheres	826421	0.7330	- 2.6711	- 0.8904
	1782503	0.7199		
	7176887	0.7134		
5 spheres	984887	0.6270	- 2.5717	- 0.7910
	2150878	0.6156		
	8673271	0.61075		

[a] Percentage difference between the coarse and fine meshes.
[b] Percentage difference between the intermediate and fine meshes.

Analyzing the Table 12, we observe that the results can be considered converged, since the relative difference between the intermediate meshes and the fine meshes presented and improvement of less than 0.9% in the trend of the result. So, further refinements will increase the computational cost without presenting significant improvement on the accuracy of the results obtained.

To qualitatively study the meshes and predict the accuracy and reliability of the results, we analyzed three mesh quality parameters. In this case, as presented in Table 13, we opted to observe the aspect ratio, the orthogonality and the skewness of the meshes.

For the aspect ratio and orthogonality of the grid element, the closer to 1, the better, while for skewness, the closer to zero, the better is the quality. For aspect ratio, values below 20 are considered excellent, while orthogonality and skewness are considered excellent for values greater than 0.8 and lower than 0.2, respectively (FERZIGER; PERIĆ, 2002). We observe in Table 13 that the mesh quality presented results close to the ideal for

Table 13 – Mesh quality for the three particle agglomerates studied.

Agglomerate	Number of elements	Statistic variable	Aspect ratio	Orthogonality	Skewness
3 spheres	5679637	Average	1.165	0.950	0.056
		SD (%)	0.570	0.088	0.134
4 spheres	7176887	Average	1.171	0.949	0.058
		SD (%)	0.452	0.089	0.137
5 spheres	8673271	Average	1.176	0.948	0.060
		SD (%)	0.458	0.090	0.139

all the parameters taken into account, showing that the simulations will tend to present accurate results, converging with low numerical instabilities.

5.3.2 Verification and validation of the steady formulation

The verification and validation of the modelling is useful to reduce the computational efforts. In order to see if steady RANS formulation is proper to estimate the drag coefficient, the results of simulations were compared with the experimental results. To assay if LES is feasible in this problem, we performed an initial test in the experimental conditions that presented time-dependent flow profile, for higher Reynolds numbers. For these conditions, we opted to use the boundary conditions of the particle flowing in water.

Jones & Clarke (2008) presented an extensive and detailed work on flow simulations around spheres using the FLUENT code with LES turbulence modelling for time-dependent flows. The study focused not only on the numerical methods, but also the size of the meshes and time-step to carry out the simulations. So, based on their statements, LES simulations in the present study were carried out using the PISO algorithm for pressure-velocity coupling, *PRESTO*! and QUICK methods for the pressure and momentum discretization, and the Smagorinsky-Lilly as the subgrid-scale model (LILLY, 1992). The finest meshes presented in the Table 12 attend the requirement of number of grid-points the Chapman's estimation (CHOI; MOIN, 2012). To observe a complete profile we chose to perform LES simulations for 8 seconds of physical time with a timestep of 0.005 seconds.

As the velocity of the flow decreases, the physical time to be simulated increases, but the size of the smaller vortices increases, which allows for increasing the timestep, leading to a moderate increase of computational costs. However, for LES there is a limitation to the maximum size of timestep acceptable when calculating the drag coefficient (JONES; CLARKE, 2008). So, the physical time simulated increases as the velocity decreases, but when the timestep reaches its maximum size, it must stay constant, the computational cost rapidly increases. By testing the LES, we observed that the case with less physical time to be simulated required approximately 30 times the time using SST k-ω, 140 hours for LES against 4.5 hours for SST k-ω, with no significant gains in the quality of results.

So, carrying out simulations for all the cases presented in Table 10 becomes infeasible.

Now, before carrying on the CFD study for a wide range of Reynolds numbers, it is necessary to observe if the mathematical modelling proposed indeed presents reliable results for the flow profiles observed in the range proposed. So, we performed the simulations at the boundary conditions of all the experimental data presented in Table 11 using the steady SST k-ω model, aiming to validate the numerical methods. So, an analysis of the relative deviation between the results was performed, assuming that the correct value is given by the result obtained experimentally, estimated by the Eq. 5.25

$$\delta = \frac{C_D^{sim} - C_D^{exp}}{C_D^{exp}} \cdot 100 \tag{5.25}$$

Table 14 shows the deviation between numerical and experimental results. Most of the results presented a good agreement with experimental data, showing deviations lower than ±10%, Results for Glycerin 2, where the Reynolds numbers are close to the transition range, presented high deviations for all particle agglomerates. Such behavior is expected, due to the difficulties of modelling the vortices in a transition range.

Table 14 – Comparison between numerical and experimental drag coefficient for each particle agglomerate at the boundary conditions obtained experimentally.

Agglomerate		Fluid				
		Water	Glycerin 1	Glycerin 2	Glycerin 3	Glycerin 4
3 spheres	C_D^{sim} (-)	0.737	0.884	1.363	5.172	79.335
	C_D^{exp} (-)	0.712	0.951	1.142	5.158	77.075
	δ (%)	3.42	- 7.02	19.34	0.27	2.93
4 spheres	C_D^{sim} (-)	0.714	0.836	1.223	4.802	61.442
	C_D^{exp} (-)	0.860	0.875	1.029	5.189	56.253
	δ (%)	- 16.98	- 4.54	18.82	- 7.46	9.23
5 spheres	C_D^{sim} (-)	0.611	0.747	1.126	4.080	50.524
	C_D^{exp} (-)	0.659	0.844	0.978	4.101	44.337
	δ (%)	- 7.30	- 11.49	15.23	- 0.52	13.96

Despite presenting some high deviations, we observe that most of simulations presented relative deviations lower than ± 10%, and all of them presented deviations lower than ± 20%, which is acceptable when validating CFD simulations.

5.3.2.1 Choosing the geometric parameter

To understand how the geometric parameter interferes with the correlation, we used a genetic algorithm to optimize the parameters C_1 to C_8 by reducing the root-square error (RSE) between the results obtained by CFD and the fit, given by

$$RSE = \sum_{i=1}^{N} \sqrt{(x_i - \hat{x}_i)^2} \tag{5.26}$$

where x_i is the i^{th} value obtained by CFD, $\hat{x_i}$ is the i^{th} value obtained by the fit and N is the N^{th} value to be compared. To cover all the ranges of experimental data - between 0.39 to 3289 -, we simulated the drag coefficient for a range between 0.1 and 3500, as previously presented in the Table 10. By reducing the error, we obtained the best fit of the correlation for each of the geometric parameters proposed in the subsection 5.2.5.3, as presented in the Table 15, to estimate which presents the lower deviations.

Table 15 – Fitting parameters of the new correlation for each geometric parameter tested.

Geometric	Fitting parameter							
parameter	C_1	C_2	C_3	C_4	C_5	C_6	C_7	C_8
$A.R.$	36.396	0.237	- 10.638	30.999	1.497	0.100	- 0.105	0.226
c	40.890	- 0.623	- 1.466	0.837	1.769	0.464	- 0.155	0.394
c_{surf}	27.497	0.416	4.844	- 7.254	1.292	0.019	- 0.077	0.089
f	23.239	1.477	7.811	- 5.446	0.939	- 1.016	- 0.032	- 3.972
ϕ_W	23.970	- 0.672	2.318	0.048	1.062	0.758	- 0.015	0.326
ψ	46.024	0.397	- 0.854	0.333	1.712	0.130	- 0.091	- 0.302

To choose the best geometric parameter, we have to observe the behavior of the correlation of all the fits along the simulated data. An easy way to do it is to plot the drag coefficient obtained numerically and the calculated by the correlation, as presented in Figures 22 to 24. In an initial analysis, we observe that, in general, all the parameters presented good agreement with simulated data. Most of the fit results presented deviations between ± 10%, which shows that the new correlation is able to predict the drag coefficient for laminar to turbulent flows.

Now, with a focus on identifying the optimal correlation, our objective is to find a fit that demonstrates a greater number of data points closely aligned with a perfect fit. It is evident that sphericity was the sole parameter that consistently exhibited a good agreement across the simulated range, with all results showing deviations within the range of ± 10%. Similarly, the flatness parameter demonstrated numerous results that closely approached a perfect fit, with only three points slightly exceeding a deviation of 10%, as observed in Figure 24d. To conclude which parameter yields the most favorable outcomes, it is crucial to present some statistical analysis. So, in Table 16 we present the deviations between the correlations and the numerical simulation data, while in Table 17 shows the deviations between the correlations and the experimental data.

Table 17 not only confirms the statement from graphical observations but also can be used as experimental validation of the correlation, where the flatness and sphericity fits presented deviations between ±20% for experimental data (Table 17). Flatness and sphericity presented similar deviations for both experimental and simulated data. However, we have to consider the range of geometries for which the correlations are applicable. Based on the values of the shape parameters presented in subsection 5.2.5.3, the correlation using

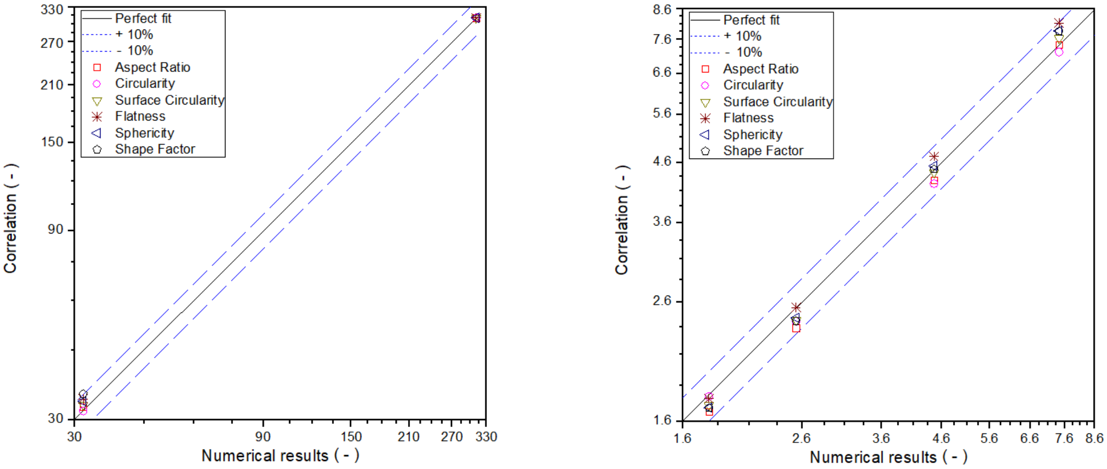

(a) Drag comparison for the range between $0.1 \leq \text{Re} \leq 1$.

(b) Drag comparison for the range between $5 \leq \text{Re} \leq 50$.

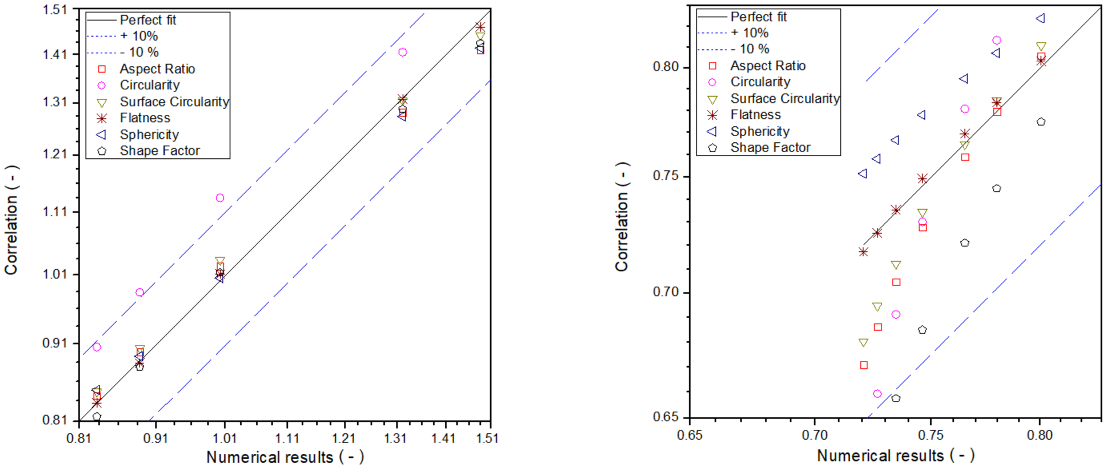

(c) Drag comparison for the range between $75 \leq \text{Re} \leq 750$.

(d) Drag comparison for the range between $1000 \leq \text{Re} \leq 3500$.

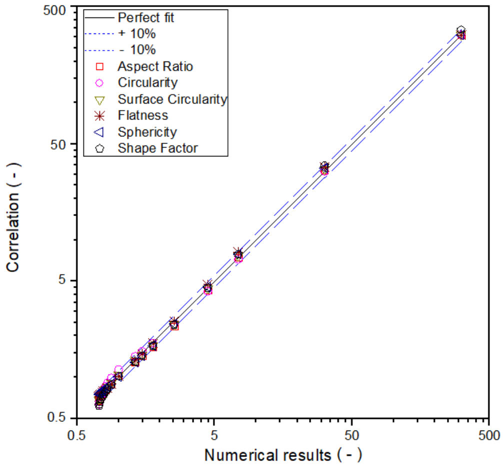

(e) Drag comparison for the range between $0.1 \leq \text{Re} \leq 3500$.

Figure 22 – Comparison between the numerical results and the fits using the new correlation (Equation 5.16) and experimental data for the agglomerate of three particles.

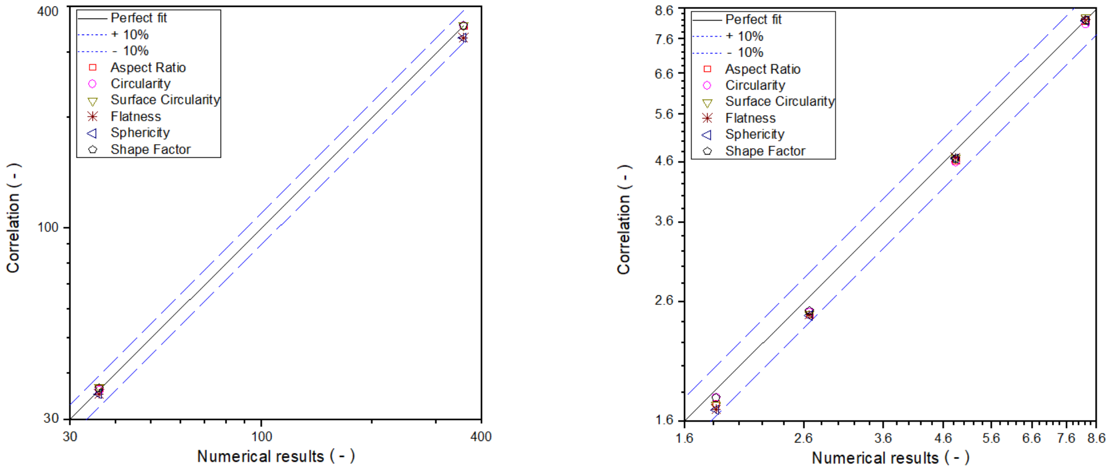

(a) Drag comparison for the range between $0.1 \leq \mathrm{Re} \leq 1$.

(b) Drag comparison for the range between $5 \leq \mathrm{Re} \leq 50$.

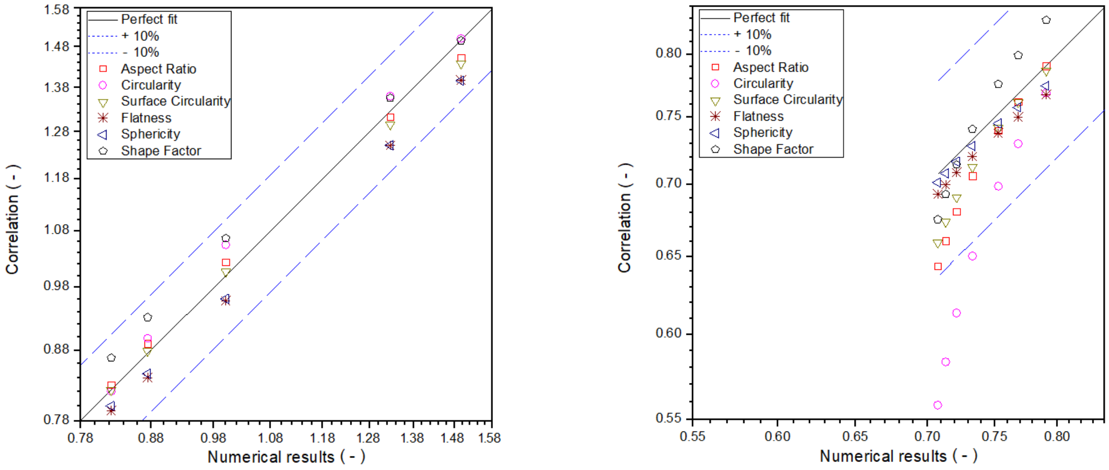

(c) Drag comparison for the range between $75 \leq \mathrm{Re} \leq 750$.

(d) Drag comparison for the range between $1000 \leq \mathrm{Re} \leq 3500$.

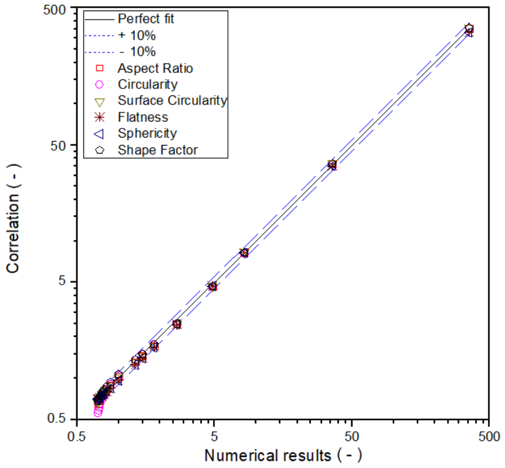

(e) Drag comparison for the range between $0.1 \leq \mathrm{Re} \leq 3500$.

Figure 23 – Comparison between the numerical results and the fits using the new correlation (Equation 5.16) and experimental data for the agglomerate of four particles.

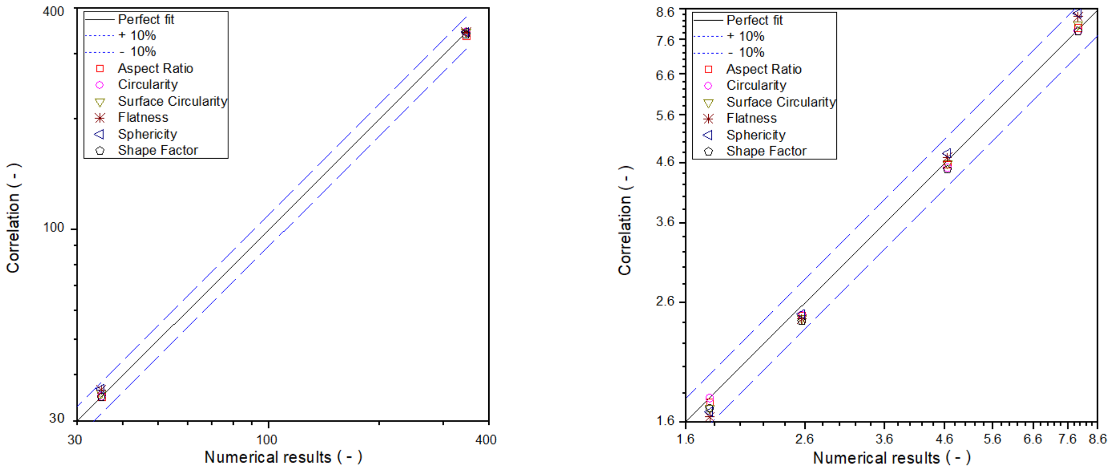

(a) Drag comparison for the range between $0.1 \leq \text{Re} \leq 1$.

(b) Drag comparison for the range between $5 \leq \text{Re} \leq 50$.

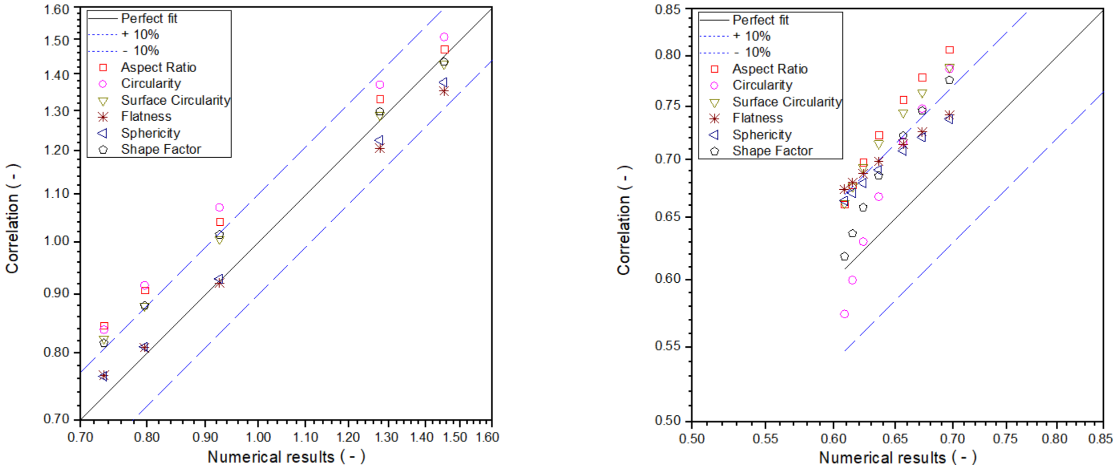

(c) Drag comparison for the range between $75 \leq \text{Re} \leq 750$.

(d) Drag comparison for the range between $1000 \leq \text{Re} \leq 3500$.

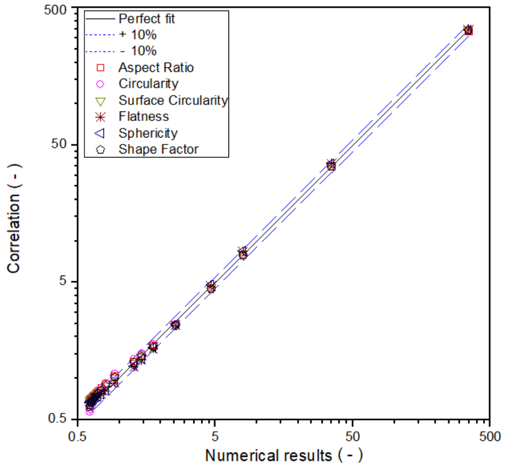

(e) Drag comparison for the range between $0.1 \leq \text{Re} \leq 3500$.

Figure 24 – Comparison between the numerical results and the fits using the new correlation (Equation 5.16) and experimental data for the agglomerate of five particles.

Table 16 – Relative deviations between the correlation fits and simulated data according to the geometric parameter tested.

Geometric parameter	δ_{min} (%)	δ_{max} (%)	δ_{ave} (%)	S.D. (%)
$A.R.$	- 7.789	14.570	4.576	6.119
c	- 21.107	15.851	5.947	8.008
c_{surf}	- 6.937	13.538	4.302	5.682
f	- 7.617	10.786	3.799	5.062
ϕ_W	- 7.814	9.181	4.007	4.769
ψ	- 14.312	11.399	4.906	6.159

Table 17 – Relative deviations between the correlation fits and experimental data according to the geometric parameter tested.

Geometric parameter	δ_{min} (%)	δ_{max} (%)	δ_{ave} (%)	S.D. (%)
$A.R.$	- 24.766	18.938	10.094	12.576
c	- 28.662	28.181	12.617	16.719
c_{surf}	- 20.484	17.402	9.938	12.048
f	- 18.367	14.367	9.601	11.115
ϕ_W	- 18.492	13.361	9.318	10.902
ψ	- 23.383	17.954	11.268	13.398

the flatness is applicable for a broader range of geometries.

5.4 Conclusions

In the present study we performed experiments to estimate the drag coefficient of three conformations of particle agglomerates, composed of spherical particles. The drag coefficient was calculated using the terminal velocity of the agglomerates in free fall using different fluids to vary the Reynolds number for a range between 0.1 and 3500, focusing on obtaining results for different types of flow profile.

The experimental results obtained were used for verification and validation of CFD simulations carried out for both steady and unsteady states, using the SST k-ω and LES turbulence modelling, respectively. Once the formulation showed to be applicable, simulations were carried out to estimate the drag coefficient for 18 Reynolds numbers between 0.1 and 3500, to propose a new drag correlation applicable in particle-laden flows from laminar to turbulent conditions carrying irregularly-shaped particles. The new correlation was fitted for the simulated results using six geometry descriptor parameters, to observe which one can better represent the drag coefficient curve. Main observations were

1. The use of steady formulation using the SST k-ω presented good agreement with experimental data, presenting, for most of the conditions, deviations lower than ± 10%.
2. For all particle agglomerates the simulations presented difficulties to estimate the drag coefficient for the solution of Glycerin 2, where the Reynolds is in a transition range. However, the values were between 15 and 19%, which can still be considered good for CFD validation.
3. The fits using flatness and sphericity presented the best results, with all deviations between -8 and 10% for simulated data, with exception of three points at the turbulent region for five spheres, where flatness presented deviations between 10.37 and 10.79%.
4. Despite the sphericity presented a maximum deviation lower than the flatness, reaching 9.18%, the average deviation were similar, 9.31% and 9.60%, respectively.
5. Since the fit using flatness presents deviations similar to the sphericity but is applicable for a wider range of geometries, we can state that the correlation using flatness presents the best results.

6 General conclusions

This work aimed to propose a new correlation to estimate the drag coefficient in irregularly shaped particles, such as particle clusters. For this purpose, three agglomeration conformations of spheres were proposed to cover different ranges of geometric parameters used in particle characterization.

After reviewing the literature, it was observed that there was a lack of studies using a steady formulation in the study of the drag coefficient in particles. Therefore, in order to fill this gap, a numerical study of turbulence models was conducted, as turbulence significantly affects pressure and velocity fields, and consequently, the drag coefficient results.

To conduct this study, simulations were performed on clusters of hypothetical geometries using five RANS (Reynolds-Averaged Navier-Stokes) turbulence models, and the obtained drag coefficient values were compared with correlations present in the literature. The geometries were proposed to cover the range of application of such correlations for both the geometric parameter characterizing the particle and the Reynolds ranges for which the drag models were proposed. The SST k-ω and Spalart-Allmaras turbulence models showed the best results for calculating the drag coefficient, but the SST k-ω model better represented the flow profile in the wake region after the cluster.

A fundamental part of the verification and validation step of using the steady formulation was the comparison between LES (Large Eddy Simulation) and steady simulations using the SST k-ω model. However, in this step, experimental results were necessary to validate the turbulence model. When analyzing the results, it was observed that LES simulations presented relatively high relative deviations, reaching values higher than 20% compared to the experimental data in fully turbulent flow conditions. In contrast, steady simulations using the SST k-ω model showed values very close to the experimental ones, with nine points having deviations within ± 5% and only two of the fifteen points showing higher deviations, close to -19%.

Once the physical coherence of the simulations was confirmed and experimental validation was carried out, the use of computational fluid dynamics became a powerful tool for extrapolating the studied phenomenon. With the simulations validated for the laminar, transitional, and turbulent flow profile ranges, simulations were then performed for the Reynolds range between 0.1 and 3500, covering fully laminar to fully turbulent flow conditions. From the numerically obtained data, a new adjustment correlation was proposed to accurately represent the behavior of the drag coefficient curve as a function of the Reynolds number. Since drag is highly dependent on the particle's geometry, the correlation was adjusted for six relevant geometric parameters observed in the literature.

Both the flattening and Wadell sphericity as geometric parameters showed good results, with relative deviations below ± 10% for all adjusted points. However, the flattening proved to be a better option, as it presented a lower average relative deviation, only 0.23%, and a standard deviation of 5.06%, in addition to being applicable to a wider range of geometries. Another advantageous aspect of using the flattening was the range of geometries to which the model applies, ranging from 1.08 to 1.28, whereas the sphericity, in this study, ranged from 0.59 to 0.71.

Comparing the new correlation with experimental values, it can be observed that the new proposal was robust for all flow ranges. The use of the flattening as a geometric parameter in the correlation was crucial for the adjustment. Regarding the experimental data, the values obtained by simulation generally showed relatively higher deviations than the values obtained by adjusting the new correlation using the flattening. Despite the deviation for the solution of glycerin flowing through three spheres presenting a relative deviation of -18.37%, it still improved compared to the simulated value, which deviates 19.54% from the experimental one.

Considering that the drag coefficient curve as a function of the Reynolds number presents four significantly different behaviors, the complexity of presenting a model that fits these conditions is high. Also, considering the wide flow range studied, with a range of drag coefficient values from 0.5 to 400, it can be stated that the new proposal proved to be quite efficient. With a maximum relative deviation of 10.78% and a minimum of -7.61%, the new correlation achieves the objectives of this study: a model of simple implementation in CFD codes, unified, capable of covering a wide range of flows, thus showing potential for application in equipment simulations.

Bibliography

ANSYS, INC. **ANSYS FLUENT 14.5 Theory Guide**. [S.l.], 2012.

BAGHERI, G.; BONADONNA, C. On the drag of freely falling non-spherical particles. **Powder Technology**, v. 301, p. 526–544, 2016. ISSN 0032-5910.

BEETSTRA, R.; HOEF, M. van der; KUIPERS, J. A lattice-Boltzmann simulation study of the drag coefficient of clusters of spheres. **Computers and Fluids**, v. 35, p. 966–970, 2006. ISSN 0045-7930.

BÜTTNER, R.; DELLINO, P.; LAVOLPE, L.; ZIMANOWSKI, B. Thermohydraulic explosions in phreatomagmatic eruptions as evidenced by the comparison between pyroclasts and products from Molten Fuel Coolant Interaction experiments. **Journal of Geophysical Research**, v. 107, p. 2277, 2002. ISSN 0148-0227.

CHEN, S.; CHEN, P.; FU, J. Drag and lift forces acting on linear and irregular agglomerates formed by spherical particles. **Physics of Fluids**, v. 32, p. 023307, 2022. ISSN 1089-7666.

CHEN, S.; DOOLEN, G. D. Lattice Boltzmann Method for fluid flows. **Annual Review of Fluid Mechanics**, v. 30, p. 329–364, 1998. ISSN 1089-7666.

CHENG, N.-S. Comparison of formulas for drag coefficient and settling velocity of spherical particles. **Powder Technology**, v. 189, p. 395–398, 2009. ISSN 0032-5910.

CHHABRA, R.; AGARWAL, L.; SINHA, N. Drag on non-spherical particles: an evaluation of available methods. **Powder Technology**, v. 101, p. 288–295, 1999. ISSN 0032-5910.

CHOI, H.; MOIN, P. Grid-point requirements for large eddy simulation: Chapman's estimates revisited. **Physics of Fluids**, v. 24, p. 011702, 2012.

CIMBALA, J. M.; ÇENGEL, Y. A. **Fluid Mechanics: Fundamentals and Applications**. New York: McGraw-Hill Education, 2000.

CLIFT, R.; GAUVIN, W. H. Motion of entrained particles in gas streams. **The Canadian Journal of Chemical Engineering**, v. 49, p. 439–448, 1971. ISSN 1939-019X.

CLIFT, R.; GRACE, J. R.; WEBER, M. E. **Bubbles, Drops and Particles**. First ed. [S.l.]: Academic Press, 1978. ISBN 0-486-44580-1.

DAVIDSON, L. Prediction of the flow around an airfoil using a reynolds stress transport model. **Journal of Fluids Engineering**, v. 117, p. 50–57, 1995. ISSN 1528-901X.

DEEN, N. G.; KRIEBITZSCH, S. H. L.; HOEF, M. A. van der; KUIPERS, J. A. M. Direct numerical simulation of flow and heat transfer in dense fluid-particle systems. **Chemical Engineering Science**, v. 81, p. 329–344, 2012. ISSN 0009-2509.

DEGLON, D.; MEYER, C. CFD modelling of stired tanks: Numerical considerations. **Minerals Engineering**, v. 19, p. 1059–1068, 2006. ISSN 0892-6875.

DELACROIX, B.; RASTOUEIX, J.; FRADETTE, L.; BERTRAND, F.; BLAIS, B. CFD-DEM simulations of solid-liquid flow in stirred tanks using a non-inertial frame of reference. **Chemical Engineering Science**, v. 230, p. 116137, 2021. ISSN 0009-2509.

DELLINO, P.; LAVOLPE, L. Image processing analysis in reconstructing fragmentation and transportation mechanisms of Pyroclastic deposits. **Journal of Volcanology and Geothermal Research**, v. 71, p. 13–29, 1996. ISSN 1872-6097.

DELLINO, P. et al. The analysis of the influence of pumice shape on its terminal velocity. **Geophysical Research Letters**, v. 32, p. 1–4, 2005. ISSN 0094-8276.

DIETZEL, M.; SOMMERFELD, M. Numerical calculation of flow resistance for agglomerates with different morphology by the Lattice-Boltzmann Method. **Powder Technology**, v. 250, p. 122–137, 2013. ISSN 0032-5910.

DOORMAAL, J. P. van; RAITHBY, G. D. Enhancements of the SIMPLE method for predicting incompressible fluid flows. **Numerical Heat Transfer**, v. 7, p. 147–163, 1983. ISSN 1521-0634.

FAN, M.; SU, D.; YANG, L. Development of a benchmark for drag correlations of nonspherical particles based on settling experiments of super-ellipsoidal particles. **Powder Technology**, v. 409, p. 117811, 2022. ISSN 0032-5910.

FERZIGER, J.; PERIĆ, M. **Computational Methods for Fluid Dynamics**. Third ed. [S.l.]: Springer, 2002. ISBN 3-540-42074-6.

GANSER, G. H. A rational approach to drag prediction of spherical and nonspherical particles. **Powder Technology**, v. 77, p. 143–153, 1993. ISSN 0032-5910.

GERHART, P. M.; GERHART, A. L.; HOCHSTEIN, J. I. **Munson, Young and Okiishi's Fundamentals of Fluid Mechanics**. Eigth edition. [S.l.]: John Wiley & Sons, 2016. ISBN 1-119-08070-3.

GIDASPOW, D. **Multiphase flow and fluidization: Continuum and kinetic theory descriptions with applications**. First ed. [S.l.]: Academic Press, 1994. ISBN 0-122-82470-9.

GOOSSENS, D. A drag coefficient equation for natural, irregularly shaped particles. **Catena**, v. 14, p. 73–99, 1987.

GOOSSENS, W. R. A. Review of the empirical correlations for the drag coefficient of rigid spheres. **Powder Technology**, v. 352, p. 350–359, 2019. ISSN 0032-5910.

GRAF, W. **Hydraulics of sediment transport**. New York: McGraw-Hill, 1971.

HAIDER, A.; LEVENSPIEL, O. Drag coefficient and terminal velocity of spherical and nonspherical particles. **Powder Technology**, v. 58, p. 63–70, 1989. ISSN 0032-5910.

HARTGE, E. U.; RATSCHOW, L.; WISCHNEWSKI, R.; WERTHER, J. CFD-simulation of a circulating fluidized bed riser. **Particuology**, v. 7, p. 283–296, 2009. ISSN 1674-2001.

HE, L.; TAFTI, D. K.; NAGENDRA, K. Evaluation of drag correlations using particle resolved simulations of spheres and ellipsoids in assembly. **Powder Technology**, v. 313, p. 332–343, 2017. ISSN 0032-5910.

HEINZ, S. A review of hybrid RANS-LES methods for turbulent flows: Concepts and applications. **Progress in Aerospace Sciences**, v. 114, p. 100597, 2020. ISSN 0376-0421.

HEISS, J. F.; COULL, J. The effect of orientation and shape on the settling velocity of non-isometric particles in a viscous medium. **Chemical Engineering Progress**, v. 48, p. 133–140, 1952.

HILL, R. J.; KOCH, D. L.; LADD, A. J. C. The first effects of fluid inertia on flows in ordered and random arrays of spheres. **Journal of Fluid Mechanics**, v. 448, p. 213–241, 2001. ISSN 0022-1120.

HILL, R. J.; KOCH, D. L.; LADD, A. J. C. Moderate-Reynolds-number flows in ordered and random arrays of spheres. **Journal of Fluid Mechanics**, v. 448, p. 243–278, 2001. ISSN 0022-1120.

HOEF, M. A. van der; BEETSTRA, R.; KUIPERS, J. A. M. Lattice-Boltzmann simulations of low reynolds number flow past mono-and bidisperse arrays of spheres: results for the permeability and drag force. **Journal of Fluid Mechanics**, v. 528, p. 233–254, 2004. ISSN 0022-1120.

HÖLZER, A.; SOMMERFELD, M. New simple correlation formula for the drag coefficient of non-spherical particles. **Powder Technology**, v. 184, p. 361–365, 2008. ISSN 0032-5910.

ISAACS, J. L.; THODOS, G. The free-settling of solid cylindrical particles in the turbulent regime. **The Canadian Journal of Chemical Engineering**, v. 45, p. 150–155, 1967. ISSN 1939-019X.

JAYAWEERA, K. O. L. F.; MASON, B. J. The behavior of freely falling cylinders and cones in viscous fluids. **Journal of Fluid Mechanics**, v. 22, p. 709–720, 1965.

JONES, D. A.; CLARKE, D. B. **Simulation of flow past a sphere using the FLUENT code.** [S.l.], 2008.

KALMAN, H.; MATANA, E. Terminal velocity and drag coefficient for spherical particles. **Powder Technology**, v. 396, p. 181–190, 2022. ISSN 0032-5910.

KASKAS, A. **Berechnung dec stationaren und instationaren Bewegung von Kugelm in rehunden und stromenden Medien**. Tese (Doutorado) — Technische Universität Berlin, Berlin, 1964.

KE, C.; SHU, S.; ZHANG, H.; YUAN, H. Drag coefficient and averaged Nusselt number of a scalene prolate ellipsoid. **Applied Mathematical Modelling**, v. 64, p. 556–571, 2018. ISSN 1872-8480.

KHAN, A. R.; RICHARDSON, J. F. The resistance to motion of a solid sphere in a fluid. **Chemical Engineering Communications**, v. 62, p. 135–150, 1987. ISSN 0098-6445.

KRAVETS, B.; ROSEMANN, T.; REINECKE, S. R.; KRUGGEL-EMDEN, H. A new drag force and heat transfer correlation derived from direct numerical lbm-simulations of flown through particle packings. **Powder Technology**, v. 345, p. 438–456, 2019. ISSN 0032-5910.

KUWAGI, K.; TAKANO, K.; HORIO, M. The effect of tangential lubrification by bridge liquid on the behavior of agglomerating fluidized beds. **Powder Technology**, v. 133, p. 287–298, 2000. ISSN 0032-5910.

LANE, G. L. Improving the accuracy of CFD predictions of turbulence in tank stirred by a hydrofoil impeller. **Chemical Engineering Science**, v. 169, p. 188–211, 2017. ISSN 0009-2509.

LANGTRY, R.; MENTER, F. Correlation-based transition modeling for unstructured parallelized computational fluid dynamics codes. **AIAA Journal**, Aerospace Research Central, v. 47, n. 12, p. 2894–2906, 2009. ISSN 1533-385X.

LÄPPLE, C. E.; SHEPHERD, C. B. Calculation of particle trajectories. **Industrial & Engineering Chemistry**, v. 32, p. 605–617, 1940.

LASSO, I. A.; WEIDMAN, P. D. Stokes drag on hollow cylinders and conglomerates. **Physics of Fluids**, v. 29, p. 3921–3934, 1986.

LAUNDER, B. E.; REECE, G. J.; RODI, W. Progress in the development of a reynolds-stress turbulence closure. **Journal of Fluid Mechanics**, v. 68, p. 537–566, 1975. ISSN 0022-1120.

LAUNDER, B. E.; SHARMA, B. I. Application of the energy dissipation model of turbulence to the calculation of flow near a spinning disc. **Letters in Heat and Mass Transfer**, v. 1, p. 131–138, 1974. ISSN 0094-4548.

LEITH, D. Drag on nonspherical objects. **Aerosol Science and Technology**, v. 6, p. 153–161, 1987. ISSN 1521-7388.

LILLY, D. K. A proposed modification of the Germano Subgrid-Scale Closure Model. **Physics of Fluids**, v. 4, p. 633–635, 1992. ISSN 1089-7666.

LIN, S.; LIU, J.; XIA, H.; ZHANG, Z.; AO, X. A numerical study of particle-laden flow around an obstacle: flow evolution and Stokes number effects. **Applied Mathematical Modelling**, v. 103, p. 287–307, 2022. ISSN 1872-8480.

LOTH, E. Drag of non-spherical solid particles of regular and irregular shape. **Powder Technology**, v. 182, p. 342–353, 2008. ISSN 0032-5910.

LUNA, C. M. R.; CARROCCI, L. R.; ARCE, G. L. A. F.; ÁVILA, I. A comparative assessment of empirical and lattice-boltzmann method-based drag models for simulation of gas-solid flow hydrodynamics in a bubbling fluidized bed. **Particuology**, v. 33, p. 129–137, 2017. ISSN 1674-2001.

MARCHILDON, E.; GAUVIN, W. H. Effects of acceleration, deceleration and particle shape on single-particle drag coefficients in still air. **AIChE Journal**, v. 25, p. 938–948, 1979. ISSN 1547-5905.

MARCHILDON, E. K.; CLAMEN, A.; GAUVIN, W. H. Drag and oscillatory motion of freely falling cylindrical particles. **Canadian Journal of Chemical Engineering**, v. 42, p. 178–182, 1964.

MCKAY, G.; MURPHY, W. R.; HILLIS, M. Settling characteristics of discs and cylinders. **Chemical Engineering Research & Design**, v. 66, p. 107–112, 1988.

MEHRABADI, M.; MURPHY, E.; SUBRAMANIAM, S. Development of a gas-solid drag law for clustered particles using particle-resolved direct numerical simulation. **Chemical Engineering Science**, v. 152, p. 199–212, 2016. ISSN 0009-2509.

MENTER, F. R. Two-equation eddy-viscosity turbulence models for engineering applications. **AIAA Journal**, v. 32, p. 1598–1605, 1994. ISSN 1533-385X.

MILITZER, J.; KAN, J. M.; HAMDULLAHPUR, F.; AMYOTTE, P. R.; TAWEEL, A. M. A. Drag coefficient for axisymmetric flow around individual spheroidal particles. **Powder Technology**, v. 57, p. 193–195, 1989. ISSN 0032-5910.

MOHAMMAD, A. F.; ZAKI, S. A.; IKEGAYA, N.; HAGISHIMA, A.; ALI, M. S. M. A new semi-empirical model for estimating the drag coefficient of the vertical random staggered arrays using LES. **Journal of Wind Engineering & Industrial Aerodynamics**, v. 180, p. 191–200, 2018. ISSN 1872-8197.

MORSI, S. A.; ALEXANDER, A. J. An investigation of particle trajectories in two-phase flow systems. **Journal of Fluid Mechanics**, v. 55, p. 193–208, 1972.

NIKOLOPOULOS, A.; PAPAFOTIOU, D.; NIKOLOPOULOS, N.; GRAMMELIS, P.; KAKARAS, E. An advanced EMMS scheme for the prediction of drag coefficient under a 1.2 MWth CFBC isothermal flow - Part I: Numerical formulation. **Chemical Engineering Science**, v. 65, p. 4080–4088, 2010. ISSN 0009-2509.

OLIVEIRA, R. A. F.; GUERRA, V. G.; LOPES, G. C. Improvement of collection efficiency in a cyclone separator using water nozzles: A numerical study. **Chemical Engineering and Processing - Process Intensification**, v. 145, p. 107667, 2019. ISSN 0255-2701.

OLIVEIRA, R. A. F.; LOPES, G. C. Drag coefficient on particle agglomerates: a cfd study with experimental validation. **Journal of the Brazilian Society of Mechanical Sciences and Engineering**, v. 45, p. 473, 2023. ISSN 1806-3691.

OLIVEIRA, R. A. F.; ZANATA, J. H.; LOPES, G. C. Numerical study of turbulence on drag coefficient determination for particle agglomerates. **Chemical Industry & Chemical Engineering Quarterly**, v. 00, p. 21–21, 2023. ISSN 2683-3867.

OUCHENE, R. Numerical simulation and modeling of the hydrodynamic forces and torque acting on individual oblate spheroids. **Physics of Fluids**, v. 32, p. 073303, 2020. ISSN 1089-7666.

PETTYJOHN, E. S.; CHRISTIANSEN, E. R. Effect of particle shape on free-settling rates of isometric particles. **Chemical Engineering Progress**, v. 44, p. 157–172, 1948.

POPE, S. B. **Turbulent Flows**. Second ed. [S.l.]: Cambridge University Press, 2000. ISBN 0-521-59886-9.

RICHTER, A.; NIKRITYUK, P. A. Drag forces and heat transfer coefficients for spherical, cuboidal and ellipsoidal particles in cross flow at sub-critical reynolds numbers. **International Journal of Heat and Mass Transfer**, v. 55, p. 1343–1354, 2012. ISSN 1879-2189.

RICHTER, A.; NIKRITYUK, P. A. New correlations for heat and fluid flow past ellipsoidal and cubic particles at different agles of attack. **Powder Technology**, v. 249, p. 463–474, 2013. ISSN 0032-5910.

ROOSTAEE, A.; VAEZI, M. Developing a standard platform to predict the drag coefficient of irregular shape particles. **Powder Technology**, v. 395, p. 314–337, 2022. ISSN 0032-5910.

SCHLICHTING, H.; GERSTEN, K. **Boundary-Layer Theory**. Ninth edition. [S.l.]: Springer-Verlag, 2017. ISBN 978-3-662-52917-1.

SENIOR, R. C.; BRERETON, C. Modelling of circulating fluidised-bed solids flow and distribution. **Chemical Engineering Science**, v. 47, p. 281–296, 1992. ISSN 0009-2509.

SPALART, P. R.; ALLMARAS, S. R. A one-equation turbulence model for aerodynamic flows. **Technical Report AIAA-92-0439**, v. 1, p. 5–21, 1992.

THOMPSON, B.; WHITELAW, J. Characteristics of a trailing-edge flow with turbulent boundary-layer separation. **Journal of Fluid Mechanics**, v. 157, p. 305–326, 1985. ISSN 0022-1120.

TRAN-CONG, S.; GAY, M.; MICHAELIDES, E. E. Drag coefficients of irregularly shaped particles. **Powder Technology**, v. 139, p. 21–32, 2004. ISSN 0032-5910.

TUKEY, J. W. **Exploratory Data Analysis**. First ed. [S.l.]: Addison-Wesley Publishing Company, 1977. ISBN 0-201-07616-0.

TUKOVIĆ Ž.; PERIĆ, M.; JASAK, H. Consistent second-order time-accurate non-iterative piso algorithm. **Computers and Fluids**, v. 166, p. 78–85, 2018. ISSN 0045-7930.

VERSTEEG, H. K.; MALALASEKERA, W. **An introduction to Computational Fluid Dynamics: The Finite Volume Method.** Segunda edição. [S.l.]: Pearson, 2007. ISBN 0-131-27498-8.

WADELL, H. Volume, Shape, and Roundness of Rock Particles. **The Journal of Geology**, v. 40, p. 443–451, 1932. ISSN 0022-1376.

WANG, K.; GE, W.; LI, J. Eulerian simulation of heterogeneous gas-solid flows in CFB risers: EMMS-based sub-grid scale model with a revised cluster description. **Chemical Engineering Science**, v. 63, p. 1553–1571, 2008. ISSN 0009-2509.

WANG, L.; WU, C.; WEI, G. Effect of particle clusters on mass transfer between gas and particles in gas-solid flows. **Powder Technology**, v. 319, p. 221–227, 2017. ISSN 0032-5910.

WEN, C. Y.; YU, Y. H. Mechanics of fluidization. In: . [S.l.]: AIChE Journal, 1966. v. 62, p. 100–111.

WEN, Y.; JOG, M. A. Variable property, steady, axi-symmetric, laminar, continuum plasma flow over spheroidal particles. **International Journal of Heat and Fluid Flow**, v. 26, p. 780–791, 2005. ISSN 1879-2278.

WILCOX, D. C. **Turbulence Modeling for CFD**. Second ed. [S.l.]: DCW Industries, 2004. ISBN 1-928729-10-X.

WILLMARTH, W. W.; HAWKS, N. E.; HARVEY, R. L. Steady and unsteady motions and wakes of freely disks. **Physics of Fluids**, v. 7, p. 197–208, 1964.

XIA, H. et al. Modeling and numerical study of particle-bubble-liquid flows using a front-tracking and discrete-element method. **Applied Mathematical Modelling**, v. 114, p. 525–543, 2023. ISSN 1872-8480.

YAKHOT, V.; ORSZAG, S. A.; THANGAM, S.; GATSKI, T. B.; SPEZIALE, C. G. Development of turbulence models for shear flows by a double expansion technique. **Physics of Fluids**, v. 7, p. 1510–1520, 1992. ISSN 1070-6631.

YOW, H. N.; PITT, M. J.; SALMAN, A. D. Drag correlations for particles of regular shape. **Advanced Powder Technology**, v. 16, p. 363–372, 2005. ISSN 1568-5527.

ZHAO, Y.; ZOU, Z.; WANG, J.; LI, H.; ZHU, Q. CFD simulation of solids residence time distributions for scaling up gas-solid bubbling fluidized bed reactors based on the modified structure-based drag model. **Canadian Journal of Chemical Engineering**, v. 99, p. 1780–1791, 2021. ISSN 1939-019X.

Scientific production related to the study

Conference articles

Oliveira, R.A.F.; Lopes, G.C. Estudo do coeficiente de arraste em aglomerados de partículas, *III Congresso Brasileiro de Fluidodinâmica Computacional - CBCFD*, 2022. Available at: Proceedings of III CBCFD

Oliveira, R.A.F.; Lopes, G.C. Uma nova correlação para cálculo de coeficiente de arraste em aglomerados de partículas, *XL Congresso Brasileiro de Sistemas Particulados - ENEMP*, 2022. Available at: 10.17648/enemp-2022-159157

Oliveira, R.A.F.; Zanata, J.H.;Lopes, G.C. Estudo do coeficiente de arraste em aglomerados de partículas utilizando fluidodinâmica computacional, *I Web Encontro Nacional de Engenharia Química - I WENDEQ*, 2021. Available at: Proceedings of I WENDEQ

Zanata, J.H.; Oliveira, R.A.F.; Lopes, G.C. Determinação numérica do coeficiente de arraste para o escoamento ao redor de esfera: avaliação do uso de modelo de turbulência para diferentes regimes de escoamento, *XXXIX Congresso Brasileiro de Sistemas Particulados - ENEMP*, 2021. Available at: Proceedings of XXXIX Congresso Brasileiro de Sistemas Particulados

Journal articles

Oliveira, R.A.F.; Lopes, G.C., 2023. Drag coefficient on particle agglomerates: A CFD study with experimental validation. *Journal of the Brazilian Society of Mechanical Sciences and Engineering*, 45, 473. **DOI:** 10.1007/s40430-023-04366-9.

Oliveira, R.A.F.; Zanata, J.H.; Lopes, G.C., 2023. Numerical study of turbulence on drag coefficient determination for particle agglomerates. *Chemical Industry & Chemical Engineering Quarterly*, 00, 21-21. **DOI:** 10.2298/CICEQ221206021O

Submitted articles

Oliveira, R.A.F.; Lopes, G.C. A new correlation for prediction of drag coefficient on particle agglomerates using CFD. Submitted to the journal *Applied Mathematical Modelling*